Laminar-specific cortico-cortical loops in mouse visual cortex

Hedi Young

Dissertation presented to obtain PhD degree in Neuroscience

Instituto de Tecnologia Química e Biológica António Xavier | Universidade Nova de Lisboa

Oeiras,
May 2021

UNIVERSIDADE NOVA DE LISBOA

Laminar-specific cortico-cortical loops in mouse visual cortex

Hedi Young

Dissertation presented to obtain PhD degree in Neuroscience

Instituto de Tecnologia Química e Biológica António Xavier | Universidade Nova de Lisboa

Research work coordinated by:

Champalimaud Foundation

FCT Fundação para a Ciência e a Tecnologia
MINISTÉRIO DA CIÊNCIA, TECNOLOGIA E ENSINO SUPERIOR

Oeiras, May 2021

ITQB UNIVERSIDADE NOVA DE LISBOA

LAMINAR-SPECIFIC CORTICO-CORTICAL LOOPS IN MOUSE VISUAL CORTEX

HEDI YOUNG

A DISSERTATION PRESENTED TO THE FACULTY OF
UNIVERSIDADE NOVA DE LISBOA IN CANDIDACY FOR THE DEGREE
OF DOCTOR OF PHILOSOPHY

SUPERVISOR: LEOPOLDO PETREANU
INTERNATIONAL NEUROSCIENCE DOCTORAL PROGRAMME
CHAMPALIMAUD RESEARCH
LISBON, PORTUGAL

OEIRAS, MAY 2021

Acknowledgments

When I first visited Lisbon in 2008 on a family holiday, little did I know that five years later, I would be returning to the city to start a PhD. I feel very lucky to have had the opportunity to do a PhD in neuroscience, and luckier still to have been able to do it at the Champalimaud Foundation in Lisbon. It has been by far and away the hardest and longest project I've ever undertaken, and there were many highs and lows along this journey. But these years have been the best of my life, and I'd like to express my gratitude and thank the people who have made it so.

To Leopoldo Petreanu, first and foremost, for welcoming me into his lab and undertaking this long journey with me. Leopoldo always made himself available to offer help and advice when needed, and it was needed often. I learnt a lot from our discussions and time together over the years, not just about the scientific process, but also about how to communicate data clearly and effectively, whether giving a talk or writing a paper. Thank you.

To Beatriz Belbut and Margarida Baeta, for their invaluable contributions to the paper and all the hard work they did to make it happen.

To Nicolas Morgenstern, for taking me under his wing when I first joined the lab. Nico taught me how to patch, and for that, I'll never forgive him.

To Maria Vito, Patrick Teca, Maria Madalena Seixas and Soraia Rodrigues for their help with solutions, to Susana Dias, Sérgio Casimiro, Maria Inês Romano, Inês Marques for their help with histology, and to Dolores Bonaparte, Rita Torre, Andreia Madalena, João Pereira and the rest of the vivarium staff for their help with the animals, anesthesia and perfusions. Doing this PhD without your help would have been much, much harder.

To my lab mates, past and present, Marina Fridman, Gabriela Fioreze, Tiago Marques, Rodrigo Dias, Radhika Rajan, Camille Mazo, Julia Nguyen, Beatriz Belbut, Margarida Baeta, Beatriz Moura, Oihane Horno, Solène Sautory, Flora Vasile, Rita Saraiva, and Francisco Semedo for making the lab such a friendly place to be in. Special thanks to Marina and Tiago for their help with code, and to Rita and Francisco for their help with lab orders.

To my INDP classmates, for being such great company and sharing this journey with me. Special thanks to Nuno Loureiro, for the many great discussions and meals, for expanding my horizons, and for providing me with some of my most enjoyable and memorable moments during these eight years. This PhD would have been much less fun without you.

To Megan Carey and Susana Lima, for the great advice and encouragement they gave me during our many thesis committee meetings.

To Nicolas Gutierrez and Jorge Ramirez, for their generous patching advice and help troubleshooting the rig.

To Bruno Miranda, for encouraging me to apply to the Champalimaud Foundation's PhD programme when we were in the same lab at UCL.

To Teresa Dias and Jorge Henriques, for their help in jumping the bureaucratic hurdles to graduation.

To my flatmates Pedro Rosmaninho and Daniel Pinto, for making Lisbon a home away from home during these many years, for being there through the good times and the bad, for the great dinners, conversations, movie night-ins, and workouts, and in the last year, for helping to preserve my sanity during the pandemic!

To Michael Pereira, Tor Stensola, Bassam Atallah, Vivek Athalye, Sam Walker, Mattia Bergomi, Dario Sarra, Sabine Renninger, João Afonso, Roberto Medina, Simone Lackner, Veronica Corrales, Katya Vinnik, Pasha Itskov, for the many great conversations, coffees, and meals.

To Liliana Silveira and Celeste Cunha, for welcoming me into your family with such generosity and warmth and for those many memorable late-afternoon Saturday lunches.

To my sister Sahra, for all her encouragement and support over these many years.

To Mum & Dad, to whom I owe everything.

Título

Ciclos cortico-corticais laminares específicos no córtex visual do ratinho.

Resumo

Muitas teorias propõem interacções recorrentes através da hierarquia cortical, mas não é claro se os circuitos corticais são selectivamente ligados para implementar cálculos em ciclo. Usando o mapeamento de circuitos subcelulares do método de canal de rodopsina 2 assistido no córtex visual do rato, comparamos a entrada sináptica de alimentação direta (feedforward, FF) ou retroalimentação (feedback, FB) cortico-cortical (CC) às células que se projectam de volta à fonte de entrada (neurónios em ciclo) com células que se projectam para uma área cortical ou subcortical diferente. Os aferentes FF e FB mostraram uma selectividade semelhante do tipo de células, fazendo ligações mais fortes com neurónios em ciclo do que com outros tipos de projecção em camadas (L)5 e L6, mas não em L2/3, resultando numa modulação selectiva da actividade em neurónios em loop. Na maioria dos casos, as ligações mais fortes em neurónios L5 em ciclo localizavam-se nos seus tufos apicais, mas não nos seus dendritos perisomáticos. Os nossos resultados revelam que as ligações CC são selectivamente ligadas para formar ciclos excitatórios monossinápticos e suportam

um papel diferencial de neurónios supragranulares e infragranulares em cálculos hierárquicos recorrentes.

Abstract

Many theories propose recurrent interactions across the cortical hierarchy, but it is unclear if cortical circuits are selectively wired to implement looped computations. Using subcellular channelrhodopsin-2-assisted circuit mapping in mouse visual cortex, we compared feedforward (FF) or feedback (FB) cortico-cortical (CC) synaptic input to cells projecting back to the input source (looped neurons) with cells projecting to a different cortical or subcortical area. FF and FB afferents showed similar cell-type selectivity, making stronger connections with looped neurons than with other projection types in layer (L)5 and L6, but not in L2/3, resulting in selective modulation of activity in looped neurons. In most cases, stronger connections in looped L5 neurons were located on their apical tufts, but not on their perisomatic dendrites. Our results reveal that CC connections are selectively wired to form monosynaptic excitatory loops and support a differential role of supragranular and infragranular neurons in hierarchical recurrent computations.

Contents

Chapter 1

"The fact that the majority of cortical cells have inter-area projections, as opposed to exclusively intra-area projections, seems already to bear an important computational message: it means that almost nothing goes on internally in one area without this activity being transmitted to at least one other area…In essence, I want to propose that the bulk of the computational work of the cortex is not carried out by one area at a time, but by information going back and forth over reciprocal pathways connecting pairs of areas."

Mumford, 1992

1

INTRODUCTION

1.1 The cortex

The mammalian neocortex is a six-layered structure forming the outer layer of the brain (Harris & Shepherd, 2015). It has expanded greatly during human evolution (Preuss, 2007), leading to its wrinkled appearance, and plays a key role in cognition, language, memory and voluntary actions, with an extraordinary capacity to flexibly adjust to different environmental contexts (Krubitzer & Prescott, 2018). Remarkably, its structure is highly conserved across mammalian species, which has led to the belief that it performs canonical computational motifs advantageous for survival and reproduction (D'Souza et al., 2020; Felleman & Van Essen, 1991; Gilbert & Li, 2013; Miller, 2016; Mumford, 1992).

In support of this view is the notion of modularity: it has been proposed that the cortex is a mosaic of modular subunits, with each subunit similar in size and internal structure and performing similar computations, albeit acting on different inputs (Eccles, 1981; Mountcastle, 1978; Szentágothai, 1978). The belief that this basic structural motif may serve to produce very different outputs, from perception to language to cognition, has informed much research

into the intricate structure of the cortex, with the hope that principles applicable to one area may be applicable to another.

But what exactly does this modular subunit, supposedly repeated throughout the cortex, consist of and how is it defined? Two different modular subunits have been hypothesized: “mini-columns” and “macro-columns”. Mini-columns comprise a vertically oriented group of ~110 cells, with a diameter of ~30 μm, and aggregate in their hundreds to form a larger processing unit, or macro-column, with a diameter estimated to be anywhere from 200–300 μm (Eccles, 1981; Szentágothai, 1978) to 500–1000 μm (Mountcastle, 1978). Such a modular organization, if it exists, promises to make the daunting task of understanding how the cortex works more surmountable, since insights gained into the function of one subunit could apply to the entire cortex.

However, others have argued that there is scant evidence for a general modular organization (Crick & Asanuma, 1986; Swindale, 1990; Towe, 1975). Swindale (1990), for example, argues that the cortex exhibits a great deal of diversity in structure and columnar organization, both within and between different cortical areas, perhaps a reflection of the diversity of information stored across these areas: “Not only does it seem wrong to describe the cortex as modular, use of the term obscures the real complexity of cortical organization and fails to do justice to the diversity of forms of columnar order that are actually present…Although it may be difficult to discard the concepts of modularity and repetitive

structural organization that have existed since 1957, the alternative insight, that the cortex is essentially non-modular in construction, may be a more powerful and helpful clue in the search for unifying principles of cortical organization".

Whether the cortex is modular or not, understanding its fine wiring, particularly at the level of the connection strengths of individual synapses, may help to unravel the computations and calculations that it performs and to reveal how they give rise to complex thought and behaviour. While a unified theory of cortical processing and immutable laws governing cortical computation may ultimately prove elusive, there may nevertheless be principles of cortical organisation that are generalisable across areas and species, even in the absence of modularity.

Yet detailed knowledge of the anatomical organisation of the cortex and of connectivity rules between cortical areas is still lacking. At the macro-scale, we have known since the beginning of the 20th century that the cortex is organised into functional areas specialised for different sensory, motor, or association functions (Brodmann, 1909). Aside from its laminated structure, one of the most important organising principles of the cortex, first derived from sensory systems, is that these areas are arranged in a hierarchy (Felleman & Van Essen, 1991; Harris et al., 2019; Markov et al., 2013; Siegle et al., 2021). Information is routed from primary sensory areas to increasingly specialised cortical areas, such that areas higher up in the hierarchy process progressively more complex features.

Importantly, as we shall discuss in the next section, each of these pathways is reciprocated, such that information flows from these higher areas back down to the lower areas they receive information from.

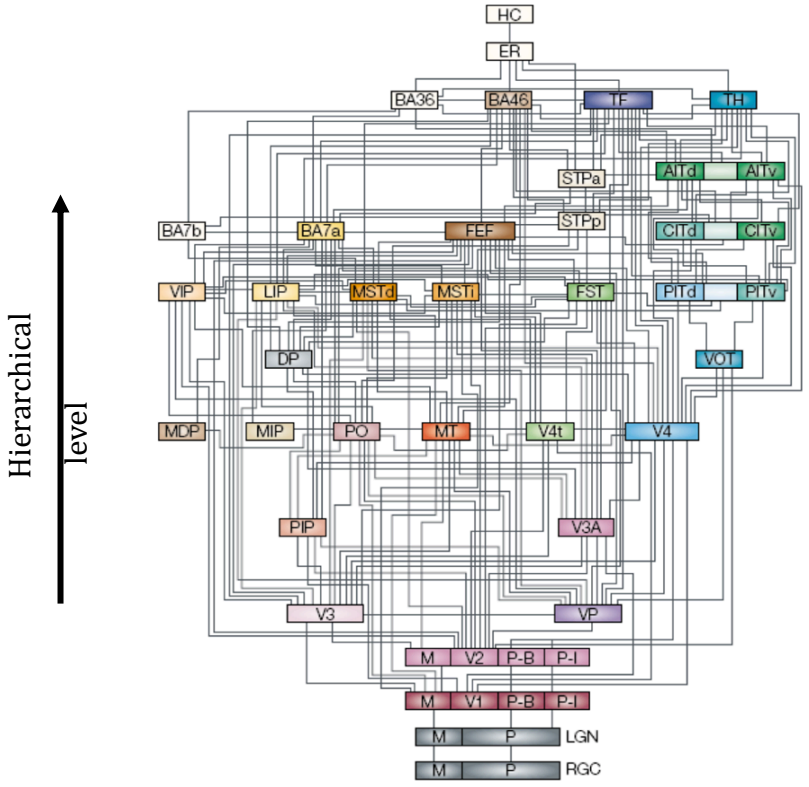

Figure 1.1 *Hierarchy of visual areas in the macaque. Lower areas are represented at the bottom, and higher areas at the top. All areas are interconnected with each other. From Felleman & Van Essen (1991).*

1.2 The canonical microcircuit and its main components

Cortical areas at different levels of the hierarchy are reciprocally connected, such that information can be said to flow bidirectionally. “Feedforward” (FF) projections convey bottom-up inputs along the hierarchy, while “feedback” (FB) projections send top-down inputs in the opposite direction. Since the work of Hubel and Wiesel (Hubel & Wiesel, 1962, 1965), we know that ascending FF projections combine to form increasingly complex representations of the world, a concept that transcended the field of neuroscience and is widely used in artificial intelligence to build neural networks performing complex tasks. However, this view left the equally prevalent descending FB connections without any function, and the various roles of FB are still being elucidated, as we shall discuss later.

There are important differences in the layers that FF and FB projections target (Rockland & Pandya, 1979), which presumably reflect their different functional roles in bottom-up and top-down processing. While ascending and descending projections share common differences across species, there is substantial variation in the precise laminar patterns that they form. In the mouse, FF cortico-cortical (CC) inputs terminate mostly in layer (L) 2/3 and L5/6 (Coogan & Burkhalter, 1990, 1993; Galloni, Ye, & Rancz, 2021; Li, Hass, Matthews, Kristl, & Glickfeld, 2020; Yang, Carrasquillo, Hooks, Nerbonne, & Burkhalter, 2013; Young, Belbut, Baeta, & Petreanu, 2021). By contrast, in the occipital lobe of the primate, FF input

ramifies largely in layer 4 (Rockland & Pandya, 1979), and in the adult cat, V1 FF input to extrastriate areas primarily targets L2/3 and avoids L4 (Price & Zumbroich, 1989). FB CC inputs, on the other hand, appear to be more consistent across species, terminating mainly in the top layer (L1) and deep layers (Coogan & Burkhalter, 1990, 1993; Galloni et al., 2021; Rockland & Pandya, 1979; Yang et al., 2013).

However, it may be noted that projections between lower and higher areas, as defined by classical hierarchical models, do not always follow these patterns. For example, L5 FF neurons in the barrel field of the mouse primary somatosensory area densely innervate L1 of the higher supplemental somatosensory area, while L2/3, L4, and L5 FF neurons in primary visual cortex (V1) all preferentially innervate L1 of dorsal anterior cingulate cortex (ACC), albeit the relatively deeper sub-layer of L1 (Harris et al., 2019). Such targeting of L1 is more usually associated with FB projection patterns. Likewise, FB pathways may display atypical patterns. Orbitofrontal cortex, which exerts top-down modulation in visual cortical areas (Liu et al., 2020), projects most densely to L2/3 of medial secondary visual areas in the mouse and appears to avoid L1 (Galloni et al., 2021), which is more in keeping with a FF projection pattern.

Together, these studies suggest an important organising feature: the long-range axons of cortical cells are not randomly distributed across the layers, but show biases for specific laminae. A

logical extension of this observation is that the axons may show biases for specific cells within those laminae, adding yet a further degree of specificity. Indeed, it has been proposed that the function of lamination is to maximise the wiring efficiency of energetically expensive axons (Chklovskii, Schikorski, & Stevens, 2002), and lamination may facilitate inter-areal communication by constraining and defining the ways in which specific cells in different areas interact e.g. by acting as a scaffold for extracellular axon guidance (Lindenmaier, Parmentier, Guo, Tissir, & Wright, 2018) or by restricting input from one or more areas to precise dendritic compartments that enable more complex computations.

An important computational feature of cortical organisation is that most cortical cells have long-range projections to other areas, such that activity in any given area is almost always relayed to another. It has been estimated that more than 50% of synapses originate from extrinsic axons (Stepanyants et al., 2008). This suggests that reciprocal pathways conveying information back and forth between pairs of interconnected areas at different levels of the hierarchy may form the backbone of cortical computations.

Another key feature of the cortex is that cells can be categorised as belonging to one of several different classes thought to perform different functions (Harris & Shepherd, 2015). The mouse is a genetically and physiologically tractable mammalian species that offers an experimentally accessible way of studying the cortex, and was the animal model of choice for this project. A brief overview of

the layers, hierarchy and cell types that make up the defining characteristics of the cortex now follows.

1.3 Mouse visual cortex

While mouse vision has roughly 100-fold lower resolution than human vision, and the fovea is absent in mice, there are nevertheless striking similarities between the visual cortices of mice and humans. Like humans, mouse visual cortex lies at the back of the brain (Rosa & Krubitzer, 1999), the thalamus provides the major source of information to L4 of V1 (Oh et al., 2014), and there is a rich array of higher-order cortical visual areas surrounding V1, which lies at the bottom of the cortical visual hierarchy (Glickfeld & Olsen, 2017).

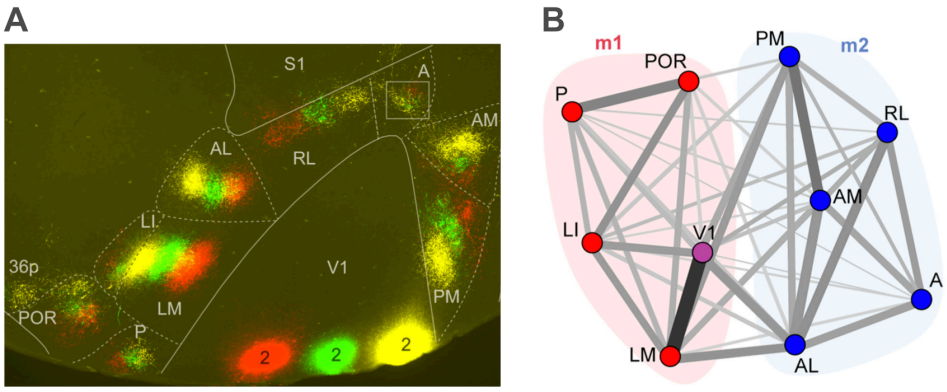

Figure 1.2 *A) Fluorescently labelled axonal projections in higher visual areas in mouse cortex after injections of three anterograde tracers at different nasotemporal locations of the upper visual field representation in V1. From Wang & Burkhalter (2007). B) Visual representation of the ventral (m1) and dorsal (m2) modules of the visual cortical areas in the mouse. The thickness of the connections*

represents the density of the projections between the cortical areas. From Wang, Sporns, & Burkhalter (2012).

Areas in mouse visual cortex are also highly interconnected, and each area is directly connected to all the others (Wang, Gao, & Burkhalter, 2011; Wang et al., 2012), as with primates (Felleman & Van Essen, 1991). However, there is considerable diversity in the projection densities from V1 to higher visual areas (HVAs), with V1 innervation of LM being the strongest (Wang et al., 2012) (Figure 1.2).

Each of these HVAs has its own retinotopic map (Dräger, 1975), and projections from V1 to these areas show retinotopic organization (Wang & Burkhalter, 2007) (Figure 1.2). Mice use vision for a range of complex behaviours, including navigation (Harvey, Collman, Dombeck, & Tank, 2009) and capturing prey (Hoy, Yavorska, Wehr, & Niell, 2016). Visual cortical cells in the mouse perform similar computations to those in the primate, from orientation selectivity (Dräger, 1975; Mangini & Pearlman, 1980; Niell & Stryker, 2008; Sohya, Kameyama, Yanagawa, Obata, & Tsumoto, 2007) to surround suppression (Adesnik, Bruns, Taniguchi, Huang, & Scanziani, 2012).

As in primates, mice display larger receptive field sizes in HVAs compared to V1 (Wang & Burkhalter, 2007) and cells in mouse visual cortex encode complex information that is not solely sensory, such as reward timing (Shuler & Bear, 2006), mismatches between predicted and actual visual feedback (Keller, Bonhoeffer, & Hübener, 2012), visual spatial attention (Speed, Del Rosario, Mikail, & Haider, 2020)

and motor- and behavioral state-dependent modulation of visual responses (Niell & Stryker, 2010).

Moreover, tracing studies show evidence of large-scale parallel information processing streams in the mouse (Wang et al., 2012; Zingg et al., 2014), analogous to the ventral and dorsal streams of primates (Kravitz, Saleem, Baker, & Mishkin, 2011; Kravitz, Saleem, Baker, Ungerleider, & Mishkin, 2013), which consist of two major cortical subnetworks of strongly interconnected areas believed to carry out different functions.

One subnetwork resembling the ventral stream in primates includes the lateral visual areas LM, LI, P and POR, which project to ventral cortical regions such as temporal association cortex involved in object recognition. The other subnetwork, similar to the dorsal stream in primates, includes the areas AL, RL, PM, AM, which project to areas involved in movement and spatial navigation such as the retrosplenial and anterior cingulate cortices. Areas PM and AM also show a preference for the temporal visual field similar to primate dorsal stream areas like MT and MST (Garrett, Nauhaus, Marshel, & Callaway, 2014).

These different anatomical pathways support the view that visual information in the mouse also travels through and is processed by distinct cortical modules. While these HVAs appear to share many properties with primate HVAs, the functions of each of the mouse HVAs is still being investigated and it is unlikely that direct comparisons between mouse and primate HVAs can be made.

Functional imaging studies have revealed functional differences between different HVAs, in particular preferences for distinct ranges of spatial and temporal frequencies, and therefore different speeds. Cells in PM, for example, show a preference for high spatial frequencies and low temporal frequencies (Andermann, Kerlin, Roumis, Glickfeld, & Reid, 2011), while cells in LM, AM, and LI show a preference for higher spatial and temporal frequencies (Marshel, Garrett, Nauhaus, & Callaway, 2011).

Given that V1 projects to all these HVAs, it is possible that the functional specialisation observed in these HVAs is a consequence of the distinct information they receive from differently tuned neurons in V1. Indeed, it has been shown in a two-photon calcium imaging study that the tuning preferences of the axons of V1 cells matches those of cells in the areas they project to (Glickfeld, Andermann, Bonin, & Reid, 2013).

Interestingly, functional differences between V1 and HVAs show variation. For instance, aside from differences in spatiotemporal preferences and receptive field size, LM appears to be functionally similar to V1 (Van Den Bergh, Zhang, Arckens, & Chino, 2010). This may be due to LM residing nearer the bottom of the hierarchy in proximity to V1, and beneath areas such as PM and AM, as suggested by multiple studies (D'Souza, Meier, Bista, Wang, & Burkhalter, 2016; Harris et al., 2019; Siegle et al., 2021).

Various methods and analyses have been employed to establish and examine the hierarchy of areas in the mouse, ranging from

anterograde tracing experiments with Cre-dependent viruses (Harris et al., 2019) to strength of recruitment of inhibition (D'Souza et al., 2016; Dong, Wang, Valkova, Gonchar, & Burkhalter, 2004; Yang et al., 2013) to functional activity (Polack & Contreras, 2012; Siegle et al., 2021).

While the concept of a cortical hierarchy originally stemmed from sensory systems, recent exhaustive studies have attempted to establish the extent to which hierarchical organization applies to the entire mouse cortex (Harris et al., 2019; Siegle et al., 2021). By performing more than 1000 viral tracer injections and analysing layer-specific axonal termination patterns, Harris et al. (2019) found evidence for hierarchical organization across the mouse corticothalamic network, establishing hierarchical positions for 37 cortical areas and 24 thalamic nuclei. The authors assigned "hierarchy scores" to each region based on the number of FF and FB connections each area receives or sends out. Interestingly, they found that the difference between the highest and lowest rungs of the hierarchy was not as great as expected, perhaps a reflection of the densely interconnected network of mouse cortex (Gămănuț et al., 2018).

Indeed, it has been argued that the organization of cortical processing into a hierarchy is need of a reappraisal, and that the functional hierarchy does not map neatly onto the anatomical one (Hegdé & Felleman, 2007). The focus on the laminar patterns of interareal connectivity, which form the basis of hierarchical models,

may neglect the local microcircuitry intrinsic to each area and its contribution to the functional properties of neurons. As Hegdé & Felleman (2007) argue, "while the sustaining strength of the notion of hierarchical processing may be that it is rather simple, its fatal flaw is that it is overly simplistic". Moreover, one can conceive of scenarios in which it is difficult to ascribe a clear hierarchical order to information flow between areas. In a predictive processing framework, for example, which we shall discuss in more detail in Chapter 3, signals from a visual area to an auditory area could act as a prediction of bottom-up auditory input, and vice versa. In such cases, it is not obvious how information flowing in either pathway can be categorized as FF or FB.

While the functional hierarchy observed by Siegle et al. (2021) – obtained by simultaneously recording spiking activity from hundreds of neurons across multiple cortical areas in response to visual stimuli – largely correlates with the anatomical hierarchy of Harris et al. (2019), it appears unlikely that the cortical information flowchart strictly follows the anatomical hierarchy. For example, the axons of most FF L2/3 neurons in mouse V1 branch and share their signals with multiple higher areas located at different hierarchical levels (Han et al., 2018). Furthermore, inconsistencies may be found not just between the functional and anatomical hierarchies, but within the anatomical hierarchy itself. For example, Harris et al. (2019) noted that the hierarchical position they assigned to a given area could not fully account for its FF and FB connections.

1.4 Cortical Cell Types

Neurons in the cortex can be divided into two main classes: pyramidal neurons and interneurons. Pyramidal cells account for almost all output from the cortex and are responsible for communication between brain areas. They are large pyramid-shaped cells with spiny dendrites, excitatory (releasing the neurotransmitter glutamate), constitute ~80% of cells in the cortex (in contrast to regions such as the olfactory bulb and the cerebellum in which interneurons dominate), project locally as well as to long-range targets and can be divided into three main types (Douglas & Martin, 2004; Harris & Mrsic-Flogel, 2013; Harris & Shepherd, 2015; Mumford, 1992).

Intratelencelephalic (IT) neurons project to areas within the telencephalon (most notably the neocortex, but also structures such as the striatum, amygdala and claustrum), pyramidal tract (PT) neurons project to subcortical structures such as the superior colliculus and corticothalamic (CT) neurons project to the thalamus (Harris & Shepherd, 2015). These cells differ not just in their long-range connectivity, but also in their morphology, gene expression profile, intrinsic physiology, and laminar position. Indeed, differences in connectivity and physiology can exist not just across cell classes but within them (even for neurons belonging to the same class and layer). In the primate, for example, IT neurons contributing projections to the dorsal and ventral streams display different firing patterns, suggesting that they belong to distinct IT subtypes

(Movshon & Newsome, 1996; Nassi & Callaway, 2009). IT neurons are distributed across all layers of the cortex (except for L1), while PT and CT neurons are restricted to L5 and L5/L6, respectively (Harris & Shepherd, 2015).

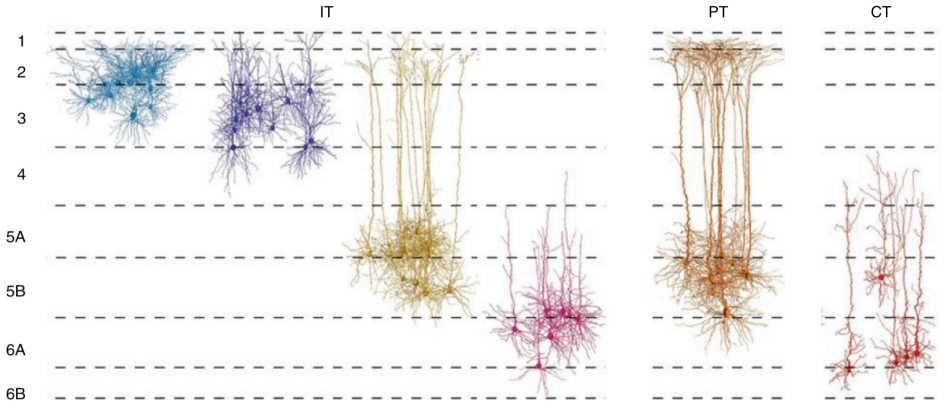

Figure 1.3 *Dendritic morphology of the three types of excitatory cortical cells in somatosensory cortex. Intratelencelephalic (IT) cells are present in all layers except L1, while pyramidal tract (PT) cells and corticothalamic (CT) neurons are present in L5 and L5/6, respectively. From Harris & Shepherd (2015).*

Interneurons constitute the remaining 20% of neurons, and unlike excitatory neurons, their projections are nearly all intra-areal and restricted to cells within the local vicinity, such that their effect on cortical output is modulatory rather than direct. They tend to be small cells with spineless dendrites, and most importantly, they are inhibitory (releasing the neurotransmitter GABA). This carries an important computational message: long-range projections are almost exclusively excitatory, and not inhibitory.

Like the pyramidal neurons, interneurons can be subdivided into three major classes that can be distinguished by their different genetic profiles, and include parvalbumin-expressing (PV), somatostatin-expressing (SST) and vasoactive intestinal peptide expressing (VIP) neurons (Tremblay, Lee, & Rudy, 2016). They also differ in their connectivity and laminar positions. For example, PV and SST neurons are distributed across the cortical layers, while VIP neurons can be found mainly in superficial layers, and are prominent in L1. Given that this thesis is concerned principally with principal cells and the long-range connections they form, focus will be given to the IT, PT and CT cells in the following sections.

1.5 Layers of the cortex

1.5.1 Layer 1

L1, the topmost layer of the cortex, does not contain any excitatory cells and instead contains the apical tufts of L2/3 and L5 cells, interneurons, and axon terminations from higher cortical areas and subcortical nuclei (Garcia-Munoz & Arbuthnott, 2015; Schuman, Dellal, Prönneke, Machold, & Rudy, 2021). The “crowning mystery” of the cortex (Hubel, 1982), L1 is thought to be the principal locus for top-down FB modulation of visual responses. Importantly, FB axons do not just reside in L1, and target both excitatory and inhibitory neurons in L2/3 and the deeper layers (Yang et al., 2013).

Since FB to apical dendrites in L1 arrives at the most electrically remote region of the cell, it may not in and of itself be able to induce spike generation in the cell, but it can induce dendritic calcium spikes that amplify a cell's responses to FF sensory information arriving simultaneously at perisomatic synapses (Larkum, Zhu, & Sakmann, 1999; Larkum, Senn, & Lüscher, 2004). In this way FB input in L1 may amplify sensory responses depending on the context of the animal's behaviour.

1.5.2 Layer 2/3

This layer consists of IT neurons exclusively. While the full spectrum of L2/3 IT subtypes are still being established, it is already clear that subtypes can be distinguished by their different long-range targets, gene expression, firing patterns and response properties (Chen, Carta, Soldado-Magraner, Schneider, & Helmchen, 2013; Greig, Woodworth, Galazo, Padmanabhan, & Macklis, 2013; Harris & Mrsic-Flogel, 2013; Molyneaux et al., 2009; Sato & Svoboda, 2010; Yamashita et al., 2013). The projections of L2/3 cells are principally restricted to the cerebral cortex, specifically to higher order and contralateral cortices. Their local axon collaterals also branch extensively in L5, but not in L4 or L6, and this appears to be a recurring feature in different cortical areas and species (Douglas & Martin, 2004; Petreanu, Huber, Sobczyk, & Svoboda, 2007; Thomson & Lamy, 2007). Moreover, individual L2/3 cells in mouse V1 display remarkably diverse long-range axonal projection patterns and

broadcast their signals to multiple HVAs rather than to a single target area.

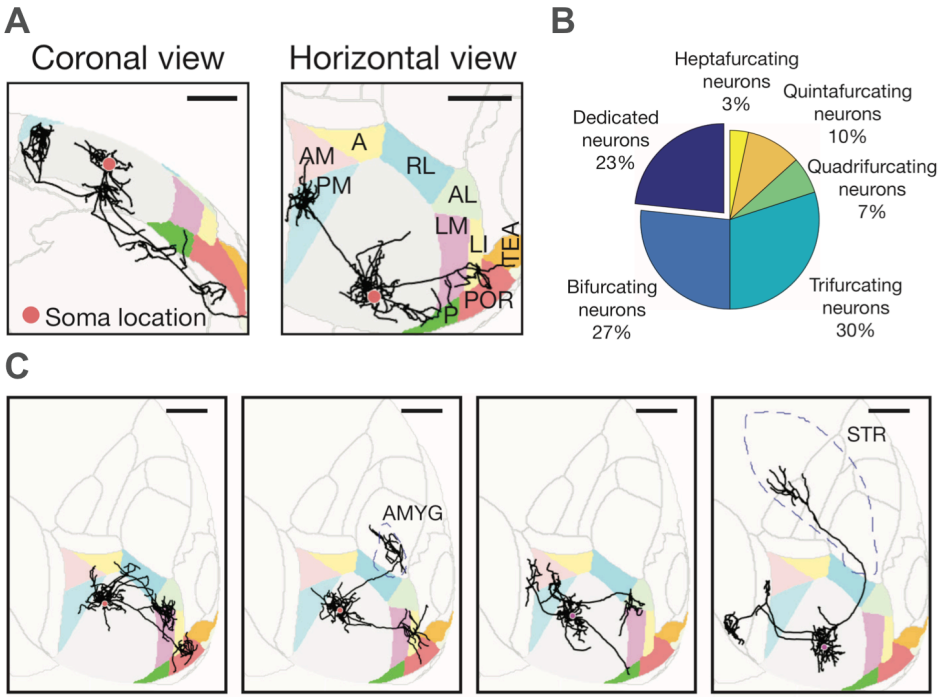

Figure 1.4 *A) Coronal and horizontal views of the axonal projections of a traced L2/3 neuron overlaid in the Allen Reference Atlas space. Scale bar, 1 mm. B) The number of areas targeted by the long-range axons of L2/3 cells projecting out of V1. C) Four examples of traced single neurons overlaid in Allen Reference Atlas space, horizontal view. Dashed lines denote non-visual target areas. AMYG, amygdala; STR, striatum. Scale bar, 1 mm. From Han et al. (2018).*

L2/3 cells employ a sparse information code, with low firing rates, and a limited range of features to which they respond. It has been proposed that this sparseness arises from selective excitation

and robust indiscriminate inhibition (Harris & Mrsic-Flogel, 2013). Activating L2/3 cells optogenetically has mostly inhibitory effects in other L2/3 cells (Adesnik et al., 2012; Beltramo et al., 2013). Reconstruction of the axons of individual L2/3 cells has revealed a wide array of long-range targets, and considerable diversity in their projections (Yamashita et al., 2018), with most neurons targeting more than one cortical area such that signals are simultaneously routed through multiple functional pathways (Han et al., 2018).

Among the L2/3 subtypes that have been identified are the L2 marginal neurons (L2MNs) (Luo, Hasegawa, Liu, & Song, 2017). These L2 neurons are distinguished by their distinct morphological and electrophysiological properties and lie in upper L2 below the L1-L2 border. They exhibit a higher firing rate than other L2/3 cells, and may play a different functional role in cortical circuits compared to their L2/3 neighbours. Indeed, the finding that cells located in different sublaminae of L2/3 differ in their sensory responses suggests that L2/3 is not a homogenous layer, and that important differences may exist between L2 and L3 that are only starting to be uncovered (Meng, Winkowski, Kao, & Kanold, 2017).

1.5.3 Layer 5

L5 is seen as the classic output layer of the cortex and cells here project more widely than L2/3 cells, and can broadly be categorised as either IT cells or PT cells. L5 ITs generally spike more than L2/3 ITs, but not as much as PT neurons (O'Connor, Peron, Huber, &

Svoboda, 2010; Sakata & Harris, 2009), and they send projections to ipsilateral and contralateral cortex and have dense projections to the striatum (Shepherd, 2013) as well as local ascending projections to L2/3 (Hooks et al., 2011; Shepherd, Stepanyants, Bureau, Chklovskii, & Svoboda, 2005). Not all L5 CC pyramids project to the striatum, and some consider these cells to be a separate class with different genetic, electrophysiological and morphological properties. For example, they display a greater affinity for high spatial frequencies, suggesting a role in visual acuity (Kim, Juavinett, Kyubwa, Jacobs, & Callaway, 2015).

L5 IT cells can be further subdivided into subtypes depending on whether they are based in upper or lower L5, or on which areas they project to (Gerfen, Economo, & Chandrashekar, 2018). Moreover, it is becoming possible to map the projection collaterals of individual neurons, which is revealing the full complexity of projection patterns in these cells. For example, the axon collaterals of a single L5 IT neuron in the secondary motor cortex was found to target at least 10 areas (Economo et al., 2018).

PT neurons, on the other hand, have different anatomical and physiological properties than L5 IT cells, and so likely mediate different perceptual and behavioural information channels (Kim et al., 2015). They are larger than L5 IT cells, have thicker apical trunks and more elaborate apical tufts in L1 (Maruoka, Kubota, Kurokawa, Tsuruno, & Hosoya, 2011), and are traditionally classified as L5B neurons, since they mostly reside in the deeper sublayer of L5. PTs

often display intrinsic bursting firing patterns (Christophe et al., 2005), and show strong expression of hyperpolarization-activated currents (Dembrow & Johnston, 2014; Sheets et al., 2011; Shepherd, 2013; Suter, Migliore, & Shepherd, 2013).

PT neurons have limited local projections (Brown & Hestrin, 2009) such that their output is mostly relayed outside the cortex to structures including the brainstem, spinal cord and midbrain, ipsilateral striatum and higher-order thalamus (Reiner, Hart, Lei, & Deng, 2010; Sherman, 2012). They can also project to ipsilateral cortex, projections which have been classified as FB rather than FF (Nelson et al., 2013; Ueta, Hirai, Otsuka, & Kawaguchi, 2013), and they receive extensive local input from IT cells across different layers (Brown & Hestrin, 2009; Kiritani, Wickersham, Seung, & Shepherd, 2012).

As a result, PT neurons integrate the results of cortical computations, and relay these signals in a strong and sustained manner to non-cortical areas. It should be noted, however, that like IT cells, there is a substantial amount of diversity in the axonal projection patterns of PT neurons, even for those in the same area (Kita & Kita, 2012) and PT cells are multi-projectional. For example, individual PT neurons in V1 can project to different subcortical targets, including the superior colliculus, LGN, LP or pons (Bourassa & Deschênes, 1995). Moreover, different subclasses of PT cells can be differentiated by their electrophysiological properties (Tseng & Prince, 1993), not just by their axonal targets.

Unlike L2/3 IT cells, PT cells employ a dense information code, and have the highest in vivo firing rates observed in excitatory cortical cells (De Kock, Bruno, Spors, & Sakmann, 2007; Niell & Stryker, 2008), which may help to strengthen the signal they broadcast to output areas. Researchers using monosynaptic rabies virus-based tracing found that PT cells receive more input from areas such as the retrosplenial and anterior cingulate cortex, while L5 IT cells receive more input from higher visual cortical areas (Kim et al., 2015). The same study found that PT cells showed greater direction selectivity and stronger tuning for fast stimuli compared to IT cells, suggesting that PT cells may be specialised for processing visual motion, with IT cells more specialised for object recognition.

1.5.4 Layer 6

The deepest layer in cortex, L6 is perhaps the least studied of the cortical layers. It comprises two major cell classes, L6 IT cells and CT cells. L6 IT cells are characterised by fairly rudimentary dendritic arbors and heterogeneous morphology including inverted cell bodies and bipolar cells (Thomson, 2010). They possess long-range horizontal axons and typically project to other areas in ipsilateral and contralateral cortex, and in V1 they receive inputs from local deep-layer neurons (Vélez-Fort et al., 2014). The sublaminar distribution of L6 ITs can differ across areas (Watakabe et al., 2012). A subset of L6 IT cells with projections to claustrum have also been identified, and have even been considered to constitute a third cell class (Thomson, 2010). These cells are characterised by long thin

apical dendrites that show minimal branching and extend all the way to L1 (Katz, 1987).

CT cells project principally to ipsilateral thalamus, but also have locally ascending axon collaterals, and have distinct molecular and developmental traits (Greig et al., 2013; Thomson, 2010). They are smaller than their neighbouring L6 IT cells, with apical tufts in L4/5 and it has been suggested that they receive most of their inputs from higher order cortical areas, and thereby convey long-range inputs to the thalamus (Harris & Shepherd, 2015; Vélez-Fort et al., 2014).

As with the other cell classes, various CT subtypes have been identified. For example, L6 CT cells that project only to first-order thalamic nuclei have been identified in upper L6 (Bourassa & Deschênes, 1995), while a subtype of CT cells in deep L6 projects to higher-order thalamic nuclei (Deschênes, Veinante, & Zhang, 1998). Unlike PT cells whose strong inputs to the thalamus are thought to drive the thalamus, CT cells generally form weak synapses such that their thalamic inputs are thought to be modulatory.

While the functions of L6 remain to be elucidated, some have proposed that it plays a suppressive role since optogenetically activating L6 in vivo leads to inhibition of cortical activity. For example, V1 CT cells have been reported to inhibit layers above through activation of PV cells (Bortone, Olsen, & Scanziani, 2014; Olsen, Bortone, Adesnik, & Scanziani, 2012).

CT and L6 IT cells display different electrophysiological properties and connectivity patterns (Mercer et al., 2005; Thomson, 2010). In response to sustained depolarisation, IT cells show strong adaptation in their spike frequency while CT cells show weak adaptation (Mercer et al., 2005). This may reflect different functional roles, with IT cells broadcasting strongly phasic signals, perhaps relaying information related to novelty, and CT cells firing tonically and in a more sustained manner. In terms of their local connectivity, CT cells innervate other L6 pyramidal cells much less frequently than IT cells, while IT cells innervate interneurons less frequently than CT cells (Mercer et al., 2005). In turn, CT cells receive significantly more inhibitory synapses on their somata relative to neighbouring cells, at least in primate V1 (Lund, Griffiths, Rumberger, & Levitt, 2001). This may contribute to the observation made by Harris & Shepherd (2015) that "most CT neurons in vivo are remarkably silent, even during various behaviors".

1.6 Cortical connections

Knowledge of micro-scale connectivity in the cortex is still rudimentary, especially with regard to long-range connectivity. Much of our assumptions about the wiring diagram of interareal cortical connections stem from studies examining the extent to which long-range excitatory axons overlap with the dendrites of individual neurons. Peters' rule states that the probability of functional synaptic connections can be predicted from axo-dendritic overlap (Rees, Moradi, & Ascoli, 2017). However, axo-dendritic overlap is not

always a good predictor of connection probability (Dantzker & Callaway, 2000; Galloni et al., 2021; Shepherd et al., 2005; White, 2002).

1.6.1 Local connectivity

We have a perhaps more complete understanding of local connectivity, which is still dominated by Gilbert & Wiesel's simplified classical model of cortical circuits (Douglas & Martin, 2004; Gilbert, 1983; Gilbert & Wiesel, 1983). In this model, inputs from the thalamus arrive in L4, and L4 excitatory cells subsequently send ascending projections to L2/3. Cells in L2/3 in turn send FF projections to L4 of higher cortical areas as well as local descending projections to L5. L5 cells then project to L6, which closes the loop by projecting up to L4 as well as to the thalamus. In addition, neurons from both L2/3 and L5 send long-range FB projections to lower cortical areas.

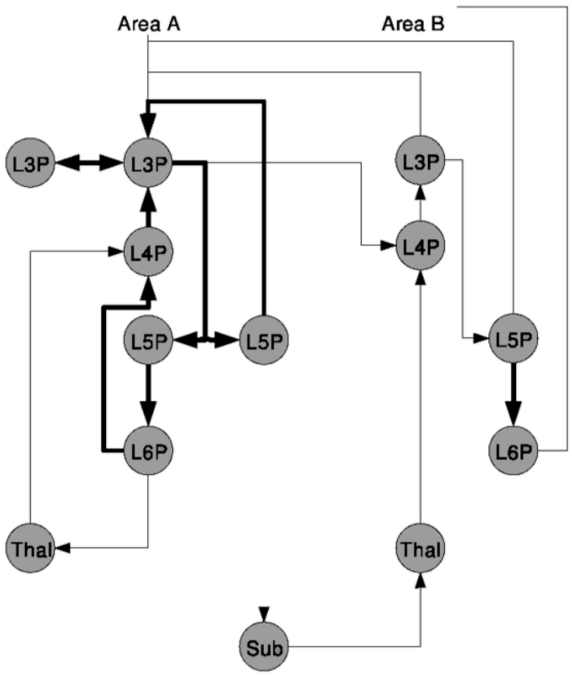

Figure 1.5 *Diagram illustrating the principal intra- and interareal connections between excitatory pyramidal cell types (P), represented by nodes, in the neocortex and their subcortical relations. Nodes are organized vertically to indicate laminar position. Thick arrows represent local intraareal connections, as described by Gilbert & Wiesel for visual cortex (Gilbert, 1983; Gilbert & Wiesel, 1983), and thin arrows represent interareal connections with cortical or subcortical regions. Thal, thalamus; Sub, subcortical structures (e.g. basal ganglia). From Douglas & Martin (2004).*

How does local connectivity in the cortex relate to sensory tuning? In mouse visual cortex, it seems that cells which share selectivity for similar visual features are more likely to be connected to each other, forming interconnected excitatory subnetworks of

cells that code for similar sensory properties (Ko et al., 2011). Connection probability appears to increase in particular for cells that have similar responses to natural movies. Interestingly, not all cells that are connected respond similarly, and vice versa. This appears to be a recurring feature in the cortex: where preferential connectivity exists, it is not absolute but graded. For example, in the previous study, even for pairs of cells with similar responses to natural movies or orientation, connection probability is still less than 50%.

Similarly, connection probabilities between neighbouring L5 callosal projection neurons in rat frontal cortex are higher if the pair exhibit similar physiological properties and firing patterns (Otsuka & Kawaguchi, 2011), and bidirectional connections between pairs of cells are more likely to be found if they share common intra- or inter-laminar input (Otsuka & Kawaguchi, 2011; Yoshimura, Dantzker, & Callaway, 2005).

Such functionally specific recurrent connectivity may serve to both amplify (Douglas et al., 2016; L. Y. Li, Li, Zhou, Tao, & Zhang, 2013; Li, Ibrahim, Liu, Zhang, & Tao, 2013; Lien & Scanziani, 2013) and prolong (Li et al., 2013; Li et al., 2013; Lien & Scanziani, 2013) cortical sensory responses, reducing noise interference and allowing for overlapping interactions with later sensory inputs or FB signals, respectively. Given that preferential connectivity for functionally similar cells is not exclusive, connections also exist between cells with different feature preferences. Recurrent excitation could therefore link neuronal populations selective for different sensory

properties, which could serve to amplify responses to combinations of specific sensory features that carry behavioural relevance.

1.6.2 Long-range connectivity

There is increasing evidence that local and long-range connectivity are related to each other. In rat visual cortex, V1 neurons projecting to LM make frequent local synaptic connections with each other (Johnson & Burkhalter, 1997). Strong interconnectivity between FF neurons sharing the same projection target could serve to amplify their FB input. In mouse visual cortex, connected pairs of pyramidal neurons in L4 share more common thalamic input than unconnected pairs, while connected pairs of neurons in L4 and L2/3 are also more likely to be innervated by the same thalamocortical axons compared to unconnected L4-L2/3 pairs (Morgenstern, Bourg, & Petreanu, 2016). This indicates that FF thalamic input is amplified by intra- and inter-laminar networks involving L4 neurons.

Numerous studies have shown that the target of long-range projection neurons may influence their local connectivity patterns (Brown & Hestrin, 2009; Le Bé, Silberberg, Wang, & Markram, 2007; Mercer et al., 2005; Morishima & Kawaguchi, 2006). For example, in mouse cortex, monosynaptic connections between neurons projecting to the same long-range target are more frequent among corticostriatal neurons than they are among CC or corticotectal

neurons, and CC axons are more likely to synapse onto nearby corticotectal neurons than onto CC neurons (Brown & Hestrin, 2009).

Recent large-scale attempts have been made to uncover long-range CC wiring patterns (Gămănuţ et al., 2018; Harris et al., 2019). Perhaps one of the most important principles of CC connections is that they are almost entirely constituted by one class of pyramidal neurons, namely, IT neurons, with CC projections from PT and CT neurons being relatively sparse (Harris et al., 2019; Harris & Shepherd, 2015).

Using Cre lines and mapping long-range axonal projections with cell-class resolution, Harris et al. (2019) describe anatomical rules governing CC connections. In general, they identify L2/3 and L4 cells as having predominantly FF-like axonal lamination patterns, while L5 and L6 neurons display a mixture of both FF- and FB-like patterns. Specifically, L2/3 and L4 cells projections largely avoid L1, and instead mostly target L2/3–L5, with another group of L4 cells targeting L1 in addition to L2/3 or L5. L5 IT neurons, on the other hand, generally target L1 and L2/3, but also L6 (since the authors were unable to identify a suitable Cre line for L6 IT cells, the axonal patterns of this population were not characterized). Of course, like many “rules” or “generalizable principles” in biology, there are notable exceptions. For example, in this same study, L2/3 cells in higher areas AL and the supplemental somatosensory area are a prominent source of FB projections to the upper and lower layers of V1 and the barrel field of primary somatosensory area, respectively.

Nevertheless, there appear to be consistent differences in the laminar origin of projection neurons both within and between FF and FB connections (Harris et al., 2019), as in the primate (Felleman & Van Essen, 1991; Markov et al., 2014). For example, FF cells projecting to higher areas residing at different hierarchical levels show differences in their layers of origin. LM-projecting V1 cells appear to have a greater percentage of neurons in L2/3 and a lower percentage of neurons in L5/6 compared to AM-projecting V1 cells (Kim et al., 2020). Similarly, relative to their L5 counterparts, L2/3 cells in V1 contribute much more to the FF projection to AL than they do to the FF projection to more hierarchically distant dorsal ACC (Harris et al., 2019).

Do long-distance cortical connections relay sensory signals in a target-specific manner? Interestingly, the excitatory cortical input received by cells in mouse visual and auditory cortex appears to match the sensory tuning of direct thalamic input (Li et al., 2013; Li et al., 2013; Lien & Scanziani, 2013), and long-range horizontal inputs in the cat preferentially synapse onto cells with similar sensory tuning (Gilbert & Wiesel, 1989). Moreover, silencing FB to V1 from HVAs AL or PM (areas which exhibit different visual properties), leads to a greater reduction in the firing rate of V1 cells with matching visual properties compared to cells with non-matching properties (Huh, Peach, Bennett, Vega, & Hestrin, 2018). This suggests that FB neurons from HVAs display differential connectivity in V1, such that they preferentially boost the activity of V1 cells that have similar visual responses.

Given that V1 cells with similar response properties to AL or PM are more likely to project to those areas (Glickfeld et al., 2013), this suggests the presence of functionally specific FF-FB loops. Supporting this view, it has been shown in the rat that individual V1 cells receive FB input from cells located in the area that they target (Johnson & Burkhalter, 1997). If such functionally specific loops exist, they may also be layer-specific. Anatomical tracing in the rat indicates that projections from deep layers of V1 are biased to the deep layers of HVAs, and that the same projection bias is found between superficial layers (Coogan & Burkhalter, 1993).

Together, these results point to a like-to-like functional organisation which may play an important role in sensory systems and across the cortex more generally. For example, there is also evidence that projections between HVAs originate from functionally and anatomically distinct subpopulations of cells. Projections from LM to other HVAs AL and PM have been found to be functionally target specific (Glickfeld et al., 2013), and LM→V1 FB and LM→AL FF projections arise from largely separate subpopulations of cells in LM (Berezovskii, Nassi, & Born, 2011).

1.6.3 Genetic vs. environmental influences in development

It remains unknown to what extent the wiring of these long-range connectivity patterns is determined by genetic and developmental processes as opposed to environmental ones. The

functionally specific subnetworks discussed so far could represent genetically distinct subpopulations of cells. Indeed, connectional probability and tuning similarity has been found to be greater in neurons generated from the same progenitor cell (Gao, Sultan, Zhang, & Shi, 2013). Just as gene modules determine the differentiation of excitatory cells into PT, CT and IT subtypes, it is possible that a common set of genes underlie differences not just in physiology and morphology, but also in long-range connectivity. Together with area-specific molecular gradients, different combinatorial expression of these genes in distinct subclasses of IT neurons could therefore guide long-range CC axons to their respective targets during development. For example, latexin- and Nr4a2-expressing neurons in the deep layers of different sensory cortices send FB projections to the corresponding primary sensory area, yet seldom send FF projections (Bai, Ishida, & Arimatsu, 2004), and V1→AL and V1→PM cells in L2/3 showed differential expression of more than 800 genes, suggesting that genetic differences do indeed contribute to the specification of long-range projections (Kim et al., 2020).

However, it is clear that cortical connectivity patterns are not entirely determined by genetic and molecular cues. For one, FF and FB projections continue to develop for weeks after eye opening, suggesting that maturation of these pathways is dependent upon activity induced by sensory experience (Berezovskii et al., 2011; Dong et al., 2004; Smith, Townsend, Huh, Zhu, & Smith, 2017). Indeed, studies in L2/3 of visual cortex have found that after eye opening more connections were added preferentially between

neurons with similar feature selectivity (Ko et al., 2013), suggesting that visual experience also contributes to functionally specific connectivity.

1.7 FB and FF interactions in the cortical hierarchy

While the FF model of hierarchical visual processing can explain how progressively more complex, abstract representations of the environment arise (Marr, 1982), the role of FB projections is less clear. However, there is increasing evidence that FB projections encode a wide array of cognitive, behavioural and sensory features (Petreanu et al., 2012), mediating cognitive processes such as spatial attention, feature binding, prior experience and expectation (W. Li, Piëch, & Gilbert, 2008; Roelfsema & de Lange, 2016), and amplifying the responses of cells carrying behaviourally relevant information (D'Souza et al., 2020; Desimone & Duncan, 1995; Gilbert & Li, 2013; Larkum, 2013; Moore & Zirnsak, 2017).

Figure 1.6 *FB processing reveals the dalmation dog. From Mumford (1992).*

For example, in primates it is known that the retinotopy of V2 FB axons matches those of target positions in V1 (Stettler, Das, Bennett, & Gilbert, 2002), and in the mouse LM→V1 FB inputs show tuning-dependent retinotopic specificity (Marques, Nguyen, Fioreze, & Petreanu, 2018). FB inputs from the anterior cingulate cortex can increase orientation selectivity in V1 neurons and enhance visual discrimination through recruitment of local inhibitory neurons (Zhang et al., 2014), and inactivating FB inputs from V2 and V3 reduces surround suppression in V1 (Nassi, Lomber, & Born, 2013).

While it is clear that FB inputs carry diverse signals and enable cells in lower areas to perform more complex computations beyond straightforward FF processing, the precise connectivity of FB axons

and whether they target specific FF neurons is still being investigated. Likewise, much remains to be learned about how FF connections innervate different projection neurons in higher areas. Understanding the organization of FF and FB connectivity at the level of individual neurons and their projection targets promises to shed light on the role of CC connections in cortical processing.

Recently, hierarchical processing theories such as predictive coding (Keller & Mrsic-Flogel, 2018) and error backpropagation (Richards & Lillicrap, 2019) have been gaining traction. These theories, which we shall discuss in more detail in Chapter 3, posit a recurrent dialogue between ascending and descending projections, working together towards a common goal, and require FF and FB CC neurons to selectively engage with each other via long-range loops.

Various studies have already identified the presence of CC monosynaptic inputs to "looped" cells that project back to the source of those inputs (Johnson & Burkhalter, 1997; Kinnischtzke, Fanselow, & Simons, 2016; Mao et al., 2011; Suter & Shepherd, 2015; Yamawaki, Radulovic, & Shepherd, 2016). An early study in rat visual cortex, which used anterograde degeneration to label LM FB axons and biotinylated dextran amine to retrogradely label FF neurons in V1, found that LM FB projections formed strong monosynaptic inputs to looped cells in V1 (Johnson & Burkhalter, 1997). Even so, the presence of strong monosynaptic inputs to looped cells does not show, in and of itself, that CC pathways selectively engage with looped neurons, since neighboring cells with different projection

targets could receive similarly strong inputs. More recent efforts, though, have shown cases of CC connections specifically targeting looped neurons. A study using sCRACM to measure CC connections between barrel cortex (vS1) and vibrissal motor cortex (vM1) in the mouse reported that retrogradely labelled vS1-projecting cells in both supragranular and infragranular layers of vM1 received significantly stronger input from vS1 relative to nearby non-labelled neurons (Mao et al., 2011). Rabies tracing studies, which we cover in Chapter 3, have also found evidence of CC projections selectively interacting with neurons projecting back to the source of these inputs (Kim et al., 2020; Siu, Balsor, Merlin, Federer, & Angelucci, 2020; Zhang et al., 2016).

Conversely, there is evidence that CC connections do not selectively engage in monosynaptic looped interactions. vM1 projections to vS1 do not preferentially target looped, vM1-projecting cells in L2/3 or L5A when compared to neighboring non-labelled cells (Mao et al., 2011). In another study, S2 axons in L5B of M1 show similar connectivity to looped IT cells and neighboring PT cells, while in the reverse direction, M1 axons in L5B of S2 preferentially target PT neurons over looped IT neurons (Suter & Shepherd, 2015). Furthermore, projections from the rostral retrosplenial cortex (RSC) to posterior secondary motor cortex (M2) do not preferentially target looped IT neurons over non-looped IT neurons in L2/3 and L5B, and also do not distinguish between looped IT neurons and adjacent PT or CT neurons (Yamawaki et al., 2016). Given that other studies suggest CC projections weakly

innervate PT (Mao et al., 2011) and CT neurons (Kinnischtzke et al., 2016) relative to IT neurons, it appears that different CC projections vary in their connectivity patterns with IT, PT and CT cells. It is also clear that the strength of CC projections varies across layers. For example, projections from vS1 to vM1 innervate L2/3 and L5A cells more strongly than L5B and L6 cells (Mao et al., 2011). Input from M2 axons in RSC innervate looped L2/3 IT cells more strongly than looped L5 IT cells (Yamawaki et al., 2016), while M1 inputs to S1 innervate looped L6 IT cells more strongly than looped L5A IT cells (Kinnischtzke et al., 2016). These results suggest that CC connections innervate looped cells differently across layers, and that if a preference for looped over non-looped cells exists, it may not hold true across all layers.

We thus set out to determine the extent to which CC connections are selectively wired to innervate looped IT neurons over non-looped IT, PT and CT neurons across upper and lower layers in mouse visual cortex. Importantly, it remains unknown whether selectivity for looped cells exists for both ascending and descending projections linking two areas, as may be required for looped cortical computations. We therefore measured the specificity of CC connections in both FF and FB directions. It is also unknown whether a preference for looped wiring in CC connections differs across dendritic compartments. Given that basal and apical dendrites may be specialized for receiving FF and FB inputs, respectively (Schuman et al., 2021), we used subcellular Channelrhodopsin-2-assisted circuit mapping (sCRACM) (Petreanu, Mao, Sternson, &

Svoboda, 2009) to analyze the dendritic distribution of FF and FB monosynaptic inputs. Finally, if looped interactions perform a canonical computation in neocortex, we might expect to find selectivity for looped wiring across different CC projections. For this reason, we measured FF and FB inputs across two different CC pathways linking V1 with two higher-order visual cortical areas.

We found that CC connections in both ascending and descending directions are specifically wired to form interareal monosynaptic loops, providing connectional evidence that the mouse visual cortical hierarchy is selectively wired to implement long-range looped interactions. Both FF and FB axons provided stronger inputs to looped neurons projecting back to the source of these inputs. Interestingly, selective innervation of looped neurons was laminar-specific, involving only neurons residing in the deep layers of the cortex (layers 5 and 6), suggesting that hierarchical interactions might play different roles in superficial and deep cortical layers. Moreover, both FB and FF projections provided stronger inputs to looped pyramidal neurons in layer 5 when contacting their apical tufts but not their perisomatic dendrites. Thus, our results suggest a specialized role in looped hierarchical processes for the mysterious distal tufts of L5 neurons. Consequently, we hope that these findings open up new perspectives on the role of distal inputs and dendritic processes in cortical function.

Adesnik, H., Bruns, W., Taniguchi, H., Huang, Z. J., & Scanziani, M. (2012). A neural circuit for spatial summation in visual cortex. *Nature*, *490*(7419), 226–230. https://doi.org/10.1038/nature11526

Andermann, M. L., Kerlin, A. M., Roumis, D. K., Glickfeld, L. L., & Reid, R. C. (2011). Functional specialization of mouse higher visual cortical areas. *Neuron*, *72*(6), 1025–1039. https://doi.org/10.1016/j.neuron.2011.11.013

Bai, W. Z., Ishida, M., & Arimatsu, Y. (2004). Chemically defined feedback connections from infragranular layers of sensory association cortices in the rat. *Neuroscience*, *123*(1), 257–267. https://doi.org/10.1016/j.neuroscience.2003.08.056

Beltramo, R., D'Urso, G., Dal Maschio, M., Farisello, P., Bovetti, S., Clovis, Y., … Fellin, T. (2013). Layer-specific excitatory circuits differentially control recurrent network dynamics in the neocortex. *Nature Neuroscience*, *16*(2), 227–234. https://doi.org/10.1038/nn.3306

Berezovskii, V. K., Nassi, J. J., & Born, R. T. (2011). Segregation of feedforward and feedback projections in mouse visual cortex. *Journal of Comparative Neurology*, *519*(18), 3672–3683. https://doi.org/10.1002/cne.22675

Bortone, D. S., Olsen, S. R., & Scanziani, M. (2014). Translaminar inhibitory cells recruited by layer 6 corticothalamic neurons suppress visual cortex. *Neuron*, *82*(2), 474–485. https://doi.org/10.1016/j.neuron.2014.02.021

Bourassa, J., & Deschênes, M. (1995). Corticothalamic projections from

the primary visual cortex in rats: a single fiber study using biocytin as an anterograde tracer. *Neuroscience*, *66*(2), 253–263. https://doi.org/10.1016/0306-4522(95)00009-8

Brodmann, K. (1909). Vergleichende Lokalisationslehre der Grosshirnrinde in ihren Prinzipien dargestellt auf Grund des Zellenbaues : Brodmann, K : Free Download, Borrow, and Streaming : Internet Archive, *44*(0). Retrieved from https://archive.org/details/b28062449/page/n4

Brown, S. P., & Hestrin, S. (2009). Intracortical circuits of pyramidal neurons reflect their long-range axonal targets. *Nature*, *457*(7233), 1133–1136. https://doi.org/10.1038/nature07658

Chen, J. L., Carta, S., Soldado-Magraner, J., Schneider, B. L., & Helmchen, F. (2013). Behaviour-dependent recruitment of long-range projection neurons in somatosensory cortex. *Nature*, *499*(7458), 336–340. https://doi.org/10.1038/nature12236

Chklovskii, D. B., Schikorski, T., & Stevens, C. F. (2002). Wiring optimization in cortical circuits. *Neuron*, *34*(3), 341–347. https://doi.org/10.1016/S0896-6273(02)00679-7

Christophe, E., Doerflinger, N., Lavery, D. J., Molnár, Z., Charpak, S., & Audinat, E. (2005). Two populations of layer V pyramidal cells of the mouse neocortex: Development and sensitivity to anesthetics. *Journal of Neurophysiology*, *94*(5), 3357–3367. https://doi.org/10.1152/jn.00076.2005

Coogan, T. A., & Burkhalter, A. (1990). Conserved patterns of cortico-cortical connections define areal hierarchy in rat visual cortex.

Experimental Brain Research, *80*(1), 49–53. https://doi.org/10.1007/BF00228846

Coogan, T. A., & Burkhalter, A. (1993). Hierarchical organization of areas in rat visual cortex. *Journal of Neuroscience*, *13*(9), 3749–3772. https://doi.org/10.1523/jneurosci.13-09-03749.1993

Crick, F., & Asanuma, C. (1986). Parallel Distributed Processing: Explorations in the Microstructure of Cognition. In J. L. McClelland & D. E. Rumelhart (Eds.). MIT press. https://doi.org/https://doi.org/10.7551/mitpress/5236.003.0011

D'Souza, Meier, A. M., Bista, P., Wang, Q., & Burkhalter, A. (2016). Recruitment of inhibition and excitation across mouse visual cortex depends on the hierarchy of interconnecting areas. *ELife*, *5*(September2016), 1–19. https://doi.org/10.7554/eLife.19332

D'Souza, R. D., Wang, Q., Ji, W., Meier, A. M., Kennedy, H., Knoblauch, K., & Burkhalter, A. (2020). Canonical and noncanonical features of the mouse visual cortical hierarchy. *BioRxiv*. https://doi.org/10.1101/2020.03.30.016303

Dantzker, J. L., & Callaway, E. M. (2000). Laminar sources of synaptic input to cortical inhibitory interneurons and pyramidal neurons. *Nature Neuroscience*, *3*(7), 701–707. https://doi.org/10.1038/76656

De Kock, C. P. J., Bruno, R. M., Spors, H., & Sakmann, B. (2007). Layer- and cell-type-specific suprathreshold stimulus representation in rat primary somatosensory cortex. *Journal of Physiology*, *581*(1), 139–154. https://doi.org/10.1113/jphysiol.2006.124321

Dembrow, N., & Johnston, D. (2014). Subcircuit-specific neuromodulation in the prefrontal cortex. *Frontiers in Neural Circuits*, *8*(JUNE), 1–9. https://doi.org/10.3389/fncir.2014.00054

Deschênes, M., Veinante, P., & Zhang, Z. W. (1998). The organization of corticothalamic projections: Reciprocity versus parity. *Brain Research Reviews*, *28*(3), 286–308. https://doi.org/10.1016/S0165-0173(98)00017-4

Desimone, R., & Duncan, J. (1995). Neural mechanisms of selective visual attention. *Annual Review of Neuroscience*, *18*, 193–222. https://doi.org/10.1146/annurev.ne.18.030195.001205

Dong, H., Wang, Q., Valkova, K., Gonchar, Y., & Burkhalter, A. (2004). Experience-dependent development of feedforward and feedback circuits between lower and higher areas of mouse visual cortex. *Vision Research*, *44*(28 SPEC.ISS.), 3389–3400. https://doi.org/10.1016/j.visres.2004.09.007

Douglas, R. J., Koch, C., Mahowald, M., Martin, K. A. C., Suarez, H. H., Douglas, R. J., … Suarezt, H. H. (2016). Recurrent Excitation in Neocortical Circuits Published by : American Association for the Advancement of Science Stable URL : http://www.jstor.org/stable/2887714 Accessed : 22-04-2016 16 : 07 UTC Your use of the JSTOR archive indicates your acceptance of t, *269*(5226), 981–985.

Douglas, R. J., & Martin, K. A. C. (2004). Neuronal circuits of the neocortex. *Annual Review of Neuroscience*, *27*, 419–451. https://doi.org/10.1146/annurev.neuro.27.070203.144152

Dräger, U. C. (1975). Receptive fields of single cells and topography in mouse visual cortex. *Journal of Comparative Neurology*, *160*(3), 269–289. https://doi.org/10.1002/cne.901600302

Eccles, J. C. (1981). The modular operation of the cerebral neocortex considered as the material basis of mental events. *Neuroscience*, *6*(10), 1839–1855. https://doi.org/https://doi.org/10.1016/0306-4522(81)90027-0

Economo, M. N., Viswanathan, S., Tasic, B., Bas, E., Winnubst, J., Menon, V., … Svoboda, K. (2018). Distinct descending motor cortex pathways and their roles in movement. *Nature*, *563*(7729), 79–84. https://doi.org/10.1038/s41586-018-0642-9

Felleman, D. J., & Van Essen, D. C. (1991). Distributed hierarchical processing in the primate cerebral cortex. *Cerebral Cortex*, *1*(1), 1–47. https://doi.org/10.1093/cercor/1.1.1-a

Galloni, A. R., Ye, Z., & Rancz, E. (2021). Dendritic distribution of synaptic inputs to layer 5 pyramidal neurons Dendritic domain-specific sampling of long-range axons shapes feedforward and feedback connectivity of L5 neurons. *BioRxiv*, 2021.01.31.429033. Retrieved from https://doi.org/10.1101/2021.01.31.429033

Gămănuţ, R., Kennedy, H., Toroczkai, Z., Ercsey-Ravasz, M., Van Essen, D. C., Knoblauch, K., & Burkhalter, A. (2018). The Mouse Cortical Connectome, Characterized by an Ultra-Dense Cortical Graph, Maintains Specificity by Distinct Connectivity Profiles. *Neuron*, *97*(3), 698-715.e10. https://doi.org/10.1016/j.neuron.2017.12.037

Gao, P., Sultan, K. T., Zhang, X. J., & Shi, S. H. (2013). Lineage-dependent circuit assembly in the neocortex. *Development (Cambridge)*, *140*(13), 2645–2655. https://doi.org/10.1242/dev.087668

Garcia-Munoz, M., & Arbuthnott, G. W. (2015). Basal ganglia—thalamus and the "crowning enigma." *Frontiers in Neural Circuits*, *9*(November), 1–10. https://doi.org/10.3389/fncir.2015.00071

Garrett, M. E., Nauhaus, I., Marshel, J. H., & Callaway, E. M. (2014). Topography and areal organization of mouse visual cortex. *Journal of Neuroscience*, *34*(37), 12587–12600. https://doi.org/10.1523/JNEUROSCI.1124-14.2014

Gerfen, C. R., Economo, M. N., & Chandrashekar, J. (2018). Long distance projections of cortical pyramidal neurons. *Journal of Neuroscience Research*, *96*(9), 1467–1475. https://doi.org/10.1002/jnr.23978

Gilbert, C. D. (1983). Microcircuitry of the visual cortex. *Annual Review of Neuroscience*, *Vol. 6*, 217–247. https://doi.org/10.1146/annurev.ne.06.030183.001245

Gilbert, C. D., & Li, W. (2013). Top-down influences on visual processing. *Nature Reviews Neuroscience*, *14*(5), 350–363. https://doi.org/10.1038/nrn3476

Gilbert, C. D., & Wiesel, T. N. (1983). Functional Organization of the Visual Cortex. *Progress in Brain Research*, *58*(C), 209–218. https://doi.org/10.1016/S0079-6123(08)60022-9

Gilbert, & Wiesel, T. N. (1989). Columnar specificity of intrinsic horizontal and corticocortical connections in cat visual cortex. *Journal of Neuroscience*, *9*(7), 2432–2422. https://doi.org/10.1523/jneurosci.09-07-02432.1989

Glickfeld, L. L., Andermann, M. L., Bonin, V., & Reid, R. C. (2013). Cortico-cortical projections in mouse visual cortex are functionally target specific. *Nature Neuroscience*, *16*(2), 219–226. https://doi.org/10.1038/nn.3300

Glickfeld, L. L., & Olsen, S. R. (2017). Higher-Order Areas of the Mouse Visual Cortex. *Annual Review of Vision Science*, *3*, 251–273. https://doi.org/10.1146/annurev-vision-102016-061331

Greig, L. C., Woodworth, M. B., Galazo, M. J., Padmanabhan, H., & Macklis, J. D. (2013). Molecular logic of neocortical projection neuron specification, development and diversity. *Nature Reviews Neuroscience*, *14*(11), 755–769. https://doi.org/10.1038/nrn3586

Han, Y., Kebschull, J. M., Campbell, R. A. A., Cowan, D., Imhof, F., Zador, A. M., & Mrsic-Flogel, T. D. (2018). The logic of single-cell projections from visual cortex. *Nature*, *556*(7699), 51–56. https://doi.org/10.1038/nature26159

Harris, J. A., Mihalas, S., Hirokawa, K. E., Whitesell, J. D., Choi, H., Bernard, A., … Zeng, H. (2019). Hierarchical organization of cortical and thalamic connectivity. *Nature*, *575*(7781), 195–202. https://doi.org/10.1038/s41586-019-1716-z

Harris, K. D., & Mrsic-Flogel, T. D. (2013). Cortical connectivity and sensory coding. *Nature*, *503*(7474), 51–58.

https://doi.org/10.1038/nature12654

Harris, K. D., & Shepherd, G. M. G. (2015). The neocortical circuit: themes and variations. *Nature Neuroscience*, *18*(2), 170–181. https://doi.org/10.1038/nn.3917

Harvey, C. D., Collman, F., Dombeck, D. A., & Tank, D. W. (2009). Intracellular dynamics of hippocampal place cells during virtual navigation. *Nature*, *461*(7266), 941–946. https://doi.org/10.1038/nature08499

Hegdé, J., & Felleman, D. J. (2007). Reappraising the functional implications of the primate visual anatomical hierarchy. *Neuroscientist*, *13*(5), 416–421. https://doi.org/10.1177/1073858407305201

Hooks, B. M., Hires, S. A., Zhang, Y. X., Huber, D., Petreanu, L., Svoboda, K., & Shepherd, G. M. G. (2011). Laminar analysis of excitatory local circuits in vibrissal motor and sensory cortical areas. *PLoS Biology*, *9*(1). https://doi.org/10.1371/journal.pbio.1000572

Hoy, J. L., Yavorska, I., Wehr, M., & Niell, C. M. (2016). Vision Drives Accurate Approach Behavior during Prey Capture in Laboratory Mice. *Current Biology*, *26*(22), 3046–3052. https://doi.org/10.1016/j.cub.2016.09.009

Hubel, D. H. (1982). Cortical Neurobiology. *Annual Review of Neuroscience*, *5*, 363–370.

Hubel, D. H., & Wiesel, T. (1962). AND FUNCTIONAL ARCHITECTURE IN THE CAT ' S VISUAL CORTEX From the Neurophysiolojy

Laboratory , Department of Pharmacology central nervous system is the great diversity of its cell types and inter- receptive fields of a more complex type (Part I) and to. *Most*, 106–154.

Hubel, D. H., & Wiesel, T. N. (1965). Receptive archi- tecture in two nonstriate visual areas (18 and 19) of the cati. *Journal of Neurophysiology*, *28*(2), 229–289.

Huh, C. Y. L., Peach, J. P., Bennett, C., Vega, R. M., & Hestrin, S. (2018). Feature-Specific Organization of Feedback Pathways in Mouse Visual Cortex. *Current Biology*, *28*(1), 114-120.e5. https://doi.org/10.1016/j.cub.2017.11.056

Johnson, R. R., & Burkhalter, A. (1997). A polysynaptic feedback circuit in rat visual cortex. *Journal of Neuroscience*, *17*(18), 7129–7140. https://doi.org/10.1523/jneurosci.17-18-07129.1997

Katz, L. C. (1987). Local circuitry of identified projection neurons in cat visual cortex brain slices. *Journal of Neuroscience*, *7*(4), 1223–1249. https://doi.org/10.1523/jneurosci.07-04-01223.1987

Keller, G. B., Bonhoeffer, T., & Hübener, M. (2012). Sensorimotor Mismatch Signals in Primary Visual Cortex of the Behaving Mouse. *Neuron*, *74*(5), 809–815. https://doi.org/10.1016/j.neuron.2012.03.040

Keller, G. B., & Mrsic-Flogel, T. D. (2018). Predictive Processing: A Canonical Cortical Computation. *Neuron*, *100*(2), 424–435. https://doi.org/10.1016/j.neuron.2018.10.003

Kim, E. J., Juavinett, A. L., Kyubwa, E. M., Jacobs, M. W., & Callaway,

E. M. (2015). Three Types of Cortical Layer 5 Neurons That Differ in Brain-wide Connectivity and Function. *Neuron*, *88*(6), 1253–1267. https://doi.org/10.1016/j.neuron.2015.11.002

Kim, E. J., Zhang, Z., Huang, L., Ito-Cole, T., Jacobs, M. W., Juavinett, A. L., … Callaway, E. M. (2020). Extraction of Distinct Neuronal Cell Types from within a Genetically Continuous Population. *Neuron*, *107*(2), 274-282.e6. https://doi.org/10.1016/j.neuron.2020.04.018

Kinnischtzke, A. K., Fanselow, E. E., & Simons, D. J. (2016). Target-specific M1 inputs to infragranular S1 pyramidal neurons. *Journal of Neurophysiology*, *116*(3), 1261–1274. https://doi.org/10.1152/jn.01032.2015

Kiritani, T., Wickersham, I. R., Seung, H. S., & Shepherd, G. M. G. (2012). Hierarchical connectivity and connection-specific dynamics in the corticospinal-corticostriatal microcircuit in mouse motor cortex. *Journal of Neuroscience*, *32*(14), 4992–5001. https://doi.org/10.1523/JNEUROSCI.4759-11.2012

Kita, T., & Kita, H. (2012). The subthalamic nucleus is one of multiple innervation sites for long-range corticofugal axons: A single-axon tracing study in the rat. *Journal of Neuroscience*, *32*(17), 5990–5999. https://doi.org/10.1523/JNEUROSCI.5717-11.2012

Ko, H., Cossell, L., Baragli, C., Antolik, J., Clopath, C., Hofer, S. B., & Mrsic-Flogel, T. D. (2013). The emergence of functional microcircuits in visual cortex. *Nature*, *496*(7443), 96–100. https://doi.org/10.1038/nature12015

Ko, H., Hofer, S. B., Pichler, B., Buchanan, K. a, Sjöström, P. J., &

Mrsic-Flogel, T. D. (2011). Functional specificity of local synaptic connections in neocortical networks. *Nature*, *473*(7345), 87–91. https://doi.org/10.1038/nature09880

Kravitz, D. J., Saleem, K. S., Baker, C. I., & Mishkin, M. (2011). A new neural framework for visuospatial processing. *Nature Reviews Neuroscience*, *12*(4), 217–230. https://doi.org/10.1038/nrn3008

Kravitz, D. J., Saleem, K. S., Baker, C. I., Ungerleider, L. G., & Mishkin, M. (2013). The ventral visual pathway: An expanded neural framework for the processing of object quality. *Trends in Cognitive Sciences*, *17*(1), 26–49. https://doi.org/10.1016/j.tics.2012.10.011

Krubitzer, L. A., & Prescott, T. J. (2018). The Combinatorial Creature: Cortical Phenotypes within and across Lifetimes. *Trends in Neurosciences*, *41*(10), 744–762. https://doi.org/10.1016/j.tins.2018.08.002

Larkum, M. (2013). A cellular mechanism for cortical associations: An organizing principle for the cerebral cortex. *Trends in Neurosciences*, *36*(3), 141–151. https://doi.org/10.1016/j.tins.2012.11.006

Larkum, M E, Zhu, J. J., & Sakmann, B. (1999). A new cellular mechanism for coupling inputs arriving at different cortical layers. *Nature*, *398*(6725), 338–341. https://doi.org/10.1038/18686

Larkum, Matthew E., Senn, W., & Lüscher, H. R. (2004). Top-down dendritic input increases the gain of layer 5 pyramidal neurons. *Cerebral Cortex*, *14*(10), 1059–1070. https://doi.org/10.1093/cercor/bhh065

Le Bé, J. V., Silberberg, G., Wang, Y., & Markram, H. (2007). Morphological, electrophysiological, and synaptic properties of corticocallosal pyramidal cells in the neonatal rat neocortex. *Cerebral Cortex*, *17*(9), 2204–2213. https://doi.org/10.1093/cercor/bhl127

Li, J., Hass, C. A., Matthews, I., Kristl, A. C., & Glickfeld, L. L. (2020). Distinct recruitment of feed-forward and recurrent pathways across higher-order areas of mouse visual cortex. *BioRxiv*.

Li, L. Y., Li, Y. T., Zhou, M., Tao, H. W., & Zhang, L. I. (2013). Intracortical multiplication of thalamocortical signals in mouse auditory cortex. *Nature Neuroscience*, *16*(9), 1179–1181. https://doi.org/10.1038/nn.3493

Li, W., Piëch, V., & Gilbert, C. D. (2008). Learning to Link Visual Contours. *Neuron*, *57*(3), 442–451. https://doi.org/10.1016/j.neuron.2007.12.011

Li, Y., Ibrahim, L. a, Liu, B., Zhang, L. I., & Tao, H. W. (2013). Linear transformation of thalamocortical input by intracortical excitation. *Nature Neuroscience*, *16*(9), 1324–1330. https://doi.org/10.1038/nn.3494

Lien, A. D., & Scanziani, M. (2013). Tuned thalamic excitation is amplified by visual cortical circuits. *Nature Neuroscience*, *16*(9), 1315–1323. https://doi.org/10.1038/nn.3488

Lindenmaier, L. B., Parmentier, N., Guo, C., Tissir, F., & Wright, K. M. (2018). Dystroglycan is a scaffold for extracellular axon guidance decisions. *BioRxiv*, 1–26. https://doi.org/10.1101/410944

Liu, D., Deng, J., Zhang, Z., Zhang, Z. Y., Sun, Y. G., Yang, T., & Yao, H. (2020). Orbitofrontal control of visual cortex gain promotes visual associative learning. *Nature Communications*, *11*(1), 1–14. https://doi.org/10.1038/s41467-020-16609-7

Lund, J. S., Griffiths, S., Rumberger, A., & Levitt, J. B. (2001). Inhibitory synapse cover on the somata of excitatory neurons in macaque monkey visual cortex. *Cerebral Cortex*, *11*(9), 783–795. https://doi.org/10.1093/cercor/11.9.783

Luo, H., Hasegawa, K., Liu, M., & Song, W. J. (2017). Comparison of the upper marginal neurons of cortical layer 2 with layer 2/3 pyramidal neurons in mouse temporal cortex. *Frontiers in Neuroanatomy*, *11*(December), 1–14. https://doi.org/10.3389/fnana.2017.00115

Mangini, N. J., & Pearlman, A. L. (1980). Laminar distribution of receptive field properties in the primary visual cortex of the mouse. *Journal of Comparative Neurology*, *193*(1), 203–222. https://doi.org/10.1002/cne.901930114

Mao, T., Kusefoglu, D., Hooks, B. M., Huber, D., Petreanu, L., & Svoboda, K. (2011). Long-Range Neuronal Circuits Underlying the Interaction between Sensory and Motor Cortex. *Neuron*, *72*(1), 111–123. https://doi.org/10.1016/j.neuron.2011.07.029

Markov, N. T., Ercsey-Ravasz, M., Van Essen, D. C., Knoblauch, K., Toroczkai, Z., & Kennedy, H. (2013). Cortical high-density counterstream architectures. *Science*, *342*(6158). https://doi.org/10.1126/science.1238406

Markov, N. T., Vezoli, J., Chameau, P., Falchier, A., Quilodran, R.,

Huissoud, C., … Kennedy, H. (2014). Anatomy of hierarchy: Feedforward and feedback pathways in macaque visual cortex. *Journal of Comparative Neurology*, *522*(1), 225–259. https://doi.org/10.1002/cne.23458

Marques, T., Nguyen, J., Fioreze, G., & Petreanu, L. (2018). The functional organization of cortical feedback inputs to primary visual cortex. *Nature Neuroscience*, *21*(5), 757–764. https://doi.org/10.1038/s41593-018-0135-z

Marr, D. (1982). Vision: A computational investigation into the human representation.

Marshel, J. H., Garrett, M. E., Nauhaus, I., & Callaway, E. M. (2011). Functional specialization of seven mouse visual cortical areas. *Neuron*, *72*(6), 1040–1054. https://doi.org/10.1016/j.neuron.2011.12.004

Maruoka, H., Kubota, K., Kurokawa, R., Tsuruno, S., & Hosoya, T. (2011). Periodic organization of a major subtype of pyramidal neurons in neocortical layer V. *Journal of Neuroscience*, *31*(50), 18522–18542. https://doi.org/10.1523/JNEUROSCI.3117-11.2011

Meng, X., Winkowski, D. E., Kao, J. P. Y., & Kanold, P. O. (2017). Sublaminar subdivision of mouse auditory cortex layer 2/3 based on functional translaminar connections. *Journal of Neuroscience*, *37*(42), 10200–10214. https://doi.org/10.1523/JNEUROSCI.1361-17.2017

Mercer, A., West, D. C., Morris, O. T., Kirchhecker, S., Kerkhoff, J. E., & Thomson, A. M. (2005). Excitatory connections made by

presynaptic cortico-cortical pyramidal cells in layer 6 of the neocortex. *Cerebral Cortex*, *15*(10), 1485–1496. https://doi.org/10.1093/cercor/bhi027

Miller, K. D. (2016). Canonical computations of cerebral cortex. *Current Opinion in Neurobiology*, *37*, 75–84. https://doi.org/10.1016/j.conb.2016.01.008

Molyneaux, B. J., Arlotta, P., Fame, R. M., MacDonald, J. L., MacQuarrie, K. L., & Macklis, J. D. (2009). Novel subtype-specific genes identify distinct subpopulations of callosal projection neurons. *Journal of Neuroscience*, *29*(39), 12343–12354. https://doi.org/10.1523/JNEUROSCI.6108-08.2009

Moore, T., & Zirnsak, M. (2017). Neural Mechanisms of Selective Visual Attention. *Annual Review of Psychology*, *68*, 47–72. https://doi.org/10.1146/annurev-psych-122414-033400

Morgenstern, N. A., Bourg, J., & Petreanu, L. (2016). Multilaminar networks of cortical neurons integrate common inputs from sensory thalamus. *Nature Neuroscience*, *19*(8), 1034–1040. https://doi.org/10.1038/nn.4339

Morishima, M., & Kawaguchi, Y. (2006). Recurrent connection patterns of corticostriatal pyramidal cells in frontal cortex. *Journal of Neuroscience*, *26*(16), 4394–4405. https://doi.org/10.1523/JNEUROSCI.0252-06.2006

Mountcastle, V. (1978). An organizing principle for cerebral function: the unit module and the distributed system. *The Mindful Brain*.

Movshon, J. A., & Newsome, W. T. (1996). Visual response properties of striate cortical neurons projecting to area MT in macaque monkeys. *Journal of Neuroscience*, *16*(23), 7733–7741. https://doi.org/10.1523/jneurosci.16-23-07733.1996

Mumford, D. (1992). On the computational architecture of the neocortex - II The role of cortico-cortical loops. *Biological Cybernetics*, *66*(3), 241–251. https://doi.org/10.1007/BF00198477

Nassi, J. J., & Callaway, E. M. (2009). Parallel processing strategies of the primate visual system. *Nat.Rev.Neurosci.*, *10*(1471-0048 (Electronic)), 360–372. https://doi.org/10.1038/nrn2619

Nassi, J. J., Lomber, S. G., & Born, R. T. (2013). Corticocortical feedback contributes to surround suppression in V1 of the alert primate. *The Journal of Neuroscience : The Official Journal of the Society for Neuroscience*, *33*(19), 8504–8517. https://doi.org/10.1523/JNEUROSCI.5124-12.2013

Nelson, A., Schneider, D. M., Takatoh, J., Sakurai, K., Wang, F., & Mooney, R. (2013). A circuit for motor cortical modulation of auditory cortical activity. *Journal of Neuroscience*, *33*(36), 14342–14353. https://doi.org/10.1523/JNEUROSCI.2275-13.2013

Niell, C. M., & Stryker, M. P. (2008). Highly selective receptive fields in mouse visual cortex. *J Neurosci*, *28*(30), 7520–7536. https://doi.org/10.1523/JNEUROSCI.0623-08.2008

Niell, C. M., & Stryker, M. P. (2010). Modulation of Visual Responses by Behavioral State in Mouse Visual Cortex. *Neuron*, *65*(4), 472–479. https://doi.org/10.1016/j.neuron.2010.01.033

O'Connor, D. H., Peron, S. P., Huber, D., & Svoboda, K. (2010). Neural activity in barrel cortex underlying vibrissa-based object localization in mice. *Neuron*, *67*(6), 1048–1061. https://doi.org/10.1016/j.neuron.2010.08.026

Oh, S. W., Harris, J. A., Ng, L., Winslow, B., Cain, N., Mihalas, S., … Zeng, H. (2014). A mesoscale connectome of the mouse brain. *Nature*, *508*(7495), 207–214. https://doi.org/10.1038/nature13186

Olsen, S. R., Bortone, D. S., Adesnik, H., & Scanziani, M. (2012). Gain control by layer six in cortical circuits of vision. *Nature*, *483*(7387), 47–52. https://doi.org/10.1038/nature10835

Otsuka, T., & Kawaguchi, Y. (2011). Cell diversity and connection specificity between callosal projection neurons in the frontal cortex. *Journal of Neuroscience*, *31*(10), 3862–3870. https://doi.org/10.1523/JNEUROSCI.5795-10.2011

Petreanu, L., Gutnisky, D. a, Huber, D., Xu, N., O'Connor, D. H., Tian, L., … Svoboda, K. (2012). Activity in motor-sensory projections reveals distributed coding in somatosensation. *Nature*, *489*(7415), 299–303. https://doi.org/10.1038/nature11321

Petreanu, L., Huber, D., Sobczyk, A., & Svoboda, K. (2007). Channelrhodopsin-2-assisted circuit mapping of long-range callosal projections. *Nature Neuroscience*, *10*(5), 663–668. https://doi.org/10.1038/nn1891

Petreanu, L., Mao, T., Sternson, S. M., & Svoboda, K. (2009). The subcellular organization of neocortical excitatory connections. *Nature*, *457*(7233), 1142–1145. https://doi.org/10.1038/nature07709

Polack, P. O., & Contreras, D. (2012). Long-range parallel processing and local recurrent activity in the visual cortex of the mouse. *Journal of Neuroscience*, *32*(32), 11120–11131. https://doi.org/10.1523/JNEUROSCI.6304-11.2012

Preuss, T. (2007). Evolutionary Specializations of Primate Brain Systems. https://doi.org/10.1007/978-0-387-33507-0_18

Price, D. J., & Zumbroich, T. J. (1989). Postnatal development of corticortical efferents from area 17 in the cat's visual cortex. *Journal of Neuroscience*, *9*(2), 600–613. https://doi.org/10.1523/jneurosci.09-02-00600.1989

Rees, C. L., Moradi, K., & Ascoli, G. A. (2017). Weighing the Evidence in Peters' Rule: Does Neuronal Morphology Predict Connectivity? *Trends in Neurosciences*, *40*(2), 63–71. https://doi.org/10.1016/j.tins.2016.11.007

Reiner, A., Hart, N. M., Lei, W., & Deng, Y. (2010). Corticostriatal projection neurons - Dichotomous types and dichotomous functions. *Frontiers in Neuroanatomy*, *4*(OCT), 1–15. https://doi.org/10.3389/fnana.2010.00142

Richards, B. A., & Lillicrap, T. P. (2019). Dendritic solutions to the credit assignment problem. *Current Opinion in Neurobiology*, *54*, 28–36. https://doi.org/10.1016/j.conb.2018.08.003

Rockland, K. S., & Pandya, D. N. (1979). Laminar origins and terminations of cortical connections of the occipital lobe in the rhesus monkey. *Brain Research*, *179*(1), 3–20. https://doi.org/10.1016/0006-8993(79)90485-2

Roelfsema, P. R., & de Lange, F. P. (2016). Early Visual Cortex as a Multiscale Cognitive Blackboard. *Annual Review of Vision Science*, *2*, 131–151. https://doi.org/10.1146/annurev-vision-111815-114443

Rosa, M. G. P., & Krubitzer, L. A. (1999). The evolution of visual cortex: Where is V2? *Trends in Neurosciences*, *22*(6), 242–248. https://doi.org/10.1016/S0166-2236(99)01398-3

Sakata, S., & Harris, K. D. (2009). Laminar Structure of Spontaneous and Sensory-Evoked Population Activity in Auditory Cortex. *Neuron*, *64*(3), 404–418. https://doi.org/10.1016/j.neuron.2009.09.020

Sato, T. R., & Svoboda, K. (2010). The functional properties of barrel cortex neurons projecting to the primary motor cortex. *Journal of Neuroscience*, *30*(12), 4256–4260. https://doi.org/10.1523/JNEUROSCI.3774-09.2010

Schuman, B., Dellal, S., Prönneke, A., Machold, R., & Rudy, B. (2021). Neocortical Layer 1: An Elegant Solution to Top-Down and Bottom-Up Integration. *Annual Review of Neuroscience*, *44*(1), 221–252. https://doi.org/10.1146/annurev-neuro-100520-012117

Sheets, P. L., Suter, B. A., Kiritani, T., Savio Chan, C. S., James Surmeier, D., & Shepherd, G. M. G. (2011). Corticospinal-specific HCN expression in mouse motor cortex: I h)-dependent synaptic integration as a candidate microcircuit mechanism involved in motor control. *Journal of Neurophysiology*, *106*(5), 2216–2231. https://doi.org/10.1152/jn.00232.2011

Shepherd, G. M. G. (2013). Corticostriatal connectivity and its role in disease. *Nature Reviews Neuroscience*, *14*(4), 278–291.

https://doi.org/10.1038/nrn3469

Shepherd, G. M. G., Stepanyants, A., Bureau, I., Chklovskii, D., & Svoboda, K. (2005). Geometric and functional organization of cortical circuits. *Nature Neuroscience*, *8*(6), 782–790. https://doi.org/10.1038/nn1447

Sherman, S. M. (2012). Thalamocortical interactions. *Current Opinion in Neurobiology*, *22*(4), 575–579. https://doi.org/10.1016/j.conb.2012.03.005

Shuler, M. G., & Bear, M. F. (2006). Reward Timing in the Primary Visual Cortex. *Science*, *311*(2006), 1606–1610. https://doi.org/10.1126/science.1123513

Siegle, J. H., Jia, X., Durand, S., Gale, S., Bennett, C., Graddis, N., … Koch, C. (2021). Survey of spiking in the mouse visual system reveals functional hierarchy. *Nature*, *592*(7852), 86–92. https://doi.org/10.1038/s41586-020-03171-x

Siu, C., Balsor, J., Merlin, S., Federer, F., & Angelucci, A. (2020). A direct interareal feedback-to-feedforward circuit in primate visual cortex. https://doi.org/10.1101/2020.07.07.192450

Smith, I. T., Townsend, L. B., Huh, R., Zhu, H., & Smith, S. L. (2017). Stream-dependent development of higher visual cortical areas. *Nature Neuroscience*, *20*(2), 200–208. https://doi.org/10.1038/nn.4469

Sohya, K., Kameyama, K., Yanagawa, Y., Obata, K., & Tsumoto, T. (2007). GABAergic neurons are less selective to stimulus

orientation than excitatory neurons in layer II/III of visual cortex, as revealed by in vivo functional Ca2+ imaging in transgenic mice. *Journal of Neuroscience*, *27*(8), 2145–2149. https://doi.org/10.1523/JNEUROSCI.4641-06.2007

Speed, A., Del Rosario, J., Mikail, N., & Haider, B. (2020). Spatial attention enhances network, cellular and subthreshold responses in mouse visual cortex. *Nature Communications*, *11*(1). https://doi.org/10.1038/s41467-020-14355-4

Stepanyants, A., Hirsch, J. A., Martinez, L. M., Kisvárday, Z. F., Ferecskó, A. S., & Chklovskii, D. B. (2008). Local potential connectivity in cat primary visual cortex. *Cerebral Cortex*, *18*(1), 13–28. https://doi.org/10.1093/cercor/bhm027

Stettler, D. D., Das, A., Bennett, J., & Gilbert, C. D. (2002). Lateral connectivity and contextual interactions in macaque primary visual cortex. *Neuron*, *36*(4), 739–750. https://doi.org/10.1016/S0896-6273(02)01029-2

Suter, B. A., Migliore, M., & Shepherd, G. M. G. (2013). Intrinsic electrophysiology of mouse corticospinal neurons: A class-specific triad of spike-related properties. *Cerebral Cortex*, *23*(8), 1965–1977. https://doi.org/10.1093/cercor/bhs184

Suter, B. A., & Shepherd, G. M. G. (2015). Reciprocal interareal connections to corticospinal neurons in mouse MI and S2. *Journal of Neuroscience*, *35*(7), 2959–2974. https://doi.org/10.1523/JNEUROSCI.4287-14.2015

Swindale, N. V. (1990). Is the cerebral cortex modular? *Trends in*

Neurosciences, *13*(12), 487–492. https://doi.org/10.1016/0166-2236(90)90082-L

Szentágothai, J. (1978). The Ferrier Lecture, 1977. The neuron network of the cerebral cortex: a functional interpretation. *Proceedings of the Royal Society of London. Series B, Biological Sciences*, *201*(1144), 219–248. https://doi.org/10.1098/rspb.1978.0043

Thomson, A. M. (2010). Neocortical layer 6, a review. *Frontiers in Neuroanatomy*, *4*(MARCH), 1–14. https://doi.org/10.3389/fnana.2010.00013

Thomson, A. M., & Lamy, C. (2007). Functional Maps of Neocortical Local Circuitry. *Frontiers in Neuroscience*, *1*(1), 19–42. https://doi.org/10.3389/neuro.01.1.1.002.2007

Towe, A. L. (1975). Notes on the hypothesis of columnar organization in somatosensory cerebral cortex. *Brain, Behavior and Evolution*, *11*(1), 16–47. https://doi.org/10.1159/000123621

Tremblay, R., Lee, S., & Rudy, B. (2016). GABAergic Interneurons in the Neocortex: From Cellular Properties to Circuits. *Neuron*, *91*(2), 260–292. https://doi.org/10.1016/j.neuron.2016.06.033

Tseng, G. -F, & Prince, D. A. (1993). Heterogeneity of rat corticospinal neurons. *Journal of Comparative Neurology*, *335*(1), 92–108. https://doi.org/10.1002/cne.903350107

Ueta, Y., Hirai, Y., Otsuka, T., & Kawaguchi, Y. (2013). Direction- and distance-dependent interareal connectivity of pyramidal cell subpopulations in the rat frontal cortex. *Frontiers in Neural Circuits*,

7(OCT), 1–16. https://doi.org/10.3389/fncir.2013.00164

Van Den Bergh, G., Zhang, B., Arckens, L., & Chino, Y. M. (2010). Receptive-field properties of V1 and V2 neurons in mice and macaque monkeys. *Journal of Comparative Neurology*, *518*(11), 2051–2070. https://doi.org/10.1002/cne.22321

Vélez-Fort, M., Rousseau, C. V., Niedworok, C. J., Wickersham, I. R., Rancz, E. A., Brown, A. P. Y., … Margrie, T. W. (2014). The stimulus selectivity and connectivity of layer six principal cells reveals cortical microcircuits underlying visual processing. *Neuron*, *83*(6), 1431–1443. https://doi.org/10.1016/j.neuron.2014.08.001

Wang, Q., & Burkhalter, A. (2007). Area map of mouse visual cortex. *Journal of Comparative Neurology*, *502*.

Wang, Q., Gao, E., & Burkhalter, A. (2011). Gateways of ventral and dorsal streams in mouse visual cortex. *Journal of Neuroscience*, *31*(5), 1905–1918. https://doi.org/10.1523/JNEUROSCI.3488-10.2011

Wang, Q., Sporns, O., & Burkhalter, A. (2012). Network analysis of corticocortical connections reveals ventral and dorsal processing streams in mouse visual cortex. *Journal of Neuroscience*, *32*(13), 4386–4399. https://doi.org/10.1523/JNEUROSCI.6063-11.2012

Watakabe, A., Hirokawa, J., Ichinohe, N., Ohsawa, S., Kaneko, T., Rockland, K. S., & Yamamori, T. (2012). Area-specific substratification of deep layer neurons in the rat cortex. *Journal of Comparative Neurology*, *520*(16), 3553–3573. https://doi.org/10.1002/cne.23160

White, E. L. (2002). Specificity of cortical synaptic connectivity: Emphasis on perspectives gained from quantitative electron microscopy. *Journal of Neurocytology*, *31*(3-5 SPEC. ISS.), 195–202. https://doi.org/10.1023/A:1024109606722

Yamashita, T., Pala, A., Pedrido, L., Kremer, Y., Welker, E., & Petersen, C. C. H. (2013). Membrane potential dynamics of neocortical projection neurons driving target-specific signals. *Neuron*, *80*(6), 1477–1490. https://doi.org/10.1016/j.neuron.2013.10.059

Yamashita, T., Vavladeli, A., Pala, A., Galan, K., Crochet, S., Petersen, S. S. A., & Petersen, C. C. H. (2018). Diverse long-range axonal projections of excitatory layer 2/3 neurons in mouse barrel cortex. *Frontiers in Neuroanatomy*, *12*(May). https://doi.org/10.3389/fnana.2018.00033

Yamawaki, N., Radulovic, J., & Shepherd, G. M. G. (2016). A corticocortical circuit directly links retrosplenial cortex to M2 in the mouse. *Journal of Neuroscience*, *36*(36), 9365–9374. https://doi.org/10.1523/JNEUROSCI.1099-16.2016

Yang, W., Carrasquillo, Y., Hooks, B. M., Nerbonne, J. M., & Burkhalter, A. (2013). Distinct balance of excitation and inhibition in an interareal feedforward and feedback circuit of mouse visual cortex. *The Journal of Neuroscience : The Official Journal of the Society for Neuroscience*, *33*(44), 17373–17384. https://doi.org/10.1523/JNEUROSCI.2515-13.2013

Yoshimura, Y., Dantzker, J. L. M., & Callaway, E. M. (2005). Excitatory cortical neurons form fine-scale functional networks. *Nature*,

433(7028), 868–873. https://doi.org/10.1038/nature03252

Young, H., Belbut, B., Baeta, M., & Petreanu, L. (2021). Laminar-specific cortico-cortical loops in mouse visual cortex. *ELife*, *10*, 1–25. https://doi.org/10.7554/eLife.59551

Zhang, S., Xu, M., Chang, W. C., Ma, C., Hoang Do, J. P., Jeong, D., … Dan, Y. (2016). Organization of long-range inputs and outputs of frontal cortex for top-down control. *Nature Neuroscience*, *19*(12), 1733–1742. https://doi.org/10.1038/nn.4417

Zhang, S., Xu, M., Kamigaki, T., Do, J. P. H., Chang, W. C., Jenvay, S., … Dan, Y. (2014). Long-range and local circuits for top-down modulation of visual cortex processing. *Science*, *345*(6197), 660–665. https://doi.org/10.1126/science.1254126

Zingg, B., Hintiryan, H., Gou, L., Song, M. Y., Bay, M., Bienkowski, M. S., … Dong, H. W. (2014). Neural networks of the mouse neocortex. *Cell*, *156*(5), 1096–1111. https://doi.org/10.1016/j.cell.2014.02.023

Chapter 2

"The connectivity [of the neocortex] is extensive. For instance, there are 305 connections described among 32 areas processing visual information in nonhuman primates in the original Felleman & Van Essen (1991) study. Understanding how different areas of the cortex interact and how the cortex communicates with the rest of the brain is key to deciphering how the cortex performs its functions."

Schuman, Dellal, Prönneke, Machold, & Rudy (2021)

Laminar-specific cortico-cortical loops in mouse visual cortex

Hedi Young, Beatriz Belbut, Margarida Baeta, Leopoldo Petreanu*

Champalimaud Research, Champalimaud Center for the Unknown, Lisbon, Portugal

Abstract Many theories propose recurrent interactions across the cortical hierarchy, but it is unclear if cortical circuits are selectively wired to implement looped computations. Using subcellular channelrhodopsin-2-assisted circuit mapping in mouse visual cortex, we compared feedforward (FF) or feedback (FB) cortico-cortical (CC) synaptic input to cells projecting back to the input source (looped neurons) with cells projecting to a different cortical or subcortical area. FF and FB afferents showed similar cell-type selectivity, making stronger connections with looped neurons than with other projection types in layer (L)5 and L6, but not in L2/3, resulting in selective modulation of activity in looped neurons. In most cases, stronger connections in looped L5 neurons were located on their apical tufts, but not on their perisomatic dendrites. Our results reveal that CC connections are selectively wired to form monosynaptic excitatory loops and support a differential role of supragranular and infragranular neurons in hierarchical recurrent computations.

Introduction

The complex network of cortical areas can be hierarchically ordered based on the anatomy of interareal cortico-cortical (CC) projections. Lower areas send bottom-up 'feedforward' (FF) inputs to higher areas, which reciprocate with anatomically distinct top-down 'feedback' (FB) inputs, while areas at the same hierarchical level interact through 'lateral' or 'mixed' inputs (***Felleman and Van Essen, 1991***; ***Markov et al., 2013***). The fact that a similar hierarchical architecture is observed across areas and across species (***D'Souza et al., 2020***; ***Felleman and Van Essen, 1991***; ***Harris et al., 2019***) suggests that FF and FB interactions reside at the core of cortical function. As with local cortical circuits, posited to implement a conserved canonical computation in different cortical areas (***Douglas and Martin, 2004***; ***Harris and Shepherd, 2015***), long-range cortical connections could be performing stereotyped functions in different areas and in different species. However, the precise function of FF and FB interactions in hierarchical processing remains poorly understood.

Several theories of hierarchical computation involve looped interactions between areas, in which FF and FB pathways selectively influence each other in a bidirectional manner (***Bastos et al., 2012***; ***Guerguiev et al., 2017***; ***Keller and Mrsic-Flogel, 2018***; ***Lillicrap et al., 2016***; ***Rao and Ballard, 1999***; ***Roelfsema and Holtmaat, 2018***; ***Sacramento et al., 2018***). It is well established that cortical areas are densely interconnected and that FF pathways are always reciprocated by FB projections (***Felleman and Van Essen, 1991***; ***Gămănuţ et al., 2018***; ***Oh et al., 2014***; ***Zingg et al., 2014***). However, whether CC connections are wired to selectively facilitate looped computations remains unknown.

One possibility is that CC inputs specifically modulate neurons projecting back to the source of those inputs (looped neurons) indirectly via intermediary inhibitory or excitatory cells in the local circuit. Another possibility, not mutually exclusive to the previous one, is that CC projections selectively synapse onto looped neurons directly to form interareal monosynaptic loops, which would be excitatory since most long-range cortical afferents are glutamatergic.

Cortical projection neurons can be divided into three broad classes: intratelencephalic (IT) neurons, which project to cortical areas, pyramidal tract (PT) neurons, which project to multiple

***For correspondence:** leopoldo.petreanu@neuro.fchampalimaud.org

Competing interests: The authors declare that no competing interests exist.

Funding: See page 21

Received: 01 June 2020
Accepted: 29 January 2021
Published: 01 February 2021

Reviewing editor: Solange P Brown, Johns Hopkins University, United States

subcerebral areas including the midbrain, and corticothalamic (CT) neurons, which project predominantly to the thalamus (**Gerfen et al., 2018**; **Harris and Shepherd, 2015**). Thus, long-range CC projections could selectively participate in excitatory monosynaptic loops by preferentially contacting looped IT neurons, while avoiding neighboring non-looped IT, PT, and CT neurons. Previous studies have found that CC inputs form monosynaptic loops in sensorimotor (**Kinnischtzke et al., 2016**; **Mao et al., 2011**; **Yamawaki et al., 2016**), frontal (**Zhang et al., 2016**), and visual cortices (**Johnson and Burkhalter, 1997**). There is also evidence that some CC projections selectively innervate IT neurons over PT and CT neurons (**Kim et al., 2015**; **Kinnischtzke et al., 2016**; **Zhang et al., 2016**), but also evidence that some do not (**Yamawaki et al., 2016**). However, it remains unknown whether CC inputs selectively contact looped neurons over closely intermingled IT neurons projecting elsewhere (non-looped IT neurons), or whether they innervate IT neurons equally regardless of their projection pattern. Furthermore, in order to implement selective recurrent interactions, both FF and FB connections could be required to specifically engage with looped IT neurons. Yet, whether the selectivity of CC input between two areas is similar for both ascending and descending projections or whether it varies also remains unknown.

Here, we measured the strength of CC afferents to different types of projection neurons in mouse visual cortex to test whether they are wired to specifically engage in monosynaptic looped interactions. Using a combination of subcellular channelrhodopsin-2 (ChR2)-assisted circuit mapping (sCRACM) (**Petreanu et al., 2009**) and injections of multiple retrograde tracers, we found that FF and FB axons selectively provide stronger inputs to looped neurons in layer (L) 5 and L6, while in L2/3, they remain either unselective for projection type or provide stronger inputs to non-looped neurons. Thus, both ascending and descending hierarchical streams display the same selectivity for specific looped projection neurons despite their different anatomical profiles. Moreover, preferential innervation of looped L5 neurons often involved synapses made on their apical, but not basal, dendrites.

Results

Neurons with different projection patterns are intermingled in visual areas

We studied CC connections between primary visual cortex (V1), the lowest-order area of mouse visual cortex, and either the lateral visual areas (V2L) or the medial visual areas (V2M). Using dual injections of retrograde tracers, we measured the laminar distribution of different projection neurons in V1 and V2L (**Figure 1**, **Figure 1—figure supplement 1**). In each experiment, we compared the laminar distribution of V2L- or V1-projecting IT neurons with either IT neurons projecting to V2M, PT neurons projecting to the superior colliculus (SC), or CT neurons projecting to the visual thalamus. In each case, the different projection neurons were closely intermingled (**Figure 1A,B**). In both V1 and V2L, IT neurons were distributed across all layers except L1, including L4 (**Harris et al., 2019**; **Minamisawa et al., 2018**), indicating that FF and FB projections originate from neurons spanning most of the cortical depth. In contrast, PT and CT neurons were confined to L5 and L5/6, respectively, as previously described (**Harris and Shepherd, 2015**; **Figure 1A,B**). In both V1 and V2L, we found double-labeled IT neurons in L2–6 after injecting tracers in two different cortical areas, indicating that subpopulations of ascending and descending projection neurons have diverging axons innervating more than one visual cortical area (**Han et al., 2018**). However, IT neurons were rarely double-labeled when tracers were injected in a cortical and subcortical area, confirming that cortical- and subcortical-projecting neurons constitute different classes of projection neurons (**Economo et al., 2018**; **Harris and Shepherd, 2015**; **Tasic et al., 2018**). Using AAV encoding green fluorescent protein (AAV-GFP), we anterogradely traced V1→V2L FF axons and V2L→V1 FB axons and measured their laminated termination pattern (**Figure 1C,D**). FF axons in V2L were present in all layers but were denser in L2/3 and L6. FB axons in V1 arborized in L1 and L6, while avoiding middle layers. Given the laminar distribution of the different projection neurons and the termination pattern of CC afferent axons, FF and FB projections could potentially directly innervate both looped and non-looped IT neurons in each cortical layer, as well as PT and CT neurons in L5 and L6 (**Figure 2A**). Moreover, the proximity of looped IT neurons and other projection classes indicates that FF and FB axons are equally accessible to them. Thus, functional mapping of FF and FB connections is required

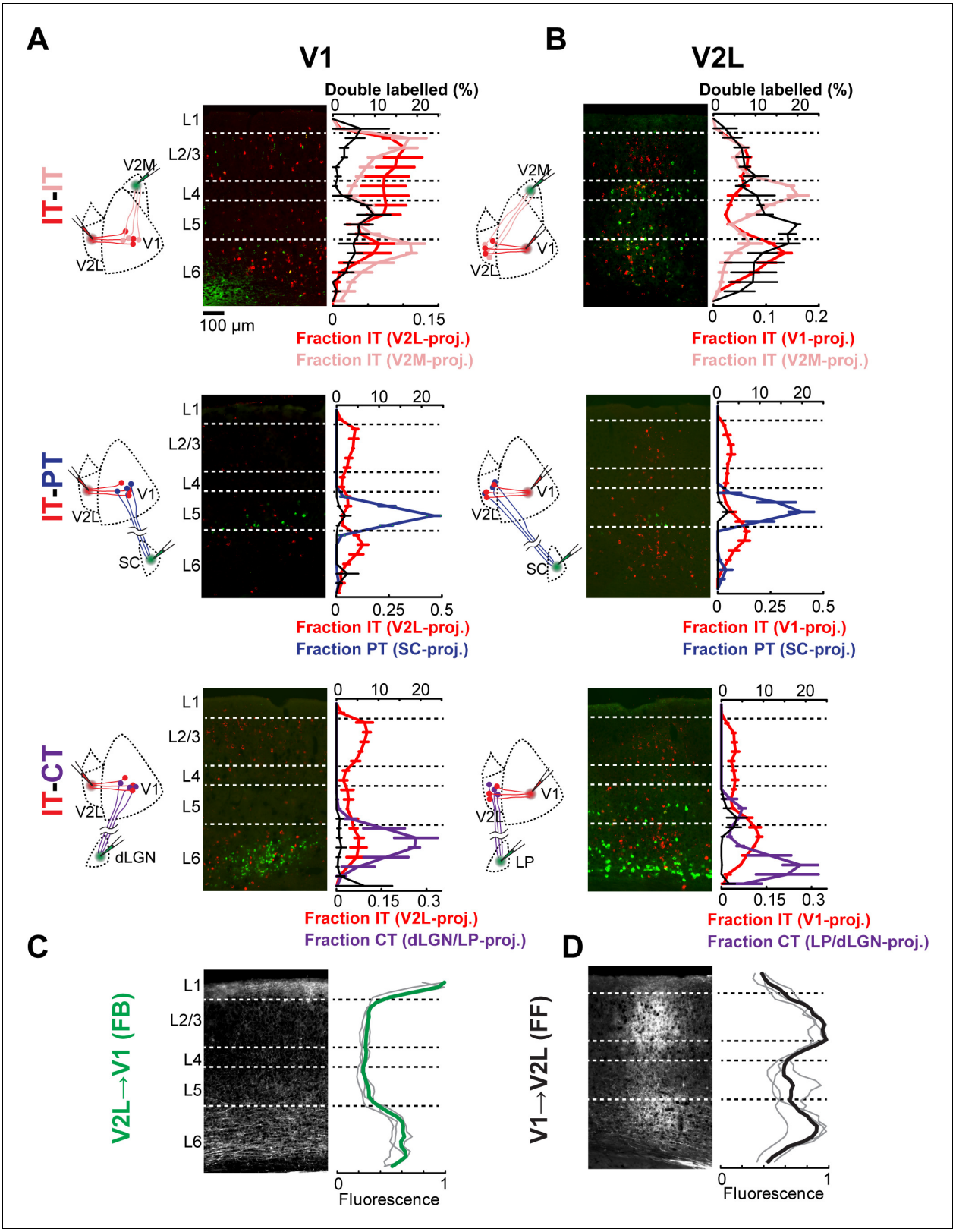

Figure 1. Cortical neurons projecting to different areas are intermingled and accessible to feedforward (FF) and feedback (FB) axons. (**A**) Distribution of retrogradely labeled projection neurons in primary visual cortex (V1) after injection of a red-fluorescent tracer in lateral visual areas (V2L) and an infrared-fluorescent tracer in either medial visual areas (V2M), superior colliculus (SC), or visual thalamus. Left, experimental configuration; center, representative fluorescent histological section, with infrared fluorescence shown in green; right, colored traces show the mean laminar distribution of

Figure 1 continued on next page

Figure 1 continued

the different projection neurons binned in 50 µm increments, while the black trace shows the percentage of retrogradely labeled neurons that are double-labeled at each depth (n = 3 animals per group). Error bars, standard error; dashed lines, approximate layer boundaries. (**B**) Distribution of retrogradely labeled projection neurons in V2L after injection of a red-fluorescent tracer in V1 and an infrared-fluorescent tracer in either V2M, SC, or visual thalamus (n = 3 animals per group). (**C**) Distribution of anterogradely labeled V2L FB axons in V1. Left, representative fluorescent histological section; right, axonal fluorescence across cortical depth binned in 50 µm increments. Individual mice, thin gray traces; average, thick green trace (n = 3 animals). (**D**) Distribution of anterogradely labeled V1 FF axons in V2L (n = 3 animals).

The online version of this article includes the following figure supplement(s) for figure 1:

Figure supplement 1. Histological and in vivo verification of lateral visual (V2L) and medial visual (V2M) area injection sites.

to reveal any underlying synaptic specificity, since axo-dendritic overlap does not always predict connectivity (***Harris and Shepherd, 2015***).

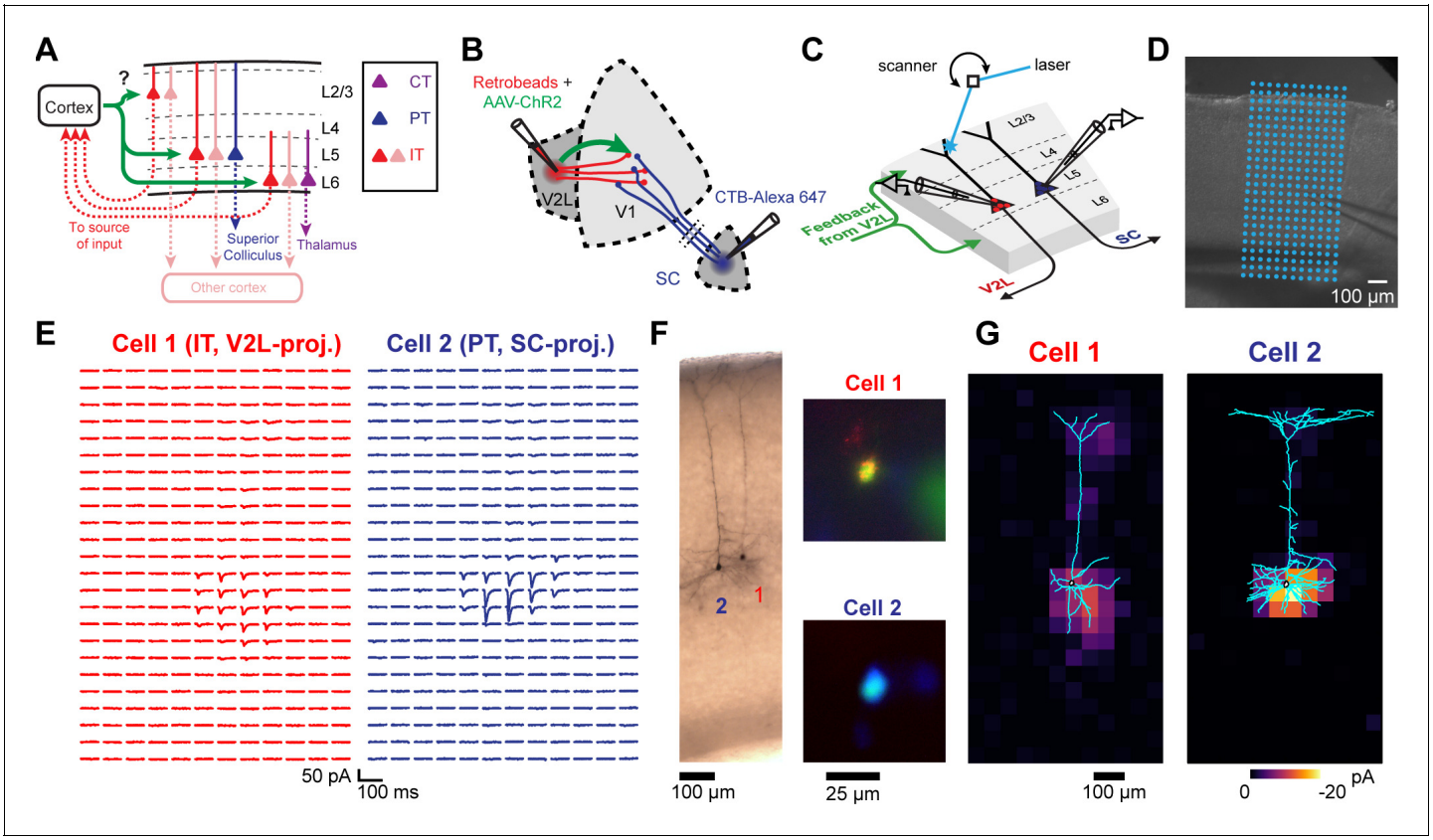

Figure 2. Measuring the strength and dendritic distribution of cortico-cortical (CC) inputs to different projection neurons. (**A**) We probed the strength of CC inputs to looped and non-looped neurons in different cortical layers. (**B**) Example experiment configuration. Retrograde tracers are injected in two areas to label different projection neurons. One cortical area is also co-injected with adeno-associated virus (AAV)-channelrhodopsin-2 (ChR2) to express ChR2 in a specific CC projection. (**C**) Example of subcellular channelrhodopsin-2 (ChR2)-assisted circuit mapping (sCRACM) experiment. Pairs of neighboring retrogradely labeled neurons in the same cortical layer were sequentially recorded. During each recording, a laser beam was scanned over the dendrites of the cell at different locations in a grid pattern. (**D**) Brightfield image of an acute coronal cortical slice showing the recording pipette and photostimulation grid. (**E**) Excitatory postsynaptic currents (EPSCs) recorded from a pair of neighboring L5 neurons, evoked by photostimulating ChR2$^+$ V2L→V1 FB terminals on a grid. (**F**) Left, dendritic morphology staining of the recorded pair. Right, identity of the recorded projection neuron was confirmed by fluorescence in the soma of both a retrograde tracer and a different-colored dye introduced from the internal patch pipette solution. (**G**) sCRACM maps of the recorded pair overlaid on their reconstructed dendrites. Responsive locations are color-coded to represent mean amplitude.

The online version of this article includes the following figure supplement(s) for figure 2:

Figure supplement 1. Total input vs. laminar depth across different projections and projection neuron classes.

Figure supplement 2. Analysis of the incidence of retrograde infection of projection neurons by adeno-associated viruses (AAVs).

Mapping the cell-type specificity of CC connections

To measure the cell-type selectivity of CC connections, we combined sCRACM (***Petreanu et al., 2009***) with multiple injections of fluorescent retrograde tracers (***Figure 2B***). We injected AAV-ChR2 mixed with a retrograde tracer in either V1, V2L, or V2M to express ChR2 in FF or FB axons and to retrogradely label looped IT neurons projecting back to the source of ChR2-expressing ($ChR2^+$) axons. We also injected a different retrograde tracer in either a second cortical area, the SC, or the thalamus to label non-looped IT, PT, or CT neurons (***Figure 2A***). We recorded from pairs of neighboring neurons in the same cortical layer in either V1 or higher-order visual areas V2L or V2M in acute brain slices containing FB or FF $ChR2^+$ axons, respectively. For each pair, one cell projected to the source of $ChR2^+$ inputs and one cell projected to a different cortical or subcortical area, as indicated by the retrograde tracer type in the soma (***Figure 2C,F***). Double-labeled cells were excluded. During the recording, we used galvanometer mirrors to rapidly photostimulate $ChR2^+$ terminals with a blue laser at different locations around the cell to evoke excitatory postsynaptic currents (EPSCs) in the presence of sodium channel blocker tetrodotoxin (TTX), potassium-channel blocker 4-aminopyridine (4-AP), and the NMDA-receptor blocker 3-((R)-2-carboxypiperazin-4-yl)-propyl-1-phosphonic acid (CPP) (***Figure 2C–E***). The onset of laser-evoked EPSCs was delayed relative to laser pulse onset in 96% (225/235) of the recorded neurons labeled with retrograde tracers, indicating that retrograde AAV-mediated transfection of ChR2 was rare, consistent with histological analyses (Materials and methods, ***Figure 2—figure supplement 2***). Thus, sCRACM maps provide a measure of both the strength and location of monosynaptic CC inputs with minimal contamination from local collaterals. We then compared the strength of monosynaptic FF or FB inputs in defined dendritic compartments in pairs of neurons projecting to different areas (***Figure 2E–G***; ***D'Souza et al., 2016***; ***Morgenstern et al., 2016***; ***Petreanu et al., 2009***; ***Yang et al., 2013***). We measured input strength of 4 CC projections (FF: V1→V2L and V1→V2M; FB: V2M→V1 and V2L→V1) to looped IT neurons in three layers (L2/3, L5, and L6), and compared it to non-looped IT, PT, or CT neurons in their vicinity (***Figure 2—figure supplement 1***).

FF and FB inputs innervate specific dendritic compartments of projection neurons

We detected monosynaptic FF and FB inputs in every cell type and analyzed their dendritic distribution (***Figure 3***). Individual sCRACM maps were normalized to their maximum response, aligned relative to pia (***Figure 3***) or soma position (***Figure 3—figure supplement 1***) and averaged. They thus represent the relative distribution of CC inputs within the dendritic tree for each class of projection neuron. Input strength to distal dendrites is underestimated in sCRACM maps as inputs are filtered and attenuated when measured from the soma due to the passive cable properties of dendritic arbors (***Petreanu et al., 2009***; ***Stuart and Spruston, 2015***; ***Williams and Mitchell, 2008***). In L2/3, FF inputs were largely confined to perisomatic dendrites. In L6, while FF connections also targeted perisomatic dendrites in both CT and IT neurons, we could detect additional FF input on the apical dendrites of IT neurons extending across L5 (***Figure 3A***, ***Figure 4F***). Similarly, FF input contacted L5 IT neurons in both the perisomatic dendrites and along their apical dendritic trunk spanning L4 and L2/3 (***Figure 3A***, ***Figure 5B***). Thus, like other long-range inputs (***Petreanu et al., 2009***), FF axons innervate several dendritic domains of L5 pyramidal neurons, revealing that targeting of apical dendrites is not an exclusive property of FB axons (see below).

As with FF inputs, FB afferents innervated the perisomatic compartments of all recorded cell types. However, when compared to FF inputs, a larger fraction of FB to L2/3 and L5 neurons was located on their distal dendrites in L1 (***Figure 3B***), consistent with previous measurements (***Petreanu et al., 2009***; ***Yang et al., 2013***) and with the laminar profile of FB axons (***Figure 1C***). Apical tuft inputs were more readily detected in L5 IT neurons than in PT neurons, suggesting differential innervation by FB fibers (***Figure 2G***, ***Figure 3B*** and ***Figure 5N***, see below).

CC inputs are selectively stronger in looped L6 neurons

We first measured the connectivity of FF and FB inputs to L6 neurons projecting to different areas. We compared the input strength to looped IT neurons (i.e., neurons projecting back to the FF or FB input source) vs. either neighboring non-looped IT neurons projecting to another cortical area or CT neurons (***Figure 4***). We measured both total input strength, summing responses over all

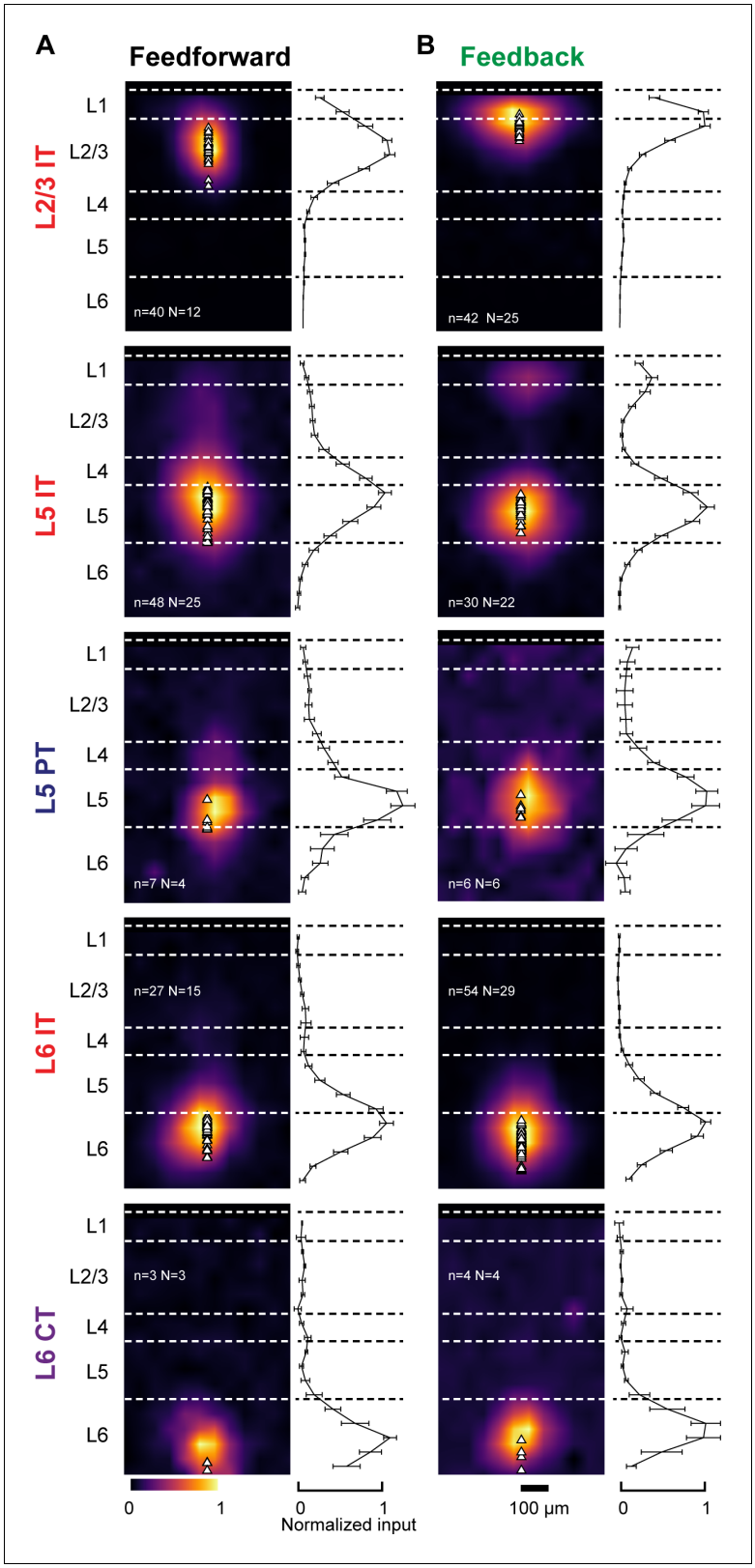

Figure 3. Dendritic distribution of feedforward (FF) and feedback (FB) inputs to different projection neuron classes. (**A**) Left, group averages of subcellular channelrhodopsin-2 (ChR2)-assisted circuit mapping (sCRACM) maps aligned by pia position showing primary visual cortex (V1) FF input to the different cell types (combining V1→V2L and V1→V2M inputs in the case of intratelencephalic [IT] neurons). Triangles, soma position. Right,

Figure 3 continued on next page

Figure 3 continued

vertical profiles of input strength. Error bars, s.e.m.; n, number of neurons; N, number of mice. (**B**) Group averages and vertical profiles of sCRACM maps showing FB input to the different cell types in V1 (combining V2L→V1 and V2M→V1 inputs in the case of IT neurons).

The online version of this article includes the following figure supplement(s) for figure 3:

Figure supplement 1. Soma-aligned dendritic distribution of feedforward (FF) and feedback (FB) inputs to different projection neuron classes.

photostimulated locations, and input strength to the perisomatic area (L6 and lower L5) and apical dendritic area (upper L5 and L4). Relative input strength between the looped IT neuron and the paired neuron was quantified using the sCRACM Response Index (SRI), which ranges from −1 to 1. The SRI has a value of 0 if input strength in the two cells is equal, −1 if there is input in the looped IT neuron but no input in the paired neuron, and 1 in the opposite case (see Materials and methods).

We first compared V1 FF inputs to looped and non-looped L6 IT neurons. For V1→V2L inputs, total strength was greater in looped IT neurons (***Figure 4—figure supplement 1***; SRI: −0.49 ± 0.23, p=0.002). This stronger innervation was present in both perisomatic (SRI: −0.50 ± 0.21, p=0.0001) and apical areas (SRI: −0.45 ± 0.45, p=0.0364) (***Figure 4A–D***). For V1→V2M inputs, we did not detect a difference in total strength between looped and non-looped IT neurons (***Figure 4—figure supplement 1***, SRI: −0.32 ± 0.48, p=0.064), but looped IT neurons again received significantly stronger input in the perisomatic area (***Figure 4C***; SRI: −0.36 ± 0.46, p=0.038). V1→V2M inputs in apical dendrites were mostly weak and not different between cell types (Apical SRI: 0.33 ± 0.69, p=0.247). We next compared V1 FF inputs to looped L6 IT neurons and same-layer CT neurons in V2L. Total input to looped neurons was consistently stronger than to CT neurons (***Figure 4—figure supplement 1***, SRI: −0.64 ± 0.23, $p=1.2\times10^{-5}$) and inputs were weaker in both perisomatic and apical areas of CT neurons (***Figure 4E–H***, Perisomatic SRI: −0.64 ± 0.26, $p=2.4\times10^{-5}$; Apical SRI: −0.69 ± 0.40, p=0.018).

Likewise, FB inputs to V1 also selectively targeted looped L6 neurons in many cases (***Figure 4I–P***). For the looped vs. non-looped comparison among IT neurons, FB from V2M preferentially connected to IT neurons projecting back to the source of FB, both when measuring total and perisomatic input (***Figure 4—figure supplement 1***, ***Figure 4I–L***, Total SRI: −0.39 ± 0.36, p=0.031; Perisomatic SRI: −0.40 ± 0.36, p=0.028), but no difference was detected in the apical area (SRI: −0.27 ± 0.85, p=0.56). FB from V2L was not significantly different in looped and non-looped L6 IT neurons (total SRI: −0.18 ± 0.35, p=0.098; perisomatic SRI: −0.14 ± 0.35, p=0.182; apical SRI: −0.02 ± 0.90, p=0.958). However, looped neurons received stronger perisomatic input from V2L compared to neighboring CT neurons (***Figure 4M–P***; total SRI: −0.40 ± 0.42, p=0.003, perisomatic SRI: −0.41 ± 0.45, p=0.005). Thus, we found that in most experiments (three out of four), FF and FB connections to L6 neurons were significantly stronger in looped IT cells than in non-looped ones. FF and FB connections were also stronger in looped IT neurons than in CT neurons.

FF and FB inputs are selectively stronger in looped L5 neurons

We next asked whether the strength of CC inputs differed among L5 pyramidal neuron types (***Figure 5***). FF and FB inputs innervated L5 neurons in both perisomatic and apical dendritic regions (***Figure 3***, ***Figure 3—figure supplement 1*** and ***Figure 5B,F,J,N***). As before, we analyzed input strength in these two innervation domains separately. First, we compared V1→V2L or V1→V2M FF inputs to looped IT neurons projecting back to V1 vs. non-looped IT neurons (***Figure 5A–D***). In V2L, total input strength did not differ between looped and non-looped L5 IT neurons (***Figure 5—figure supplement 1***; SRI: −0.03 ± 0.35, p=0.783), and neither did perisomatic input (***Figure 5C***; SRI: −0.02 ± 0.36, p=0.82). However, FF inputs terminating on the apical dendrites of L5 neurons were stronger in looped IT neurons (***Figure 5D***; SRI: −0.40 ± 0.43, p=0.009). In V2M, looped neurons received stronger V1 input than neighboring non-looped IT neurons on both their perisomatic and apical dendrites (***Figure 5—figure supplement 1*** and ***Figure 5C,D***; total SRI: −0.42 ± 0.32, p=0.002; perisomatic SRI: −0.42 ± 0.35, p=0.002; apical SRI: −0.37 ± 0.43, p=0.0174).

We then compared the strength of FF inputs to looped IT and PT neurons. FF fibers innervated the perisomatic dendrites of looped neurons more strongly, with no difference observed in apical

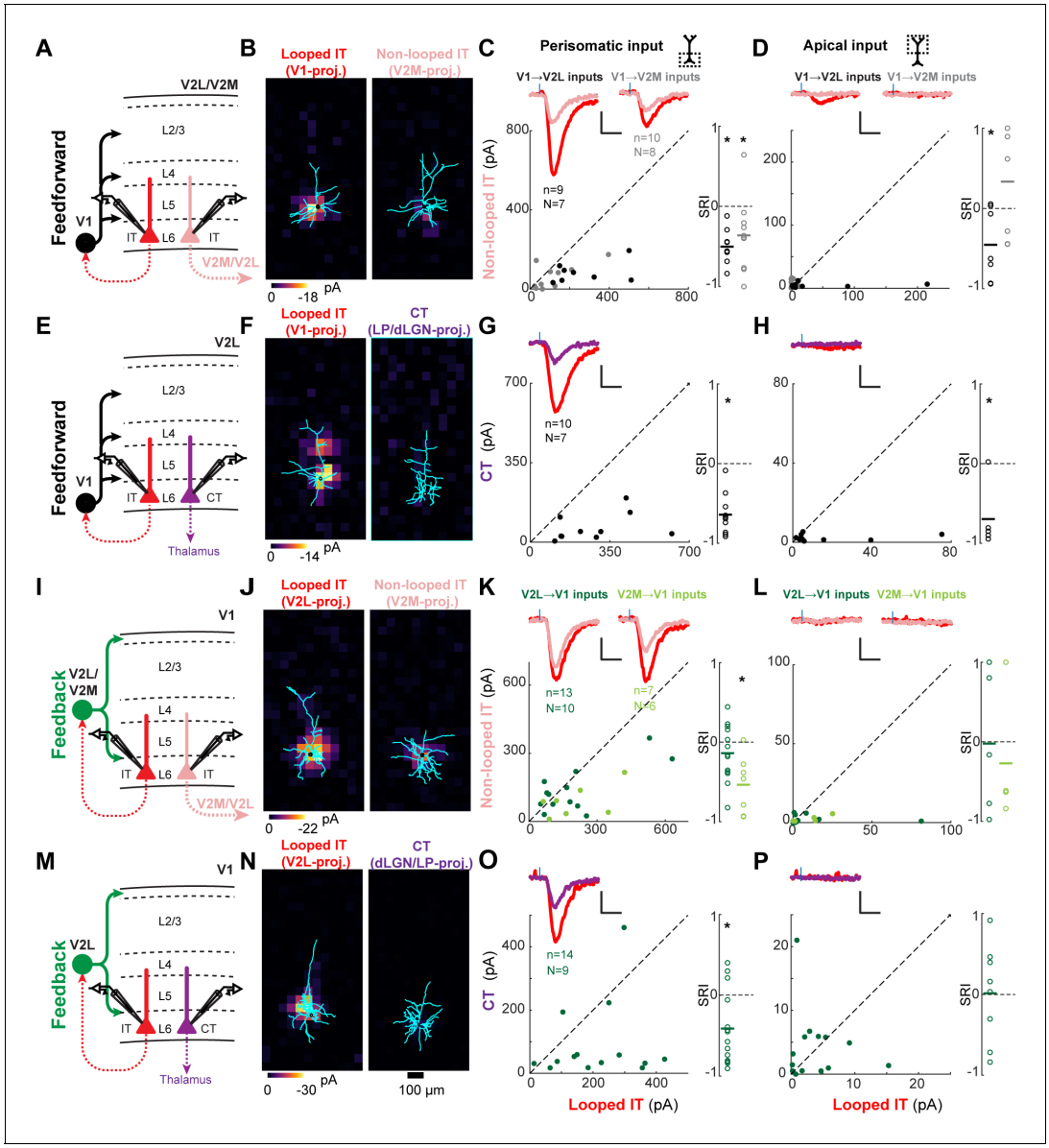

Figure 4. Most feedforward (FF) and feedback (FB) inputs are stronger in looped intratelencephalic (IT) neurons than in neighboring non-looped IT or corticothalamic (CT) neurons in L6. (**A**) Configuration of experiments comparing strength of primary visual cortex (V1) FF input to pairs of L6 looped and non-looped IT neurons in lateral visual area (V2L) or medial visual area (V2M). (**B**) Example pair of subcellular channelrhodopsin-2 (ChR2)-assisted circuit mapping (sCRACM) maps overlaid on reconstructed dendrites showing monosynaptic V1 FF inputs to a looped IT neuron (left) and an adjacent non-looped IT neuron (right) recorded in V2L. (**C**) Left, paired comparisons of perisomatic FF input to looped vs. non-looped IT neurons (n, number of cell pairs; N, number of mice); black dots, V1→V2L inputs; gray dots, V1→V2M inputs. Traces were generated by averaging the mean perisomatic excitatory postsynaptic current (EPSC) of each neuron across all neurons in the same projection class. Colors correspond to (**A**). Blue tick, laser pulse. Scale bars in all panels, 2 pA and 20 ms. Right, sCRACM Response Index (SRI) of the same data. Number of cell pairs and animals are the same as in the left plot unless otherwise specified. Horizontal line, mean. *, p<0.05, see text for exact value. (**D**) Same as C for apical inputs (SRI: V1→V2L, n = 7, N = 6; V1→V2M, n = 7, N = 6). (**E**) Configuration of experiment comparing strength of V1 FF input to pairs of L6 looped IT and CT neurons in V2L. (**F**) Example pair of sCRACM maps overlaid on reconstructed dendrites showing monosynaptic V1 FF inputs to a looped IT neuron (left) and an adjacent CT neuron (right) recorded in V2L. (**G**) Paired comparisons and SRI of perisomatic FF input to looped IT vs. CT neurons. (**H**) Paired comparisons and SRI (n = 5, N = 5) of apical FF input to looped IT vs. CT neurons. (**I**) Configuration of experiments comparing strength of V2L or V2M FB input to pairs of L6 looped and non-looped IT neurons in V1. (**J**) Example pair of sCRACM maps overlaid on reconstructed dendrites showing monosynaptic V2L FB inputs to a looped IT neuron (left) and an adjacent non-looped IT neuron (right) recorded in V1. (**K**) Paired comparisons and SRI of perisomatic FB input to looped vs. non-looped IT neurons. Dark green dots, V2L→V1 inputs; light green dots, V2M→V1 inputs. (**L**) Paired comparisons and SRI (V2L→V1, n = 5, N = 5; V2M→V1, n = 4, N = 4) of apical FB input to looped vs. non-looped IT neurons. (**M**) Configuration of experiment comparing strength of V2L FB input to pairs of L6 looped IT and CT neurons in V1. (**N**) Example pair of sCRACM maps overlaid on reconstructed dendrites showing monosynaptic V2L FB

Figure 4 continued on next page

Figure 4 continued

inputs to a looped IT neuron (left) and an adjacent CT neuron (right) recorded in V1. (**O**) Paired comparisons and SRI of perisomatic FB input to looped IT vs. CT neurons. (**P**) Paired comparisons and SRI (n = 8, N = 7) of apical FB input to looped IT vs. CT neurons.

The online version of this article includes the following figure supplement(s) for figure 4:

Figure supplement 1. Total subcellular channelrhodopsin-2 (ChR2)-assisted circuit mapping (sCRACM) input to L6 neurons.

inputs (***Figure 5—figure supplement 1*** and ***Figure 5E–H***; total SRI: −0.43 ± 0.41, p=0.003; perisomatic SRI: −0.46 ± 0.43, p=0.002; apical SRI: −0.14 ± 0.65, p=0.49). We conclude that FF inputs are selectively stronger in looped L5 neurons when compared to non-looped IT or PT neurons, and that this selectivity may result from inputs impinging on the perisomatic dendrites (V1→V2L, IT vs. PT), the apical dendrites (V1→V2L, IT vs. IT), or both regions (V1→V2M, IT vs. IT).

We next measured the strength of FB inputs to L5 neurons with different projection targets (***Figure 5I–P***). We transfected V2L or V2M FB axons with ChR2 and recorded different L5 cell types in V1. We first compared the strength of V2L→V1 and V2M→V1 FB inputs to looped vs. non-looped L5 IT neurons (***Figure 5I–L***). In both projections, total input (***Figure 5—figure supplement 1***; V2L→V1 SRI: −0.15 ± 0.54, p=0.284; V2M→V1 SRI: −0.19 ± 0.56, p=0.222) and perisomatic input (***Figure 5K***; V2L→V1 SRI: −0.09 ± 0.60, p=0.557; V2M→V1 SRI: −0.22 ± 0.57, p=0.152) were indistinguishable between the two projection types. However, inputs targeting the distal tufts in L1 were stronger in looped than non-looped IT neurons for both projections (***Figure 5L***; V2L→V1 SRI: −0.47 ± 0.51, p=0.012; V2M→V1 SRI: −0.48 ± 0.58, p=0.022). This resulted in looped neurons receiving a larger fraction of total FB input in their L1 apical domain (mean fraction of total input in L1; V2L→V1: looped, 23.1 ± 16.6%, non-looped, 11.0 ± 10.6%, p=0.01, signed-rank test; V2M→V1: looped, 18.1 ± 23.0%, non-looped, 9.4 ± 18.2%, p=0.01, signed-rank test). The presence of stronger apical inputs in looped neurons could not be explained by differences in dendritic filtering. First, V2L- and V2M-projecting populations had similar apical dendritic morphologies, with slender tufts that were indistinguishable in L1 (***Figure 5—figure supplement 2***). Second, the cell type receiving the largest fraction of distal input switched from V2L-projecting neurons in the V2L→V1 experiment to V2M-projecting neurons in the V2M→V1 experiment.

As with the looped vs. non-looped IT comparison, V2L→V1 total and perisomatic inputs did not distinguish between looped IT and PT neurons (***Figure 5—figure supplement 1***, ***Figure 5M–P***; total SRI: −0.20 ± 0.52, p=0.195; perisomatic SRI: −0.19 ± 0.62, p=0.28), but looped neurons received stronger FB input in their L1 apical compartment (***Figure 5P***; SRI: −0.46 ± 0.62, p=0.026), despite having less total dendritic length in L1 (***Figure 5—figure supplement 2***). Simulations showed that the weaker sCRACM responses in distal tufts of PT neurons cannot be explained by differences in passive dendritic filtering between the two cell types. In the absence of connectional selectivity, the thicker apical shafts and richer apical tuft arborization of PT neurons (***Figure 5—figure supplement 2***) predict that distal FB input arriving at the soma would be larger, not smaller (***Figure 5—figure supplement 3***). We also confirmed that the weaker distal FB input in PT neurons was not due to different levels of hyperpolarization-activated current (I_h) between the two cell types (***Harris and Shepherd, 2015***), since looped IT neurons still received stronger FB input in the apical tuft when measured in the presence of I_h blockers (***Figure 5—figure supplement 4***). Thus, the stronger sCRACM signals detected in L1 reflect synaptic selectivity for the terminal tufts of looped IT neurons. We conclude that the apical dendrites of L5 neurons have privileged access to FB axons when the neurons loop back to the source of those axons. Conversely, FB inputs to the basal dendrites of L5 neurons do not favor looped neurons over non-looped IT or PT neurons.

The strength of CC inputs in looped and non-looped L2/3 neurons

Finally, we examined whether CC projections to supragranular neurons would also exhibit a preference for looped connectivity. In addition to total input strength (***Figure 6—figure supplement 1***), we analyzed inputs terminating in L1 and in the perisomatic region (***Figure 6***). FF input from V1 was equally strong in looped and non-looped L2/3 IT neurons in both V2L and V2M when assessing total input strength (***Figure 6—figure supplement 1***; V1→V2L SRI: −0.04 ± 0.30, p=0.65; V1→V2M SRI: −0.05 ± 0.35, p=0.683) and perisomatic innervation (***Figure 6C***; V1→V2L SRI:−0.06 ± 0.30, p=0.564; V1→V2M SRI: −0.17 ± 0.34, p=0.167). However, when considering FF connections in L1, V1→V2M

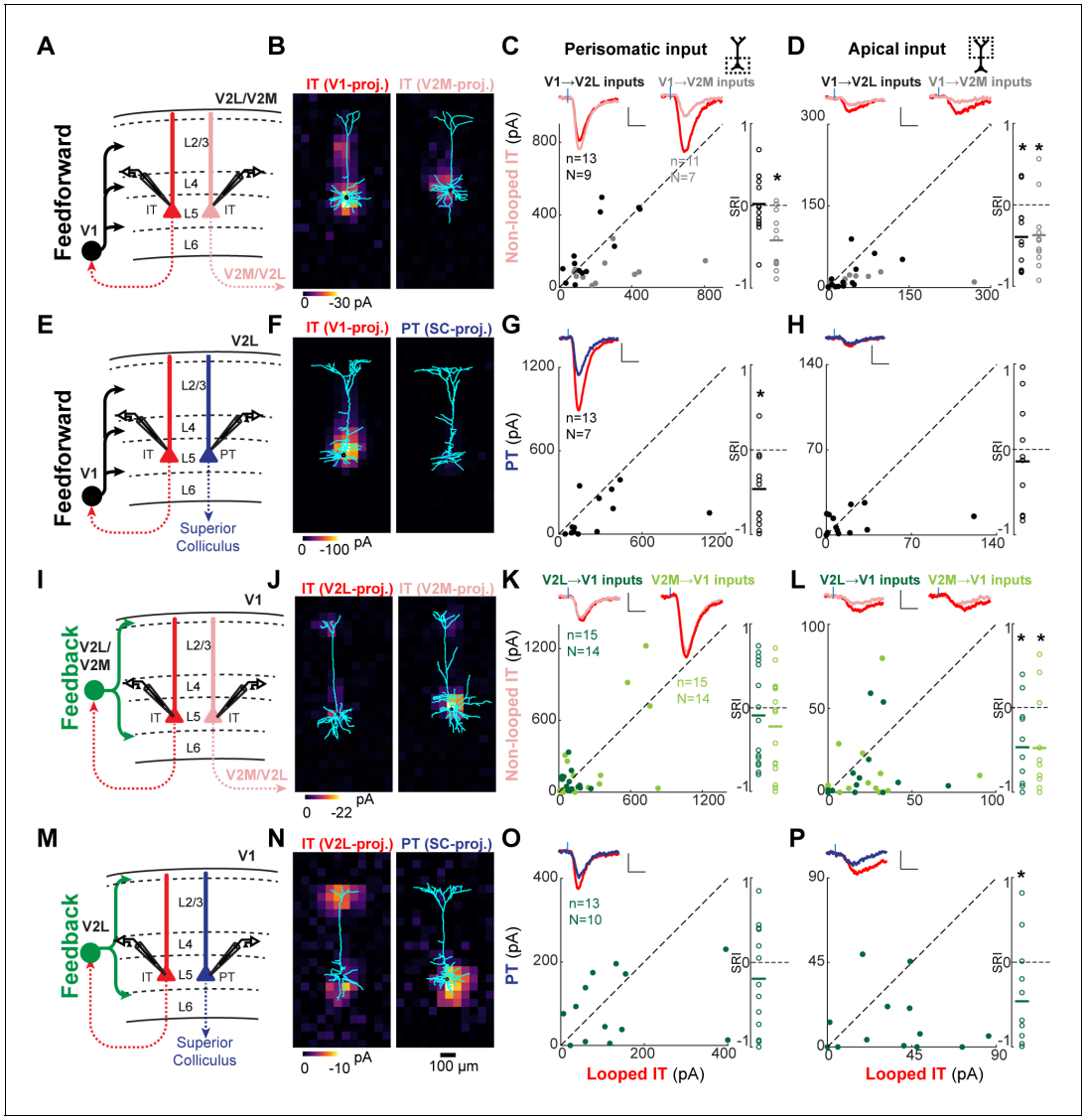

Figure 5. Feedforward (FF) and feedback (FB) inputs are stronger in looped intratelencephalic (IT) neurons than in neighboring non-looped IT or pyramidal tract (PT) neurons in L5. (**A**) Configuration of experiments comparing strength of primary visual cortex (V1) FF input to pairs of L5 looped and non-looped IT neurons in lateral visual (V2L) or medial visual (V2M) areas. (**B**) Example pair of subcellular channelrhodopsin-2 (ChR2)-assisted circuit mapping (sCRACM) maps overlaid on reconstructed dendrites showing monosynaptic V1 FF inputs to a looped IT neuron (left) and an adjacent non-looped IT neuron (right) recorded in V2L. (**C**) Left, paired comparisons of perisomatic FF input to looped vs. non-looped IT neurons; black dots, V1→V2L inputs; gray dots, V1→V2M inputs. Traces were generated by averaging the mean perisomatic excitatory postsynaptic current (EPSC) of each neuron across all neurons in the same projection class. Blue tick, laser pulse. Scale bars in all panels, 2 pA and 20 ms. Right, sCRACM Response Index (SRI) of the same data. Number of cell pairs and animals are the same as in the left plot unless otherwise specified. Horizontal line, mean. *, $p<0.05$, see text for exact value. (**D**) Same as C for apical inputs (SRI: V1→V2L, n = 12, N = 8; V1→V2M, n = 11, N = 7). (**E**) Configuration of experiment comparing strength of V1 FF input to pairs of L5 looped IT and PT neurons in V2L. (**F**) Example pair of sCRACM maps overlaid on reconstructed dendrites showing monosynaptic V1 FF inputs to a looped IT neuron (left) and an adjacent PT neuron (right) recorded in V2L. (**G**) Paired comparisons and SRI of perisomatic FF input to looped IT vs. PT neurons. (**H**) Paired comparisons and SRI (n = 11, N = 7) of apical FF input to looped IT vs. PT neurons. (**I**) Configuration of experiments comparing strength of V2L or V2M FB input to pairs of L5 looped and non-looped IT neurons in V1. (**J**) Example pair of sCRACM maps overlaid on reconstructed dendrites showing monosynaptic V2L FB inputs to a looped IT neuron (left) and an adjacent non-looped IT neuron (right) recorded in V1. (**K**) Paired comparisons and SRI of perisomatic FB input to looped vs. non-looped IT neurons. Dark green dots, V2L→V1 inputs; light green dots, V2M→V1 inputs. (**L**) Paired comparisons and SRI (V2L→V1, n = 11, N = 10; V2M→V1, n = 11, N = 10) of FB input in L1 to looped vs. non-looped IT neurons. (**M**) Configuration of experiment comparing strength of V2L FB input to pairs of L5 looped IT and PT neurons in V1. (**N**) Example pair of sCRACM maps overlaid on reconstructed dendrites showing monosynaptic V2L FB inputs to a looped IT neuron (left) and an adjacent PT neuron (right) recorded in V1. (**O**) Paired comparisons and SRI of perisomatic FB input to looped IT vs. PT neurons. (**P**) Paired comparisons and SRI (n = 12, N = 9) of FB input in L1 to looped IT vs. PT neurons.

Figure 5 continued on next page

Figure 5 continued

The online version of this article includes the following figure supplement(s) for figure 5:

Figure supplement 1. Total subcellular channelrhodopsin-2 (ChR2)-assisted circuit mapping (sCRACM) input to L5 neurons.
Figure supplement 2. Dendritic morphology of the different L5 projection neuron types in primary visual cortex (V1).
Figure supplement 3. Simulations of the dendritic filtering of distal apical inputs.
Figure supplement 4. Feedforward (FB) input to looped L5 intratelencephalic (IT) neurons vs. pyramidal tract (PT) neurons in the presence of I_h blockers.

inputs were significantly stronger in non-looped neurons projecting to V2L, while V1→V2L inputs showed no preference (***Figures 6A,B,D***; V1→V2L SRI: −0.03 ± 0.66, p=0.892; V1→V2M SRI: 0.68 ± 0.52, p=0.013). This resulted in non-looped V2M L2/3 neurons receiving a larger fraction of total V1 FF input in L1 compared to their looped neighbors (mean fraction of total input in L1; V1→V2M inputs: looped, 2.1 ± 3.7%, non-looped, 12.6 ± 13.0%, p=0.039, signed-rank test). Similarly, we measured the strength of V2M and V2L FB inputs to different L2/3 IT neurons in V1. Total input was indistinguishable between looped and non-looped neurons, as were perisomatic and L1 inputs (***Figure 6—figure supplement 1***, ***Figure 6E–H***; V2L→V1, total SRI: −0.13 ± 0.51, p=0.36, perisomatic SRI: −0.13 ± 0.54, p=0.394, L1 input SRI: −0.12 ± 0.64, p=0.553; V2M→V1, total SRI: −0.04 ± 0.36, p=0.67, perisomatic SRI: 0.03 ± 0.48, p=0.826, L1 input SRI: −0.04 ± 0.66, p=0.86). In summary, most (3/4) FF and FB inputs did not show projection-type specificity when innervating L2/3 neurons, with the exception of V1→V2M FF inputs, which were weaker, not stronger, when

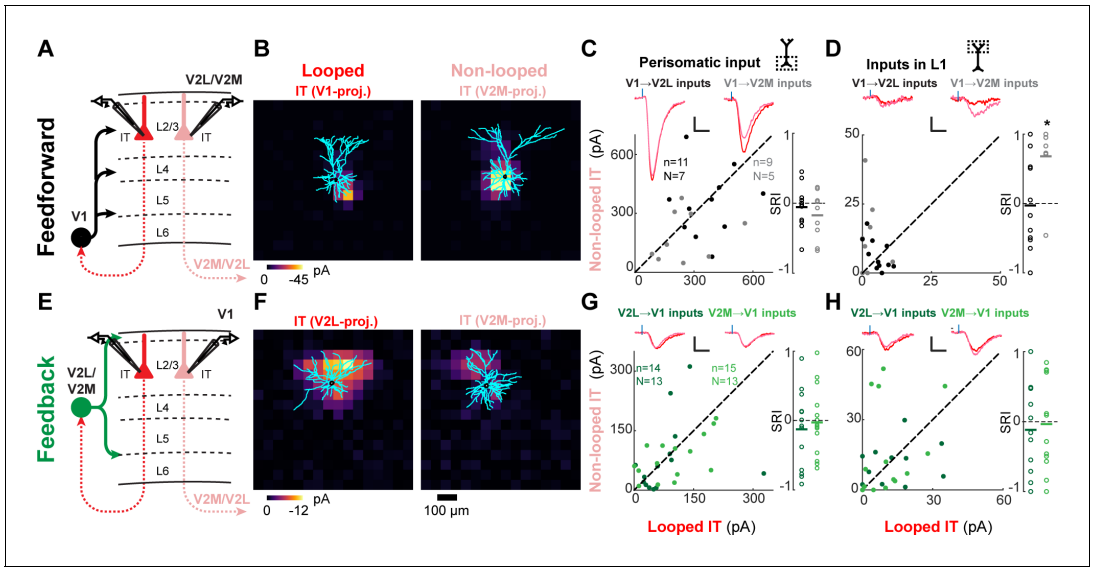

Figure 6. Feedforward (FF) and feedback (FB) connections are similar or weaker in looped L2/3 neurons. (**A**) Configuration of experiments comparing strength of primary visual cortex (V1) FF input to pairs of L2/3 looped and non-looped intratelencephalic (IT) neurons in lateral visual area (V2L) or medial visual area (V2M). (**B**) Example pair of subcellular channelrhodopsin-2 (ChR2)-assisted circuit mapping (sCRACM) maps overlaid on reconstructed dendrites showing monosynaptic V1 FF inputs to a looped IT neuron (left) and an adjacent non-looped IT neuron (right) recorded in V2L. (**C**) Left, paired comparisons of perisomatic FF input to looped vs. non-looped IT neurons; black dots, V1→V2L inputs; gray dots, V1→V2M inputs. Traces were generated by averaging the mean perisomatic excitatory postsynaptic current (EPSC) of each neuron across all neurons in the same projection class. Blue tick, laser pulse. Scale bars in all panels, 2 pA and 20 ms. Right, sCRACM Response Index (SRI) of the same data. Number of cell pairs and animals are the same as in the left plot unless otherwise specified. Horizontal line, mean. *, p<0.05, see text for exact value. (**D**) Same as C for inputs in L1 (SRI: V1→V2L, n = 11, N = 7; V1→V2M, n = 7, N = 5). (**E**) Configuration of experiments comparing strength of V2L or V2M FB input to pairs of L2/3 looped and non-looped IT neurons in V1. (**F**) Example pair of sCRACM maps overlaid on reconstructed dendrites showing monosynaptic V2L FB inputs to a looped IT neuron (left) and an adjacent non-looped IT neuron (right) recorded in V1. (**G**) Paired comparisons and SRI of perisomatic FB input to looped vs. non-looped IT neurons. Dark green dots, V2L→V1 inputs; light green dots, V2M→V1 inputs. (**H**) Same as G for inputs in L1 (SRI: V2L→V1, n = 11, N = 10; V2M→V1, n = 12, N = 11).

The online version of this article includes the following figure supplement(s) for figure 6:

Figure supplement 1. Total subcellular channelrhodopsin-2 (ChR2)-assisted circuit mapping (sCRACM) input to L2/3 neurons.

contacting dendrites of looped neurons in L1, in contrast to the looped preference observed in L5 and L6.

Selectivity for looped IT neurons differs across infragranular and supragranular layers

We then searched for common patterns in the synaptic selectivity of CC projections to different IT neurons. In each layer, we plotted the strength of FF or FB projections to looped IT neurons relative to non-looped IT neurons in the perisomatic or apical compartments, as measured using the SRI (***Figure 7***). While there was some variability across individual projections as previously described, there were some common patterns shared across projections. When comparing inputs to looped and non-looped IT neurons in L5 and L6, in seven out of eight FF/FB projections we found stronger inputs to looped IT neurons, either in the perisomatic or apical areas, or both. On the contrary, none of the four FF/FB projections to L2/3 showed stronger inputs to looped IT neurons, and in the only case in which input strength differed between looped and non-looped neurons, inputs were weaker in looped neurons rather than in non-looped ones. When comparing looped IT neurons and PT or CT neurons, we found that in all cases CC inputs were stronger in looped IT neurons. We conclude that most FF and FB connections are selectively wired to strongly innervate looped IT neurons in L5 and L6. In L5, this selectivity involved synapses on apical, but not basal, dendrites in most cases (1/3 and

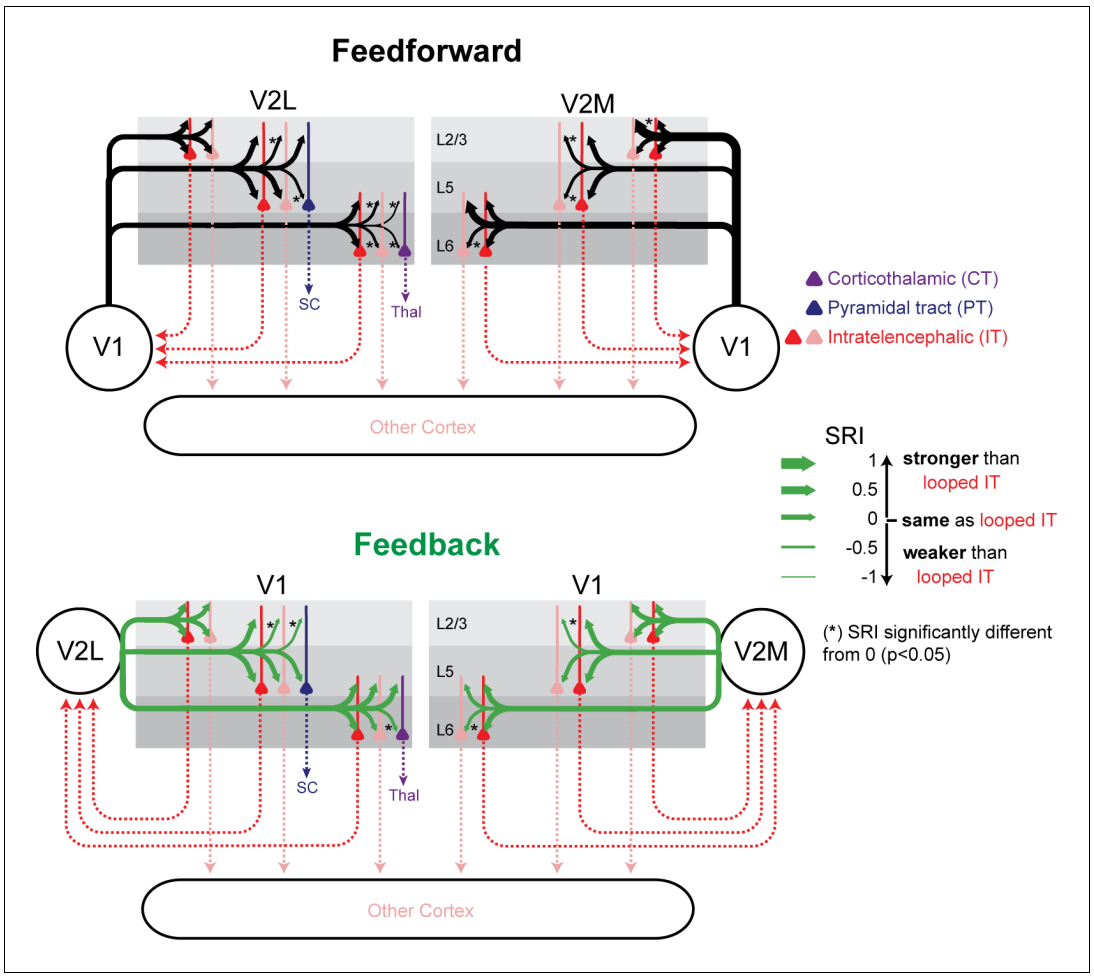

Figure 7. Summary of relative input strength across all experiments. The sCRACM Response Index (SRI) of feedforward (FF) and feedback (FB) inputs to the different cell types is represented by arrow thickness. The top and bottom arrows to L5 neurons indicate inputs to apical and perisomatic domains, respectively. Inputs to looped intratelencephalic (IT) cells in each cortical layer are assigned an SRI of 0 (medium arrow thickness). * signifies significant difference ($p<0.05$) from the looped IT population.

3/3 of FF and FB connections tested, respectively). By contrast, inputs to L2/3 were either equally strong in looped and non-looped IT neurons or weaker in looped ones.

FB inputs selectively influence the activity of looped neurons in V1

These sCRACM measurements of input strength suggest that CC inputs exert different influences on their target neurons depending on their looped connectivity. To test the functional implications of the selective innervation of infragranular looped IT neurons, we performed experiments in current clamp in the absence of channel blockers. We injected the same AAV-ChR2 in V2M and measured voltage changes and spiking activity of V2M-projecting L6 neurons in V1 upon photostimulation, comparing their responses to those of neighboring V2L-projecting neurons (***Figure 8***). The resting potential of both projection types was similar (looped: −72.35 ± 5.85 mV, non-looped: −74.52 ± 3.58 mV, p=0.38). In the absence of current injection, a brief LED light pulse resulted in depolarizations, but not spiking activity, in the recorded cells under these illumination conditions. Depolarizations were larger in looped IT L6 neurons than in non-looped ones (***Figure 8A–C***; mean amplitude; looped IT, 10.2 ± 4.8 mV; non-looped IT, 4.3 ± 3.2 mV, p=0.004, signed-rank test). We compared the relative magnitude of the evoked postsynaptic potentials using the CRACM Response Index (CRI), analogous to the SRI used in the sCRACM experiments (Materials and methods). The relative difference in input strength between looped and non-looped cells measured with current-clamp LED-induced responses was similar to that measured with

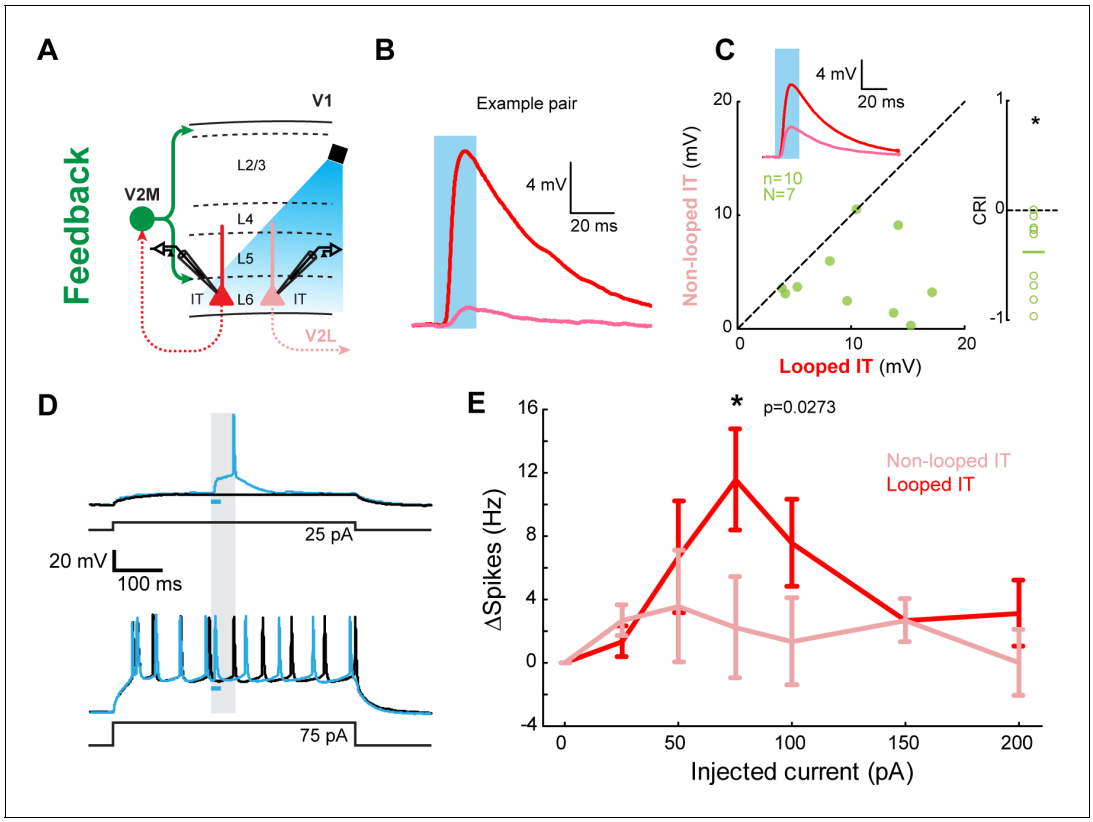

Figure 8. Feedback (FB) inputs in L6 can selectively modulate activity in looped intratelencephalic (IT) neurons. (**A**) Experiment configuration. In the absence of channel blockers, V2M→V1 FB axons were photostimulated using an LED during current-clamp recordings of looped and non-looped IT neurons in L6. (**B**) Example of excitatory postsynaptic potentials (EPSPs) from an example pair. Blue shade, light pulse. (**C**) Left, paired comparisons of EPSP amplitudes evoked in looped vs. non-looped IT neurons. Inset traces represent group averages for each projection class. Blue shade, light pulse. Right, CRACM Response Index (CRI) of the same data (n = 10, N = 7). (**D**) Example traces of FB modulation in a looped IT neuron. Cells were driven by a sustained positive current injection. Black traces, LED OFF trials; blue traces, LED ON trials. Blue bar, duration of the LED light pulse. Gray shading, time period used to analyze spiking activity in (**E**). (**E**) Spike rate difference between LED-ON and LED-OFF trials in looped and non-looped IT neurons as a function of the amount of current injected during the depolarization step. *, p=0.0273, paired t-test with Bonferroni correction for seven comparisons.

sCRACM (*Figure 8C*, *Figure 4—figure supplement 1* and *Figure 2—figure supplement 2*; current-clamp CRI: −0.38 ± 0.35; sCRACM total input SRI with AAV2/1: −0.39 ± 0.36; sCRACM total input SRI with AAV5: −0.52 ± 0.39), indicating that sCRACM reflects actual input strength in the functioning circuit. We then asked how V2M→V1 FB combines with bottom-up input in looped and non-looped L6 IT neurons. We injected steps of positive current at the soma through the recording pipette to mimic bottom-up depolarization, and measured evoked spiking activity while photostimulating FB axons (*Figure 8D–E*). Photoactivation of V2M→V1 axons induced additional spiking activity over a range of current injections (*Figure 8D–E*). Looped neurons spiked more frequently upon FB photoactivation than their non-looped neighbors (*Figure 8E*). Thus, stronger FB innervation of looped IT neurons in L6 can selectively modify their spiking activity when they are concurrently depolarized by other inputs.

Discussion

We comprehensively measured the connection strength of several ascending and descending projections to the three major classes of cortical projection neurons across layers and across areas. We found that both FF and FB preferentially innervated looped over non-looped neurons in the infragranular layers, but not in the supragranular layers, resulting in a selective modulation of spiking activity in looped neurons. Furthermore, by mapping the dendritic locations of CC synaptic inputs, we show that targeting of looped neurons is often highly subcellular, with many projections showing selectivity for the apical domains of looped neurons, but not for their basal domains.

Looped connectivity in CC interactions

Consistent with previous reports, we found that CC axons provide inputs to all neurons regardless of their projection type (*DeNardo et al., 2015*; *Kim et al., 2015*; *Kinnischtzke et al., 2016*; *Yamawaki et al., 2016*). However, input strength was consistently different across projection classes. When comparing looped IT neurons with neighboring subcortical-projecting PT or CT neurons, both FF and FB inputs always innervated looped IT neurons more strongly. Given the distinct gene-expression profiles of IT, PT, and CT neurons (*Tasic et al., 2018*), the preferential wiring of FF and FB axons to IT neurons could be guided by projection-type specific molecular cues. These findings accord with rabies virus (RV)-mediated trans-synaptic retrograde tracing experiments reporting that V1 IT neurons receive a larger proportion of their monosynaptic inputs from higher visual cortices than do V1 PT neurons (*Kim et al., 2015*). They are also consistent with studies showing that FF inputs from V1 to frontal cortices preferentially innervate looped neurons over PT neurons (*Zhang et al., 2016*) and that looped IT neurons in L6 of somatosensory cortex receive stronger input from motor cortex than subcortically projecting neurons (*Kinnischtzke et al., 2016*). Conversely, inputs from retrosplenial cortex to primary motor cortex do not show a preference for IT over CT or PT neurons (*Yamawaki et al., 2016*). Similarly, while we found a strong preference of V2L inputs for IT over CT neurons, single-cell RV tracings in V1 L6 found that CT neurons had a greater fraction of presynaptic partners from other cortical areas than IT neurons (*Vélez-Fort et al., 2014*). It remains to be elucidated to what extent these dissimilarities are due to differing selectivity across CC pathways for projection neuron types. Alternatively, since in many cases we found that projection-type specificity was present only for inputs terminating in the apical dendrites (*Figure 5*, *Figure 5—figure supplement 1*), selectivity for IT neurons may have been missed in previous studies using methods that cannot distinguish input strength in different dendritic compartments.

All the projections in this study contacted looped IT neurons, consistent with previous reports from the visual (*Johnson and Burkhalter, 1997*; *Kim et al., 2020*), somatosensory (*Kinnischtzke et al., 2016*), frontal (*Zhang et al., 2016*), and motor (*Mao et al., 2011*; *Yamawaki et al., 2016*) cortices. We extended these previous observations by comparing inputs to looped and non-looped IT neurons, and finding selectively stronger connections in looped over non-looped neurons in seven out of eight tested projections targeting infragranular layers. Thus, for all CC visual afferents in this study, IT neurons were the principal excitatory targets in deep layers, and in most of these cases, looped IT neurons were the main recipients.

The specificity of CC connections for looped neurons in infragranular layers was not absolute, as we detected monosynaptic CC inputs in all cell types. However, our measurements likely underestimate the selectivity of CC inputs for looped neurons. First, many, if not most, projection neurons

target multiple cortical areas (**Economo et al., 2016**; **Han et al., 2018**). Thus, since retrograde tracer injections only label a fraction of neurons projecting to the injection site, some non-looped neurons might in fact send a looped projection despite not being retrogradely labeled, thereby reducing our observed specificity for looped neurons. Second, looped connectivity would also be underestimated if it only involves CC afferents originating from a specific layer, as we expressed ChR2 non-specifically in projection neurons spanning multiple layers. Future experiments with layer-specific transgenic mouse lines (**Harris et al., 2019**) will make it possible to compare the specificity of projections with different laminar origins.

FF and FB connections to L2/3 neurons were consistently different from those targeting deeper neurons as they showed either no predilection for forming monosynaptic loops (three out of four projections), or were stronger, not weaker, when contacting non-looped IT neurons (V1→V2M). Pairs of L2/3 neurons were biased to upper L2/3 when measuring FB inputs and biased to lower L2/3 when measuring FF inputs (**Figure 2—figure supplement 1**). Thus, we cannot discard that FB connections also show a preference for non-looped neurons when targeting lower L2/3, as V1→V2M FF inputs do. While the axons of most L2/3 neurons branch to innervate multiple cortical areas, especially those of V1 neurons projecting to V2L (**Han et al., 2018**), the absence of loop specificity in L2/3 is unlikely to be caused by looped neurons being misattributed as non-looped neurons due to incomplete labeling from tracer injections. This is because L5 showed looped connectivity despite having a larger percentage of neurons with bifurcating axons (**Figure 1**). A recent report using RV-mediated monosynaptic input tracing found that looped L2/3 neurons in V1 had a greater percentage of presynaptic partner cells in visual areas to which they projected (**Kim et al., 2020**). Given that FB input strength in looped and non-looped L2/3 cells is similar, the presence of more presynaptic partners in the higher visual areas to which L2/3 neurons project would be consistent with our results if FB synapses in looped cells were fewer or weaker than in non-looped ones, since number of presynaptic partners does not necessarily reflect input strength. Thus, the connectivity rules of CC projections in L2/3 are different from those in deep layers, in which neurons consistently received stronger inputs from areas they innervated.

While, overall, the selectivity for looped neurons followed similar laminar-specific patterns across CC projections as described above, there was some variability in the connectivity rules (**Figure 7**). One possibility is that our measurements are underpowered to detect weaker selectivity in some projections that would result in a more coherent picture across cortical inputs. Alternatively, the selectivity of CC inputs for looped neurons might vary across individual cortical projections. This would be consistent with the stronger selectivity we observed for IT over PT/CT neurons in visual cortices and the lack of such selectivity reported in motor cortex (**Yamawaki et al., 2016**).

A role for the apical tufts of IT neurons in looped hierarchical interactions

We found that both FF and FB inputs innervated the perisomatic and apical dendrites of L5 IT pyramidal neurons, but that they differed in their apical distribution. FB innervated the distal dendritic tufts in L1 while FF inputs extended along the apical shaft up to L2 (**Figure 3**, **Figure 3—figure supplement 1**). For both FF and FB projections to looped L5 neurons, we observed stronger selectivity for apical dendrites than for perisomatic ones (**Figure 5**, **Figure 7**). This preference was found in three out of the four CC projections studied (including in all FB pathways) when comparing looped with non-looped IT neurons, suggesting an important role for the apical dendritic trees of L5 IT neurons in many looped hierarchical interactions. Inputs to apical tufts might be selectively involved in recurrent computations, while perisomatic inputs might mediate other hierarchical exchanges. Through a dynamic interplay of active and passive membrane properties, the apical arbors of L5 pyramidal neurons can perform complex computations combining inputs from different dendritic compartments (**Larkum, 2013**; **London and Häusser, 2005**; **Stuart and Spruston, 2015**). The apical dendrites of L5 IT neurons are less well understood than those of PT neurons, being thinner and less experimentally tractable. Understanding hierarchical computations will require elucidating how looped L5 IT neurons integrate CC inputs in their distal tufts with inputs arriving in other dendritic regions.

While inputs to L2/3 neurons were for the most part equally strong in looped and non-looped IT neurons, FF inputs to V2M were selectively stronger, not weaker, when contacting dendrites of non-

looped IT neurons in L1 (***Figure 6D***). Thus, as with L5 neurons, distal input in L2/3 neurons might also be selectively involved in looped interactions, albeit with different rules.

Functional implications

The stronger innervation of looped neurons resulted in the selective modulation of their spiking and subthreshold activity in an ex vivo functioning circuit (***Figure 8***), showing that the connectional selectivity measured using sCRACM has functional consequences in cortical networks. The selective engagement of looped neurons by both FF and FB afferents supports several theories advocating looped computations in CC circuitry (***Bastos et al., 2012***; ***Guerguiev et al., 2017***; ***Keller and Mrsic-Flogel, 2018***; ***Mumford, 1992***; ***Rao and Ballard, 1999***; ***Richards and Lillicrap, 2019***; ***Roelfsema and Holtmaat, 2018***; ***Sacramento et al., 2018***). Our observations suggest that L5/6 IT neurons might be preferential players in the implementation of these long-range loops. CC inputs and postsynaptic neurons in their target area have similar tuning properties (***Glickfeld et al., 2013***; ***Huh et al., 2018***; ***Zhang et al., 2018***) and overlapping receptive fields (***Marques et al., 2018***). Thus, given the prominence of looped connectivity in FF and FB visual pathways, related visual signals are likely relayed back and forth between interconnected neurons located at different hierarchical levels.

According to recent models, looped FB innervation could allow neurons embedded in a hierarchical network to optimize synaptic weights toward the global desired output, akin to the backpropagation algorithm used to train artificial neural networks (***Guerguiev et al., 2017***; ***Lillicrap et al., 2016***; ***Richards and Lillicrap, 2019***; ***Roelfsema and Holtmaat, 2018***; ***Sacramento et al., 2018***). The apical dendrites of looped neurons are integral to many such models, wherein apical inputs trigger synaptic plasticity of basal inputs to instruct learning. Thus, selective targeting of the apical compartments of looped neurons by descending inputs, as observed here, may allow L5 IT neurons to update synaptic strengths based on activity in the higher-order areas that they project to. Such a role in looped interactions does not negate the involvement of apical dendrites in other non-looped computations. For example, we found that L5 PT neurons received weaker FB inputs in their distal tufts compared to L5 IT neurons (***Figure 5***), despite having more extensive dendrites in L1 (***Figure 5—figure supplement 2***). Since L5 PT neurons receive more inputs from frontal and associative areas than IT neurons (***Kim et al., 2015***), their thicker apical dendrites might be specialized in mediating top-down processes that do not require excitatory looped connectivity, such as brain state-dependent and attentional modulations of perceptual saliency (***Manita et al., 2015***; ***Takahashi et al., 2020***; ***Takahashi et al., 2016***; ***Zhang et al., 2014***).

Models in which descending projections modulate plasticity in lower-order synapses to optimize the global output of the network result in alignment of FF and FB weights, such that synaptic strengths between pairs of reciprocally connected neurons tend to become similar (***Guerguiev et al., 2017***; ***Lillicrap et al., 2016***; ***Sacramento et al., 2018***). Whether the neocortex follows such rules is a matter of speculation (***Lillicrap et al., 2020***; ***Richards and Lillicrap, 2019***; ***Roelfsema and Holtmaat, 2018***; ***Whittington and Bogacz, 2019***). In the presence of weight symmetry, FF and FB projection neurons would be expected to receive minimal input from areas they do not project to, and to receive strong input from areas that they do. Thus, alignment of synaptic weights between neuron pairs will lead to stronger average synaptic input to looped neurons from both ascending and descending pathways, as observed here. While our results are consistent with some degree of weight alignment in neocortical circuits, our experimental approach cannot prove the existence of symmetric synaptic weights in pairs of neurons at different hierarchical levels. It remains unknown whether the monosynaptic loops that we unveil here arise from pairs of neurons selectively targeting each other in a recurrent loop. Given that ChR2 was expressed in multiple presynaptic neurons, our experiments measured the selectivity of afferent populations and do not have the resolution to resolve interareal loops with single-cell resolution. There is evidence that L5/6 cortical neurons receive long-range CC inputs preferentially from L5/6 neurons (***DeNardo et al., 2015***). Moreover, L6 IT neurons innervate deep layers in their target areas (***Tasic et al., 2018***), and L5 IT neurons have access to corresponding L5 IT neurons in distant cortical regions, as indicated by their axonal arborization pattern (***Harris et al., 2019***; ***Tasic et al., 2018***). Thus, while our findings and the laminar distribution of CC connections are consistent with pairs of same-layer neurons in different cortical areas selectively engaging in bidirectional monosynaptic loops, the prevalence of such a circuit arrangement has yet to be determined. Since input strength in L2/3 neurons was either independent of looped connectivity or weaker in looped neurons, synaptic weight symmetry, if present,

might selectively involve deep cortical layers and not superficial ones. Thus, hierarchical learning resulting in synaptic weight symmetry could also be laminar-specific.

Our observations reported here suggest that recurrent interareal cortical interactions may play different roles in supragranular and infragranular layers. They also provide a framework for future work on the role of projection neurons in different cortical layers in recurrent hierarchical processes.

Materials and methods

Key resources table

Reagent type (species) or resource	Designation	Source or reference	Identifiers	Additional information
Strain, strain background (*Mus musculus*)	C57BL/6	Jackson Laboratory	JAX:000664, RRID:IMSR_JAX:000664	Bred in-house
Antibody	Anti-GFP (rabbit polyclonal)	Thermo Fisher	Catalog # A-6455, RRID: AB_221570	(1:1000)
Antibody	Alexa Fluor 488-conjugated secondary antibody	Thermo Fisher	Catalog # A-11008, RRID:AB_143165	(1:1000)
Recombinant DNA reagent	AAV-2/1-CAG-ChR2-Venus	Addgene	RRID:Addgene_20071	
Recombinant DNA reagent	AAV5-CaMKIIa-hChR2(H134R)-EYFP	Addgene	RRID:Addgene_26969	
Recombinant DNA reagent	AAV2/1-synapsin-EGFP	UPenn Vector Core	RRID:Addgene_105539	
Peptide, recombinant protein	Cholera toxin B (Alexa Fluor 647)	Thermo Fisher	Catalog #: C34778	1 mg/ml
Chemical compound, drug	Red Retrobeads IX	Lumafluor		
Software, algorithm	Ephus	Vidrio Technologies ***Suter et al., 2010***	PMID:21960959	

Animal surgeries

All procedures were reviewed by the Champalimaud Centre for the Unknown Ethics Committee and performed in accordance with the Portuguese Veterinary General Direction guidelines. Surgeries were conducted in either male or female C57BL/6J mice (P26−P28) under anesthesia (intraperitoneal, 37.5 mg/kg ketamine, 0.5 mg/kg medetomidine). Virus expressing ChR2 (AAV-2/1-CAG-Channelrhodopsin-2-Venus, Addgene #20071; 20–25 nl, titer ~5×10^{12} vg/ml) was delivered intracortically either to V1 to label FF projections or V2L/V2M to label FB projections, and co-injected with red-fluorescent microspheres (Red Retrobeads IX, Lumafluor; 10–12.5 nl) to retrogradely label cells projecting to the source of FF/FB input. A second retrograde tracer (Cholera toxin subunit B, Alexa Fluor 647 Conjugate, Thermo Fisher, 50–60 nl, 1.0 mg/ml) was injected elsewhere to label cells projecting to a different cortical or subcortical area. For axonal quantification, we used AAV2/1-synapsin-EGFP (Penn Vector Core p1696, ~5×10^{12} vg/ml). For ***Figure 2—figure supplement 2***, we replaced AAV-2/1-CAG-Channelrhodopsin-2-Venus with AAV5-CaMKIIa-hChR2(H134R)-EYFP (Addgene #26969, ~0.5×10^{12} vg/ml) when injecting in V2M. Pulled glass injection pipettes (Drummond Scientific) had tip diameter of 15–20 µm. Stereotaxic coordinates for V1 and V2L were measured from the midline and from the posterior-most point of the transverse sinus (lateral of midline/anterior of transverse sinus/depth in mm): V1 (2.3/1.3/0.775), V2L (3.5/1.7/0.9). Stereotaxic coordinates for V2M and SC were measured from the midline and from the sinus confluence, the point at which the transverse sinuses meet the superior sagittal sinus (lateral of midline/anterior of sinus confluence/depth in mm): V2M (1.6/1.25/0.8), SC (0.5/0.4/1.5 and 1.8). We verified the accuracy of V2L and V2M

coordinates by identifying the borders of visual areas relative to the injection sites in vivo in a subset of animals (***Figure 1—figure supplement 1***). Animals were injected in V2L and V2M with red-fluorescent latex microspheres as described above. Approximately 30 days later, a circular craniotomy was performed over the visual cortex (diameter: 4 mm) and an imaging window was embedded into the craniotomy and secured in place using black dental cement. A custom-designed iron headpost was attached to the skull with dental acrylic. Intrinsic signal imaging was performed to identify the position of the visual areas relative to the injection sites as previously described (***Garrett et al., 2014***; ***Marques et al., 2018***; ***Figure 1—figure supplement 1***). In 7/7 mice screened, both V2L and V2M injections were located outside the borders of V1. V2L injections targeted mainly the lateromedial (LM) visual cortex, while V2M injections labeled the anteromedial (AM) and/or anterior part of the posteromedial (PM) visual cortices (***Wang and Burkhalter, 2007***). To label CT neurons, injections of retrograde tracers were targeted to the dorsal lateral geniculate nucleus (dLGN) for V1 recordings, and the lateral posterior nucleus (LP) of the thalamus for V2L recordings. Stereotactic coordinates were measured from the midline and from bregma (lateral of midline/posterior of bregma/depth in mm): dLGN (2.3/1.75/2.8), LP (1.35/1.75/2.65 and 2.85). We cannot discard the possibility that cholera toxin injections were not entirely confined to either dLGN or LP and encompassed both nuclei in some cases. Animals were maintained at 37˚C on a heating pad during surgery and returned to their home cages after surgery (maximum of five animals per cage). All animals were housed in a room with a regular 12 hr light/dark cycle.

Slice preparation

Fourteen to 20 days (age range P40–P48) after the surgery, mice were decapitated under deep anesthesia (isoflurane) and brains were dissected in ice-cold choline chloride solution (110 mM choline chloride, 25 mM $NaHCO_3$, 25 mM D-glucose, 11.6 mM sodium ascorbate, 7 mM $MgCl_2$, 3.1 mM sodium pyruvate, 2.5 mM KCl, 1.25 mM NaH_2PO_4, and 0.5 mM $CaCl_2$ [Sigma]; aerated with 95% O_2/5% CO_2) and sectioned in 300-µm-thick coronal slices using a Leica VT1200S vibratome. Slices were then incubated for 30 min at 37˚C in artificial cerebrospinal fluid (127 mM NaCl, 25 mM $NaHCO_3$, 25 mM D-glucose, 2.5 mM KCl, 1 mM $MgCl_2$, 2 mM $CaCl_2$, and 1.25 mM NaH_2PO_4 (Sigma); aerated with 95% O_2/5% CO_2).

Electrophysiology and photostimulation

Neurons were patched with borosilicate pipettes (resistance 3–5 MΩ, Werner Instruments) filled with potassium gluconate intracellular solution (128 mM potassium gluconate, 4 mM $MgCl_2$, 10 mM HEPES, 1 mM EGTA, 4 mM Na_2ATP, 0.4 mM Na_2GTP, 10 mM sodium phosphocreatine, 3 mM sodium L-ascorbate, 3 mg/ml biocytin [Sigma] and 5 µg/ml Alexa Fluor 488 dye [Thermo Fisher Scientific]; pH 7.25, 290 mOsm). All sCRACM recordings were performed at room temperature (22–24˚C) and with the presence of TTX (1 µM), CPP (5 µM), and 4-AP (100 µM) in the bath. For ***Figure 5—figure supplement 4***, ZD7288 (10 µM) was also applied to control for I_h differences between cell types. Areas V2L and V2M were identified by the presence of Venus-expressing FF axons. When measuring FB input strength, we verified that V2L or V2M injections resulted in the expected laminar distribution of Venus-expressing axons in V1 (***Figure 1C*** and ***Figure 2—figure supplement 2***) in the recorded slice. For sCRACM mapping, fluorescent-positive cells were recorded sequentially in voltage clamp (−70 mV) at depths of >30 µm in the same slice. Double-labeled cells were not recorded. A blue laser (473 nm, Cobolt Laser) was used for photostimulation to evoke EPSCs. Duration (1 or 4 ms) and intensity (0.1–1.1 µW) of light pulses were controlled with a Pockels cell (ConOptics) and a shutter (Thorlabs). The laser beam (diameter ~15 µm, not taking into account tissue scattering) was rapidly repositioned using galvanometer mirrors (Thorlabs) and delivered through an air immersion objective (Olympus 4X, NA 0.1) on either a 16 × 16 grid (L2/3 cells) or a 12 × 24 grid (L5 and L6 cells) with 50 µm spacing and 400 ms inter-stimulus interval. Stimuli were given in a spatial sequence pattern designed to maximize the time between neighboring locations. The stimulus pattern was flipped and rotated between maps to avoid sequence-specific responses. sCRACM maps were repeated two to five times for each cell. Laser power was manually adjusted in each experiment using a graduated neutral density filter (Edmund Optics) so that peak amplitudes smaller than 100 pA were evoked in the most excitable locations for the first recorded cell in the pair. Pairs of different projection neurons recorded at similar cortical depths in the same layer and in close proximity

(mean ± s.d.: 73.27 ± 47.41 μm) were photostimulated using the same laser power and pulse duration. The order in which cell types were recorded alternated between pairs. Data were acquired with a Multi clamp 700B amplifier (Axon Instruments) and digitalized with National Instruments acquisition boards controlled under Matlab using Ephus (***Suter et al., 2010***).

Current-clamp experiments

To examine the functional impact of selective looped interactions (***Figure 8***), recordings were performed in current clamp in the absence of channel blockers and at near-physiological temperatures (34˚C). Neurons were photostimulated with 20 ms pulses from a blue LED (Cairn Research) through a water immersion objective (Olympus 60X, NA1.0, 20 μW at the focal point). Steps of positive current (0–200 pA, 500 ms duration) were injected every second. Trials with and without the LED pulses were interleaved. In trials with current injection, the LED light pulse began 200 ms after current step onset. We compared the mean amplitude of the LED-evoked excitatory postsynaptic potentials in trials without current injection to measure synaptic strength (***Figure 8C***). Spike frequency in a 0–50 ms window after LED onset was averaged across five trials and compared in ***Figure 8E***.

Immunohistochemistry and dendritic reconstructions

After whole-cell recordings, biocytin-filled neurons were fixed overnight in 4% paraformaldehyde (PFA) at 4˚C and transferred to phosphate-buffered saline the following day. Prior to staining, slices were rinsed in phosphate buffer (PB) 0.1 M. Endogenous peroxidases were quenched with 1% H_2O_2 (Sigma) in PB 0.1 M for 45 min at room temperature. Slices were rinsed again in PB 0.1 M and incubated in the ABC reaction (Vector Laboratories) for ~12 hr at room temperature (22–24˚C). After successive PB 0.1 M and Tris-buffered saline (TBS) washings, slices were subjected to the diaminobenzidine (DAB) reaction for 30–50 min (using 30 ml of TBS, 90 μl 3% H_2O_2, 225 μl of $NiCl_2$ (250 mM), and 7 mg of DAB [Sigma]). The DAB reaction was stopped with TBS. Slices were mounted and coverslipped with Mowiol mounting medium. Dendrites were reconstructed with Neurolucida software (MBF Bioscience) using the 40x magnification objective lens of an Olympus BX61 microscope. Tracings were imported into Matlab, corrected for shrinkage and analyzed using custom routines. Dendritic length density was calculated in 50 μm bins and interpolated for display.

Laminar distribution of projection neuron subtypes and FF/FB axons

Injected animals were intracardially perfused with 4% PFA 14 days post-surgery and cryostat-sectioned in 20-μm-thick coronal slices. Slices were stained with 4′,6-diamidino-2-phenylindole dihydrochloride (DAPI) and imaged with the 20× objective of a Zeiss AxioImager M2 widefield fluorescence microscope. For quantification of different projection neurons in V1/V2L cortex (***Figure 1A, B***), three animals were used per dataset (eight slices per animal). Cells were counted within a 1000 × 1000 μm (V1) or 600 × 1000 μm (V2L) area. To normalize cell depth, fractional cortical depth (pia–cell distance/pia–white matter distance) was multiplied by average cortical thickness across the eight slices. For quantification of axons (***Figure 1C,D***), three animals were analyzed for both FF and FB datasets (eight slices per animal). Vertical fluorescence profiles of GFP-expressing axons were measured using ImageJ after subtracting background fluorescence from a hippocampal area devoid of labeled axons or somata.

Quantification of retrograde infection of ChR2-expressing AAVs

We verified that AAV-2/1-CAG-ChannelrhodopsIn-2-Venus led to minimal retrograde infection in several ways (***Figure 2—figure supplement 2***). While Venus-labeled axons were clearly visible in target regions in unstained sections, Venus-positive somata were undetectable in these regions. In coronal slices stained with rabbit anti-GFP polyclonal antibody (1:1000 dilution, Thermo Fisher, catalog #A-6455) and Alexa Fluor 488-conjugated secondary antibody (1:1000 dilution, Thermo Fisher, catalog #A-11008) to boost Venus fluorescence, we detected a very small number of Venus-positive somata (***Figure 2—figure supplement 2***). In 20 μm sections of V1, we found 2.60 ± 0.94 Venus-expressing neurons/mm^2 (n = 3, V2M-injected mice). We also stained sections (n = 3 mice) for the neural marker NeuN (rabbit monoclonal, 1:1500 dilution, Abcam, catalog #ab177487), followed by an Alexa Fluor 647-conjugated secondary antibody (donkey polyclonal, 1:800 dilution, Jackson ImmunoResearch, catalog #711-605-152) and measured the density of neurons in V1 sections using

Cellpose (***Stringer et al., 2021***). From these counts we estimate that retrogradely infected neurons expressing ChR2 comprise 1 out of every 1282 ± 578 $NeuN^+$ V1 neurons (n = 3). In addition to these anatomical analyses, we also analyzed the onset of the sCRACM response in looped neurons to verify that they did not express ChR2 (***Figure 2—figure supplement 2***). We were able to detect early-onset (<2 ms) responses, consistent with a non-synaptic ChR2-induced current, in 10/235 (4.2%) of the recorded looped IT neurons. These 10 neurons were removed from further analysis. Together, these analyses suggest that, given their sparsity, collaterals of neurons retrogradely infected with ChR2 are unlikely to contribute to our measurements. We also conducted additional recordings using AAV5-ChR2 (AAV5-CaMKIIa-hChR2(H134R)-EYFP) to examine whether the small number of neurons retrogradely infected with AAV2/1-ChR2 could nevertheless be contributing to the stronger inputs in looped IT neurons (***Figure 2—figure supplement 2***). Consistent with previous results (***Kinnischtzke et al., 2014***), we found that the AAV5 resulted in less retrograde infection than AAV-2/1-CAG-Channelrhodopsin-2-Venus in sections immunostained with anti-GFP antibody (number of retrogradely infected neurons per mm^2 in 20-μm-thick V1 sections, 0.49 ± 0.20; fraction of $NeuN^+$ V1 neurons, 1 in 7009 ± 3434, n = 3 mice). None of the recorded looped IT neurons displayed early EPSC onset with AAV5 (n = 11, ***Figure 2—figure supplement 2***). Despite the significantly lower density of retrogradely infected cells expressing ChR2 in AAV5 compared to AAV2/1 (AAV2/1-AAV5 density ratio = 5.6, p=0.0465, t-test), the relative strength of V2M→V1 inputs in looped vs. non-looped L6 IT neurons was similar using the two AAVs (***Figure 2—figure supplement 2***; total SRI, AAV2/1, −0.39 ± 0.36; AAV5, −0.52 ± 0.39, p=0.476). We conclude that local collaterals from the small number of neurons retrogradely infected with AAV2/1-ChR2 do not contribute significantly to the measurement of CC input strength.

Data analysis

In electrophysiological recordings, the boundaries between layers were established as L1: pia−90 μm; L2/3: 90–350 μm; L4: 350–450 μm; L5: 450–650 μm; L6 650–950 μm. To correct for differences in cortical thickness due to variability in slicing angle of brain sections, the fractional cortical depth of each recorded neuron was positioned on a reference cortical slice with a thickness of 950 μm. Only pairs of cells with an intersomatic distance of <200 μm were included in analyses. In cases where multiple cells were recorded in the same slice, cells nearest each other were paired. Traces were baseline-substracted (baseline period: 50 ms before laser onset) and averaged across successive sCRACM maps. Average responses at each location were calculated as the mean EPSC 0–75 ms after laser onset and are therefore a measure of charge (***D'Souza et al., 2016***; ***Petreanu et al., 2009***). In ***Figure 3*** and ***Figure 3—figure supplement 1***, sCRACM maps were aligned by pia and soma position, respectively, and linearly interpolated for display. To calculate input strength, input at responsive locations (EPSC amplitude >5 standard deviations above baseline) was summed across the entire map or within the perisomatic or apical regions. The sign was flipped so that stronger inputs resulted in larger values. Pairs in which neither cell showed detectable input (total sCRACM input <20 pA) were discarded. To calculate the SRI, we required at least one cell with summed inputs >5 pA in the region of interest. The SRI was calculated as follows:

$$\frac{\sum Responses\ of\ non\ looped\ neuron\ - \sum responses\ of\ looped\ neuron}{\sum Responses\ of\ non\ looped\ neuron + \sum responses\ of\ looped\ neuron}$$

For inclusion in fraction-to-apical analyses, both cells in the pair required detectable input. Perisomatic and apical responses in neurons of different layers were calculated by summing inputs within a given cortical depth (L2/3: perisomatic 150–650 μm, L1: 0–50 μm; L5: perisomatic: 400–900 μm, L1: 0–150 μm for FB inputs, apical: 0–300 μm for FF inputs; L6: perisomatic: 600–950 μm, apical: 0–500 μm). For L5 datasets, pairs with any cut apical dendrites were discarded. Since many L2/3 neurons were located in upper L2/3, apical and perisomatic dendrites may be intermingled in L1 in some cases. Thus, responses in L1 could include inputs made on perisomatic and apical dendrites. We therefore refer to these as 'inputs in L1'. As the resolution of sCRACM is ~60 μm (***Petreanu et al., 2009***), to better distinguish inputs in L1 from those in L2/3, we removed responses in the two rows flanking the L1–L2/3 boundary when analyzing inputs in L1 and the perisomatic area of L2/3 neurons. For L6 neurons, we could not always verify the integrity of apical dendrites, thus when no difference in apical input is observed across cell types, this may be due to incomplete arbors. To compute

average traces in ***Figures 4–6***, ***Figure 4—figure supplement 1***, ***Figure 5—figure supplement 1***, ***Figure 5—figure supplement 4*** and ***Figure 6—figure supplement 1***, EPSCs at all locations in a given region of interest (perisomatic, apical, L1, or total) were averaged for each neuron, regardless of whether the location had a detectable light-evoked response, and subsequently averaged across neurons of the same projection class. To visualize the average subcellular distribution of inputs (***Figure 3***), only cells with sCRACM input >10 pA for at least one location were included.

To quantify relative synaptic strength in the current-clamp experiments (***Figure 8C***), we calculated the CRI as follows:

$$\frac{EPSP\,amplitude\,in\,non\,looped\,neuron - EPSP\,amplitude\,in\,looped\,neuron}{EPSP\,amplitude\,in\,non\,looped\,neuron + EPSP\,amplitude\,looped\,neuron}$$

SRI and CRI values were tested using the two-tailed Student's t-test, and fraction of inputs in the apical region were tested using the two-tailed Wilcoxon signed-rank test for paired samples. Data in the text is mean ± standard deviation. No statistical tests were used to predetermine the number of cell pairs, but our sample sizes are comparable to those in similar studies (***D'Souza et al., 2016***; ***Kinnischtzke et al., 2016***; ***Mao et al., 2011***; ***Morgenstern et al., 2016***; ***Yamawaki et al., 2016***; ***Yang et al., 2013***). All statistical analyses were performed with Matlab.

Simulations of passive dendritic filtering of L1 inputs

Traced dendrites of L5 neurons in V1 were imported into the NEURON simulation environment (***Hines and Carnevale, 1997***). We set the diameter of the somata, apical trunks, and apical tuft branches for the different projection neurons using manual measurements from biocytin-stained arbors (***Figure 5—figure supplement 2***). For each cell belonging to a given projection type, segments from the same dendritic compartment were assigned the same diameter value (apical trunk width, µm: SC-projecting, 1.7, V2M-projecting, 1.14; V2L-projecting, 1; apical tuft branch width, µm: SC-projecting, 0.7, V2M-projecting, 0.4, V2L-projecting, 0.43). The biophysical properties used for simulations were as follows: cytoplasmic resistivity, R_a = 35.4 cm; specific membrane capacitance, C_m = 1 F/cm^2; resting conductance, g_{pas} = 1/20,000; resting potential, E_{pas}=–65 mV. We applied a synaptic density of 0.2 synapses per µm of apical dendritic segment when distributing passive synapses over the apical tree. The location of synapses along individual dendritic segments was randomly determined, and synaptic conductance was approximated by an alpha function, with parameters τ=0.1 ms and g_{max} = 1 µS. For each neuron, we then simulated responses to apical tuft inputs under single-electrode voltage-clamp at the soma (−70 mV, 10 MΩ resistance), assuming no axonal selectivity for postsynaptic cell types. We conducted 100 simulations for each neuron and quantified the mean charge or amplitude measured at the soma (***Figure 5—figure supplement 3***). To measure input resistance (***Figure 5—figure supplement 3E***), we simulated somatic voltage-clamp recordings and measured input resistance using a −5 mV voltage step.

Acknowledgements

We thank N Yamawaki, B Atallah, and M Fridman for critical comments on the manuscript and J Sacramento and S Keemink for discussions. This work was supported by fellowships from Fundação para a Ciência e a Tecnologia to HY and BB, and by grants from Marie Curie (PCIG12-GA-2012-334353), la Caixa Banking Foundation (LCF/PR/HR17/52150005), and Fundação para a Ciência e a Tecnologia (LISBOA-01-0145-FEDER 030328 and Congento LISBOA-01-0145-FEDER-022170), co-financed by FCT (Portugal) and Lisboa2020, under the PORTUGAL2020 agreement (European Regional Development Fund) and the Champalimaud Foundation.

Additional information

Funding

Funder	Grant reference number	Author
"la Caixa" Foundation	LCF/PR/HR17/52150005	Leopoldo Petreanu
Fundação para a Ciência e a	LISBOA-01-0145-FEDER	Leopoldo Petreanu

Tecnologia	030328	
Fundação para a Ciência e a Tecnologia	Congento LISBOA-01-0145-FEDER-022170	Hedi Young Beatriz Belbut Margarida Baeta Leopoldo Petreanu
Fundação para a Ciência e a Tecnologia	SFRH/BD/52221/2013	Hedi Young
FP7 Marie-Curie Actions	PCIG12-GA-2012–334353	Leopoldo Petreanu
Fundação para a Ciência e a Tecnologia	SFRH/BD/148468/2019	Beatriz Belbut

The funders had no role in study design, data collection and interpretation, or the decision to submit the work for publication.

Author contributions

Hedi Young, Conceptualization, Data curation, Formal analysis, Investigation, Methodology, Writing - original draft, Writing - review and editing; Beatriz Belbut, Software, Investigation; Margarida Baeta, Data curation, Investigation, Visualization; Leopoldo Petreanu, Conceptualization, Resources, Formal analysis, Supervision, Funding acquisition, Visualization, Writing - original draft, Project administration, Writing - review and editing

Author ORCIDs

Beatriz Belbut http://orcid.org/0000-0003-0341-0585
Leopoldo Petreanu https://orcid.org/0000-0003-1434-4691

Ethics

Animal experimentation: All procedures were reviewed and performed in accordance with the Champalimaud Centre for the Unknown Ethics Committee and approved by the Portuguese Veterinary General Direction (Ref.No.0421/000/000/2019).

Decision letter and Author response

Decision letter https://doi.org/10.7554/eLife.59551.sa1
Author response https://doi.org/10.7554/eLife.59551.sa2

Additional files

Supplementary files

- Transparent reporting form

Data availability

All data are publicly available on Dryad https://doi.org/10.5061/dryad.1ns1rn8r7.

The following dataset was generated:

Author(s)	Year	Dataset title	Dataset URL	Database and Identifier
Young H, Belbut B, Baeta M, Petreanu L	2020	Laminar-specific cortico-cortical loops in mouse visual cortex	https://doi.org/10.5061/dryad.1ns1rn8r7	Dryad Digital Repository, 10.5061/dryad.1ns1rn8r7

References

Bastos AM, Usrey WM, Adams RA, Mangun GR, Fries P, Friston KJ. 2012. Canonical microcircuits for predictive coding. *Neuron* **76**:695–711. DOI: https://doi.org/10.1016/j.neuron.2012.10.038, PMID: 23177956

D'Souza RD, Meier AM, Bista P, Wang Q, Burkhalter A. 2016. Recruitment of inhibition and excitation across mouse visual cortex depends on the hierarchy of interconnecting Areas. *eLife* **5**:e19332. DOI: https://doi.org/10.7554/eLife.19332, PMID: 27669144

DeNardo LA, Berns DS, DeLoach K, Luo L. 2015. Connectivity of mouse somatosensory and prefrontal cortex examined with trans-synaptic tracing. *Nature Neuroscience* **18**:1687–1697. DOI: https://doi.org/10.1038/nn.4131, PMID: 26457553

Douglas RJ, Martin KA. 2004. Neuronal circuits of the neocortex. *Annual Review of Neuroscience* **27**:419–451. DOI: https://doi.org/10.1146/annurev.neuro.27.070203.144152, PMID: 15217339

D'Souza RDD, Wang Q, Ji W, Meier AM, Kennedy H, Knoblauch K, Burkhalter A. 2020. Canonical and noncanonical features of the mouse visual cortical hierarchy. *bioRxiv*. DOI: https://doi.org/10.1101/2020.03.30.016303

Economo MN, Clack NG, Lavis LD, Gerfen CR, Svoboda K, Myers EW, Chandrashekar J. 2016. A platform for brain-wide imaging and reconstruction of individual neurons. *eLife* **5**:e10566. DOI: https://doi.org/10.7554/eLife.10566, PMID: 26796534

Economo MN, Viswanathan S, Tasic B, Bas E, Winnubst J, Menon V, Graybuck LT, Nguyen TN, Smith KA, Yao Z, Wang L, Gerfen CR, Chandrashekar J, Zeng H, Looger LL, Svoboda K. 2018. Distinct descending motor cortex pathways and their roles in movement. *Nature* **563**:79–84. DOI: https://doi.org/10.1038/s41586-018-0642-9, PMID: 30382200

Felleman DJ, Van Essen DC. 1991. Distributed hierarchical processing in the primate cerebral cortex. *Cerebral Cortex* **1**:1–47. DOI: https://doi.org/10.1093/cercor/1.1.1, PMID: 1822724

Gămănuţ R, Kennedy H, Toroczkai Z, Ercsey-Ravasz M, Van Essen DC, Knoblauch K, Burkhalter A. 2018. The mouse cortical connectome, characterized by an Ultra-Dense cortical graph, maintains specificity by distinct connectivity profiles. *Neuron* **97**:698–715. DOI: https://doi.org/10.1016/j.neuron.2017.12.037, PMID: 29420935

Garrett ME, Nauhaus I, Marshel JH, Callaway EM. 2014. Topography and areal organization of mouse visual cortex. *Journal of Neuroscience* **34**:12587–12600. DOI: https://doi.org/10.1523/JNEUROSCI.1124-14.2014, PMID: 25209296

Gerfen CR, Economo MN, Chandrashekar J. 2018. Long distance projections of cortical pyramidal neurons. *Journal of Neuroscience Research* **96**:1467–1475. DOI: https://doi.org/10.1002/jnr.23978

Glickfeld LL, Andermann ML, Bonin V, Reid RC. 2013. Cortico-cortical projections in mouse visual cortex are functionally target specific. *Nature Neuroscience* **16**:219–226. DOI: https://doi.org/10.1038/nn.3300

Guerguiev J, Lillicrap TP, Richards BA. 2017. Towards deep learning with segregated dendrites. *eLife* **6**:e22901. DOI: https://doi.org/10.7554/eLife.22901, PMID: 29205151

Han Y, Kebschull JM, Campbell RAA, Cowan D, Imhof F, Zador AM, Mrsic-Flogel TD. 2018. The logic of single-cell projections from visual cortex. *Nature* **556**:51–56. DOI: https://doi.org/10.1038/nature26159

Harris JA, Mihalas S, Hirokawa KE, Whitesell JD, Choi H, Bernard A, Bohn P, Caldejon S, Casal L, Cho A, Feiner A, Feng D, Gaudreault N, Gerfen CR, Graddis N, Groblewski PA, Henry AM, Ho A, Howard R, Knox JE, et al. 2019. Hierarchical organization of cortical and thalamic connectivity. *Nature* **575**:195–202. DOI: https://doi.org/10.1038/s41586-019-1716-z, PMID: 31666704

Harris KD, Shepherd GMG. 2015. The neocortical circuit: themes and variations. *Nature Neuroscience* **18**:170–181. DOI: https://doi.org/10.1038/nn.3917

Hines ML, Carnevale NT. 1997. The NEURON simulation environment. *Neural Computation* **9**:1179–1209. DOI: https://doi.org/10.1162/neco.1997.9.6.1179, PMID: 9248061

Huh CYL, Peach JP, Bennett C, Vega RM, Hestrin S. 2018. Feature-Specific organization of feedback pathways in mouse visual cortex. *Current Biology : CB* **28**:114–120. DOI: https://doi.org/10.1016/j.cub.2017.11.056, PMID: 29276127

Johnson RR, Burkhalter A. 1997. A polysynaptic feedback circuit in rat visual cortex. *The Journal of Neuroscience* **17**:7129–7140. DOI: https://doi.org/10.1523/JNEUROSCI.17-18-07129.1997, PMID: 9278547

Keller GB, Mrsic-Flogel TD. 2018. Predictive processing: a canonical cortical computation. *Neuron* **100**:424–435. DOI: https://doi.org/10.1016/j.neuron.2018.10.003, PMID: 30359606

Kim EJ, Juavinett AL, Kyubwa EM, Jacobs MW, Callaway EM. 2015. Three types of cortical layer 5 neurons that differ in Brain-wide connectivity and function. *Neuron* **88**:1253–1267. DOI: https://doi.org/10.1016/j.neuron.2015.11.002, PMID: 26671462

Kim EJ, Zhang Z, Huang L, Ito-Cole T, Jacobs MW, Juavinett AL, Senturk G, Hu M, Ku M, Ecker JR, Callaway EM. 2020. Extraction of distinct neuronal cell types from within a genetically continuous population. *Neuron* **107**:274–282. DOI: https://doi.org/10.1016/j.neuron.2020.04.018, PMID: 32396852

Kinnischtzke AK, Simons DJ, Fanselow EE. 2014. Motor cortex broadly engages excitatory and inhibitory neurons in somatosensory barrel cortex. *Cerebral Cortex* **24**:2237–2248. DOI: https://doi.org/10.1093/cercor/bht085, PMID: 23547136

Kinnischtzke AK, Fanselow EE, Simons DJ. 2016. Target-specific M1 inputs to infragranular S1 pyramidal neurons. *Journal of Neurophysiology* **116**:1261–1274. DOI: https://doi.org/10.1152/jn.01032.2015

Larkum M. 2013. A cellular mechanism for cortical associations: an organizing principle for the cerebral cortex. *Trends in Neurosciences* **36**:141–151. DOI: https://doi.org/10.1016/j.tins.2012.11.006

Lillicrap TP, Cownden D, Tweed DB, Akerman CJ. 2016. Random synaptic feedback weights support error backpropagation for deep learning. *Nature Communications* **7**:13276. DOI: https://doi.org/10.1038/ncomms13276

Lillicrap TP, Santoro A, Marris L, Akerman CJ, Hinton G. 2020. Backpropagation and the brain. *Nature Reviews. Neuroscience* **21**:1–12. DOI: https://doi.org/10.1038/s41583-020-0277-3, PMID: 32303713

London M, Häusser M. 2005. Dendritic computation. *Annual Review of Neuroscience* **28**:503–532. DOI: https://doi.org/10.1146/annurev.neuro.28.061604.135703, PMID: 16033324

Manita S, Suzuki T, Homma C, Matsumoto T, Odagawa M, Yamada K, Ota K, Matsubara C, Inutsuka A, Sato M, Ohkura M, Yamanaka A, Yanagawa Y, Nakai J, Hayashi Y, Larkum ME, Murayama M. 2015. A Top-Down cortical circuit for accurate sensory perception. *Neuron* **86**:1304–1316. DOI: https://doi.org/10.1016/j.neuron.2015.05.006, PMID: 26004915

Mao T, Kusefoglu D, Hooks BM, Huber D, Petreanu L, Svoboda K. 2011. Long-range neuronal circuits underlying the interaction between sensory and motor cortex. *Neuron* **72**:111–123. DOI: https://doi.org/10.1016/j.neuron.2011.07.029, PMID: 21982373

Markov NT, Vezoli J, Chameau P, Falchier A, Quilodran R, Huissoud C, Lamy C, Misery P, Giroud P, Ullman S, Barone P, Dehay C, Knoblauch K, Kennedy H. 2013. The anatomy of hierarchy: feedforward and feedback pathways in macaque visual cortex. *The Journal of Comparative Neurology* **259**:225–259. DOI: https://doi.org/10.1002/cne.23458

Marques T, Nguyen J, Fioreze G, Petreanu L. 2018. The functional organization of cortical feedback inputs to primary visual cortex. *Nature Neuroscience* **21**:757–764. DOI: https://doi.org/10.1038/s41593-018-0135-z

Minamisawa G, Kwon SE, Chevée M, Brown SP, O'Connor DH. 2018. A Non-canonical feedback circuit for rapid interactions between somatosensory cortices. *Cell Reports* **23**:2718–2731. DOI: https://doi.org/10.1016/j.celrep.2018.04.115, PMID: 29847801

Morgenstern NA, Bourg J, Petreanu L. 2016. Multilaminar networks of cortical neurons integrate common inputs from sensory thalamus. *Nature Neuroscience* **19**:1034–1040. DOI: https://doi.org/10.1038/nn.4339

Mumford D. 1992. On the computational architecture of the neocortex. II. the role of cortico-cortical loops. *Biological Cybernetics* **66**:241–251. DOI: https://doi.org/10.1007/BF00198477, PMID: 1540675

Oh SW, Harris JA, Ng L, Winslow B, Cain N, Mihalas S, Wang Q, Lau C, Kuan L, Henry AM, Mortrud MT, Ouellette B, Nguyen TN, Sorensen SA, Slaughterbeck CR, Wakeman W, Li Y, Feng D, Ho A, Nicholas E, et al. 2014. A mesoscale connectome of the mouse brain. *Nature* **508**:207–214. DOI: https://doi.org/10.1038/nature13186, PMID: 24695228

Petreanu L, Mao T, Sternson SM, Svoboda K. 2009. The subcellular organization of neocortical excitatory connections. *Nature* **457**:1142–1145. DOI: https://doi.org/10.1038/nature07709

Rao RP, Ballard DH. 1999. Predictive coding in the visual cortex: a functional interpretation of some extra-classical receptive-field effects. *Nature Neuroscience* **2**:79–87. DOI: https://doi.org/10.1038/4580, PMID: 10195184

Richards BA, Lillicrap TP. 2019. Dendritic solutions to the credit assignment problem. *Current Opinion in Neurobiology* **54**:28–36. DOI: https://doi.org/10.1016/j.conb.2018.08.003

Roelfsema PR, Holtmaat A. 2018. Control of synaptic plasticity in deep cortical networks. *Nature Reviews Neuroscience* **19**:166–180. DOI: https://doi.org/10.1038/nrn.2018.6

Sacramento J, Costa RP, Bengio Y, Senn W, Costa RP, Senn W. 2018. Dendritic cortical microcircuits approximate the backpropagation algorithm. Advances in Neural Information Processing Systems 8721–8732.

Stringer C, Wang T, Michaelos M, Pachitariu M. 2021. Cellpose: a generalist algorithm for cellular segmentation. *Nature Methods* **18**:100–106. DOI: https://doi.org/10.1038/s41592-020-01018-x, PMID: 33318659

Stuart GJ, Spruston N. 2015. Dendritic integration: 60 years of progress. *Nature Neuroscience* **18**:1713–1721. DOI: https://doi.org/10.1038/nn.4157, PMID: 26605882

Suter B, O'Connor T, Iyer V, Petreanu L, Hooks BM, Kiritani T, Svoboda K, Shepherd GMG. 2010. Ephus: multipurpose data acquisition software for neuroscience experiments. *Frontiers in Neural Circuits* **4**:100. DOI: https://doi.org/10.3389/fncir.2010.00100

Takahashi N, Oertner TG, Hegemann P, Larkum ME. 2016. Active cortical dendrites modulate perception. *Science*. **354**:1587–1590. DOI: https://doi.org/10.1126/science.aah6066

Takahashi N, Ebner C, Sigl-Glöckner J, Moberg S, Nierwetberg S, Larkum ME. 2020. Active dendritic currents gate descending cortical outputs in perception. *Nature Neuroscience* **23**:1277–1285. DOI: https://doi.org/10.1038/s41593-020-0677-8, PMID: 32747790

Tasic B, Yao Z, Graybuck LT, Smith KA, Nguyen TN, Bertagnolli D, Goldy J, Garren E, Economo MN, Viswanathan S, Penn O, Bakken T, Menon V, Miller J, Fong O, Hirokawa KE, Lathia K, Rimorin C, Tieu M, Larsen R, et al. 2018. Shared and distinct transcriptomic cell types across neocortical Areas. *Nature* **563**:72–78. DOI: https://doi.org/10.1038/s41586-018-0654-5, PMID: 30382198

Vélez-Fort M, Rousseau CV, Niedworok CJ, Wickersham IR, Rancz EA, Brown AP, Strom M, Margrie TW. 2014. The stimulus selectivity and connectivity of layer six principal cells reveals cortical microcircuits underlying visual processing. *Neuron* **83**:1431–1443. DOI: https://doi.org/10.1016/j.neuron.2014.08.001, PMID: 25175879

Wang Q, Burkhalter A. 2007. Area map of mouse visual cortex. *The Journal of Comparative Neurology* **502**:339–357. DOI: https://doi.org/10.1002/cne.21286

Whittington JCR, Bogacz R. 2019. Theories of error Back-Propagation in the brain. *Trends in Cognitive Sciences* **23**:235–250. DOI: https://doi.org/10.1016/j.tics.2018.12.005, PMID: 30704969

Williams SR, Mitchell SJ. 2008. Direct measurement of somatic voltage clamp errors in central neurons. *Nature Neuroscience* **11**:790–798. DOI: https://doi.org/10.1038/nn.2137, PMID: 18552844

Yamawaki N, Radulovic J, Shepherd GM. 2016. A corticocortical circuit directly links retrosplenial cortex to M2 in the mouse. *The Journal of Neuroscience* **36**:9365–9374. DOI: https://doi.org/10.1523/JNEUROSCI.1099-16.2016, PMID: 27605612

Yang W, Carrasquillo Y, Hooks BM, Nerbonne JM, Burkhalter A. 2013. Distinct balance of excitation and inhibition in an interareal feedforward and feedback circuit of mouse visual cortex. *Journal of Neuroscience* **33**:17373–17384. DOI: https://doi.org/10.1523/JNEUROSCI.2515-13.2013, PMID: 24174670

Zhang S, Xu M, Kamigaki T, Hoang Do JP, Chang WC, Jenvay S, Miyamichi K, Luo L, Dan Y. 2014. Selective attention. Long-range and local circuits for top-down modulation of visual cortex processing. *Science* **345**:660–665. DOI: https://doi.org/10.1126/science.1254126, PMID: 25104383

Zhang S, Xu M, Chang W-C, Ma C, Hoang Do JP, Jeong D, Lei T, Fan JL, Dan Y. 2016. Organization of long-range inputs and outputs of frontal cortex for top-down control. *Nature Neuroscience* **19**:1733–1742. DOI: https://doi.org/10.1038/nn.4417

Zhang QF, Li H, Chen M, Guo A, Wen Y, Poo MM. 2018. Functional organization of intrinsic and feedback presynaptic inputs in the primary visual cortex. *PNAS* **115**:E5174–E5182. DOI: https://doi.org/10.1073/pnas.1719711115, PMID: 29760100

Zingg B, Hintiryan H, Gou L, Song MY, Bay M, Bienkowski MS, Foster NN, Yamashita S, Bowman I, Toga AW, Dong HW. 2014. Neural networks of the mouse neocortex. *Cell* **156**:1096–1111. DOI: https://doi.org/10.1016/j.cell.2014.02.023, PMID: 24581503

Figures and figure supplements

Laminar-specific cortico-cortical loops in mouse visual cortex

Hedi Young *et al*

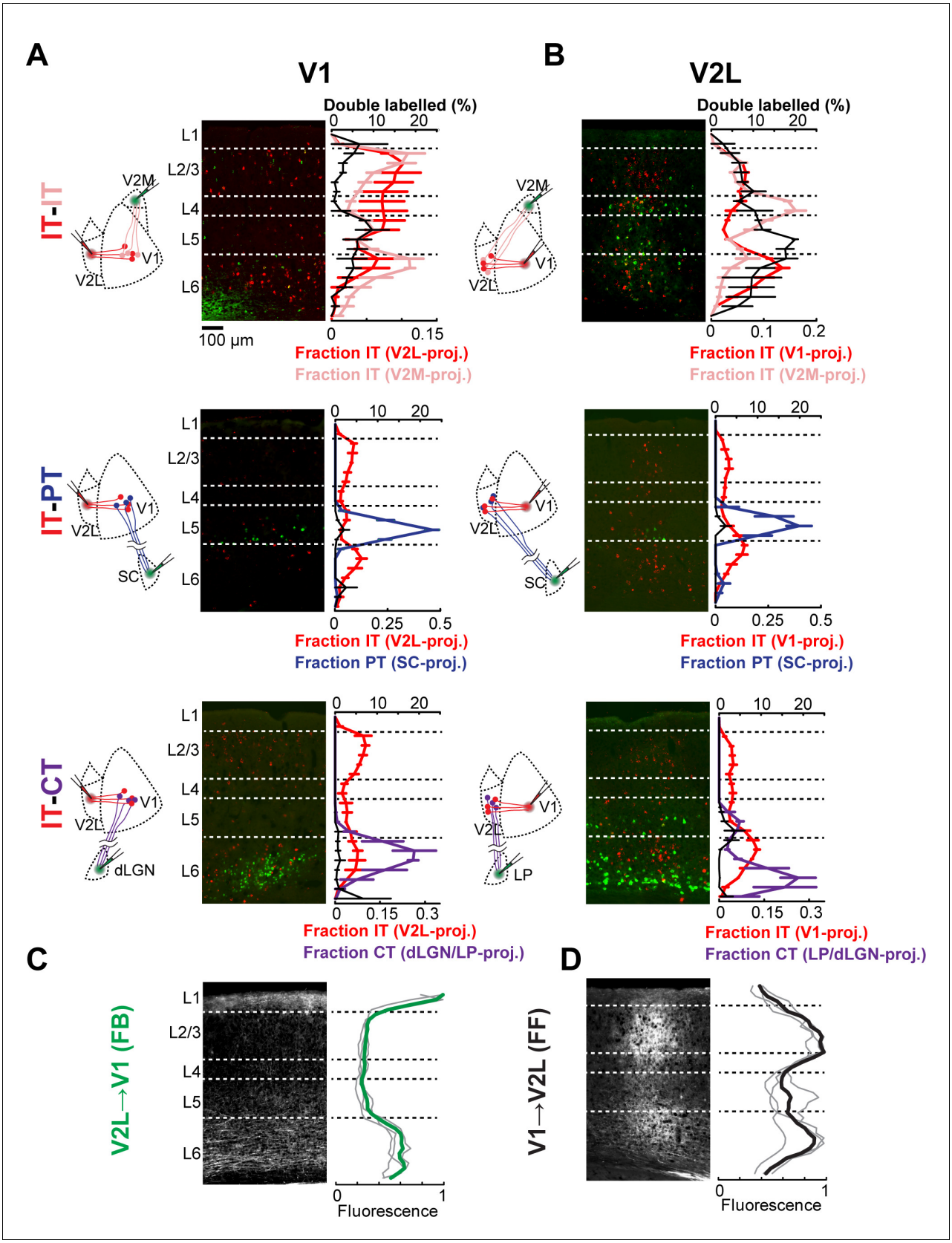

Figure 1. Cortical neurons projecting to different areas are intermingled and accessible to feedforward (FF) and feedback (FB) axons. (**A**) Distribution of retrogradely labeled projection neurons in primary visual cortex (V1) after injection of a red-fluorescent tracer in lateral visual areas (V2L) and an

Figure 1 continued on next page

Figure 1 continued

infrared-fluorescent tracer in either medial visual areas (V2M), superior colliculus (SC), or visual thalamus. Left, experimental configuration; center, representative fluorescent histological section, with infrared fluorescence shown in green; right, colored traces show the mean laminar distribution of the different projection neurons binned in 50 μm increments, while the black trace shows the percentage of retrogradely labeled neurons that are double-labeled at each depth (n = 3 animals per group). Error bars, standard error; dashed lines, approximate layer boundaries. (**B**) Distribution of retrogradely labeled projection neurons in V2L after injection of a red-fluorescent tracer in V1 and an infrared-fluorescent tracer in either V2M, SC, or visual thalamus (n = 3 animals per group). (**C**) Distribution of anterogradely labeled V2L FB axons in V1. Left, representative fluorescent histological section; right, axonal fluorescence across cortical depth binned in 50 μm increments. Individual mice, thin gray traces; average, thick green trace (n = 3 animals). (**D**) Distribution of anterogradely labeled V1 FF axons in V2L (n = 3 animals).

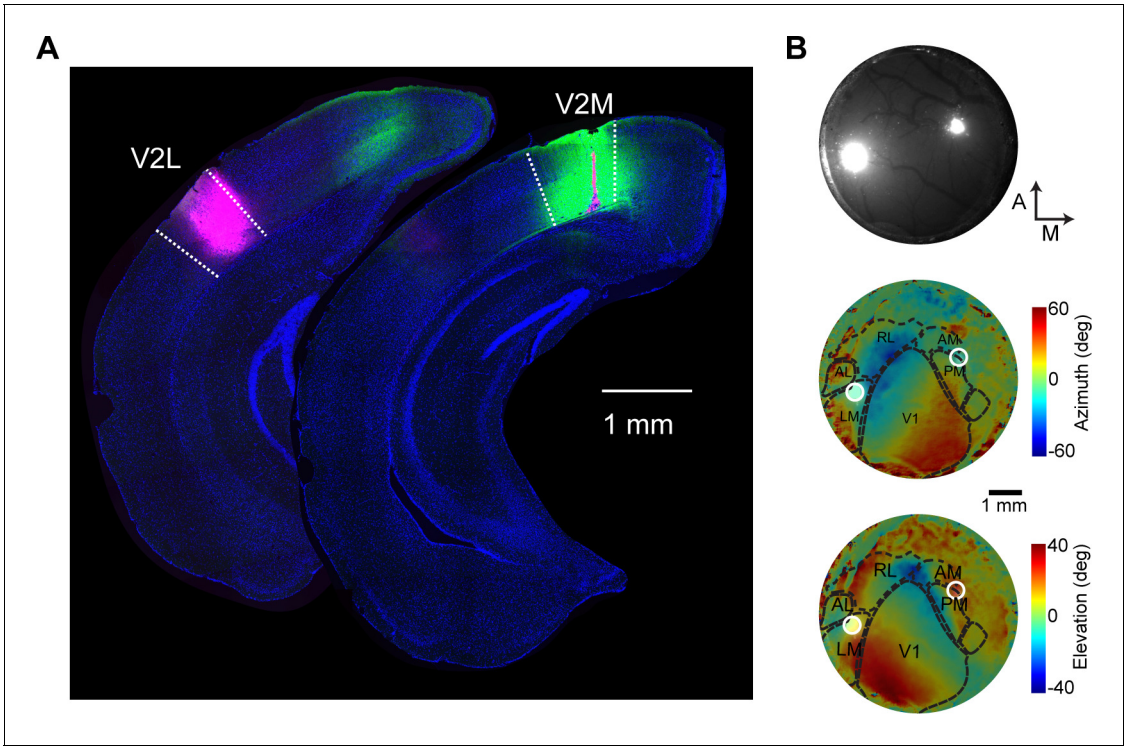

Figure 1—figure supplement 1. Histological and in vivo verification of lateral visual (V2L) and medial visual (V2M) area injection sites. (**A**) Example coronal sections of a brain injected in V2L and V2M. (**B**) Example injections in V2L and V2M visualized in vivo. Top, image of the brain vasculature and injection sites. Middle, injection sites and area borders overlaid on the azimuth map determined by intrinsic signal imaging. Bottom, elevation map. White circles, injection sites.

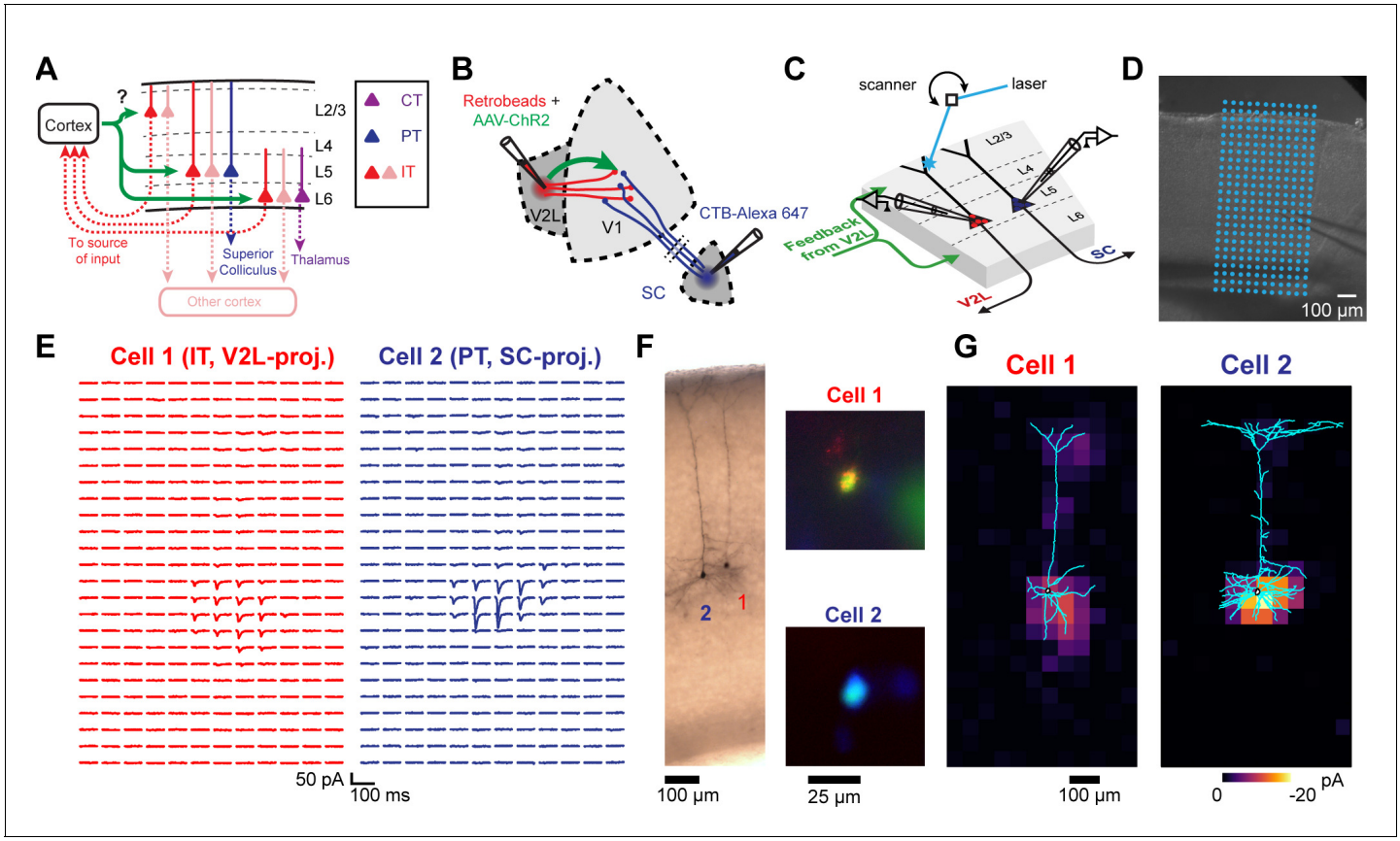

Figure 2. Measuring the strength and dendritic distribution of cortico-cortical (CC) inputs to different projection neurons. (**A**) We probed the strength of CC inputs to looped and non-looped neurons in different cortical layers. (**B**) Example experiment configuration. Retrograde tracers are injected in two areas to label different projection neurons. One cortical area is also co-injected with adeno-associated virus (AAV)-channelrhodopsin-2 (ChR2) to express ChR2 in a specific CC projection. (**C**) Example of subcellular channelrhodopsin-2 (ChR2)-assisted circuit mapping (sCRACM) experiment. Pairs of neighboring retrogradely labeled neurons in the same cortical layer were sequentially recorded. During each recording, a laser beam was scanned over the dendrites of the cell at different locations in a grid pattern. (**D**) Brightfield image of an acute coronal cortical slice showing the recording pipette and photostimulation grid. (**E**) Excitatory postsynaptic currents (EPSCs) recorded from a pair of neighboring L5 neurons, evoked by photostimulating $ChR2^+$ V2L→V1 FB terminals on a grid. (**F**) Left, dendritic morphology staining of the recorded pair. Right, identity of the recorded projection neuron was confirmed by fluorescence in the soma of both a retrograde tracer and a different-colored dye introduced from the internal patch pipette solution. (**G**) sCRACM maps of the recorded pair overlaid on their reconstructed dendrites. Responsive locations are color-coded to represent mean amplitude.

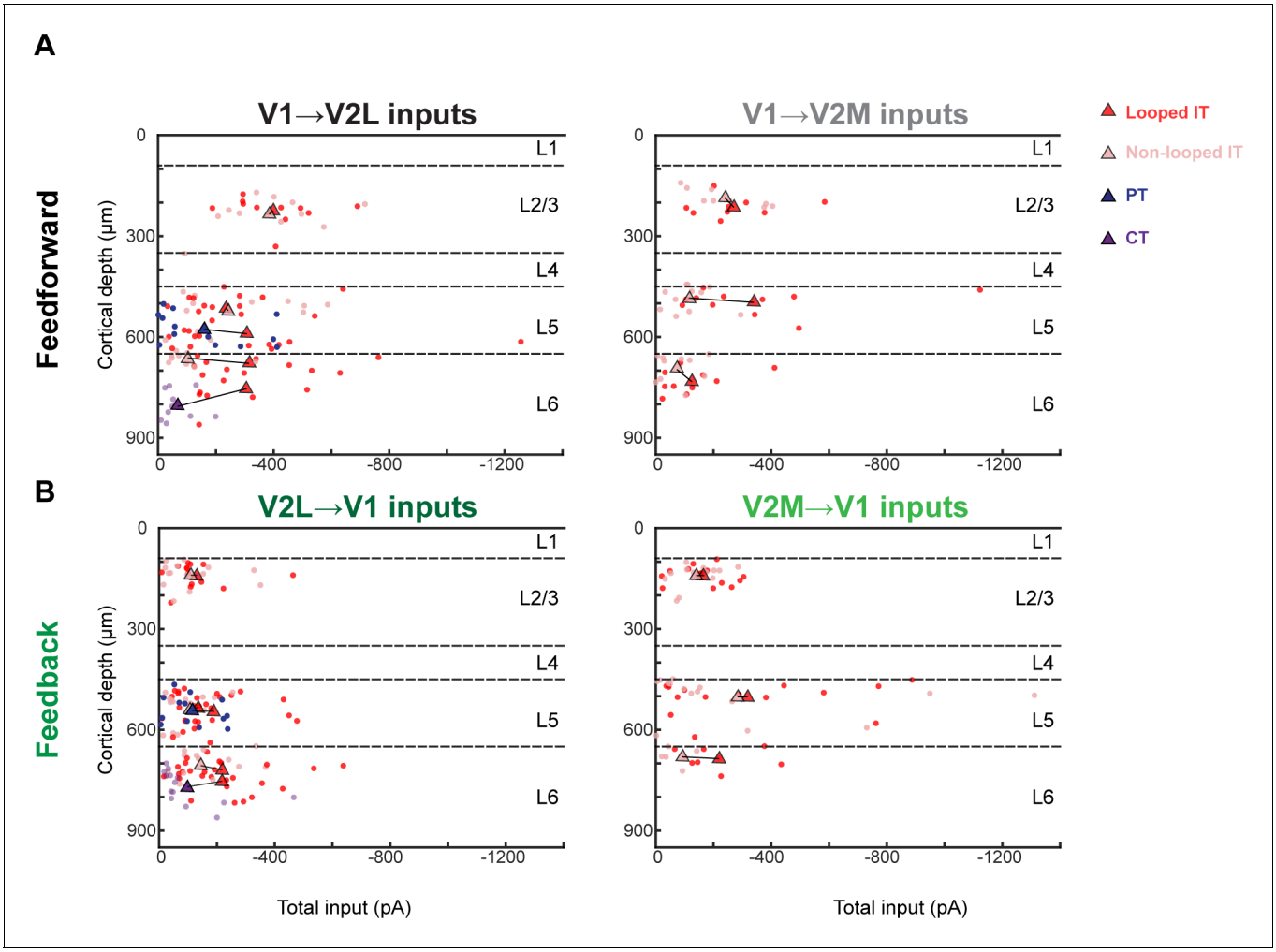

Figure 2—figure supplement 1. Total input vs. laminar depth across different projections and projection neuron classes. (**A**) Total subcellular channelrhodopsin-2 (ChR2)-assisted circuit mapping (sCRACM) input per neuron as a function of cortical depth for both feedforward (FF) projections. Circles, individual cells. Triangles, mean values per projection class for each experiment. Averages from paired data are joined by a line. Color indicates projection class. (**B**) Total sCRACM input per neuron as a function of cortical depth for both feedback (FB) projections.

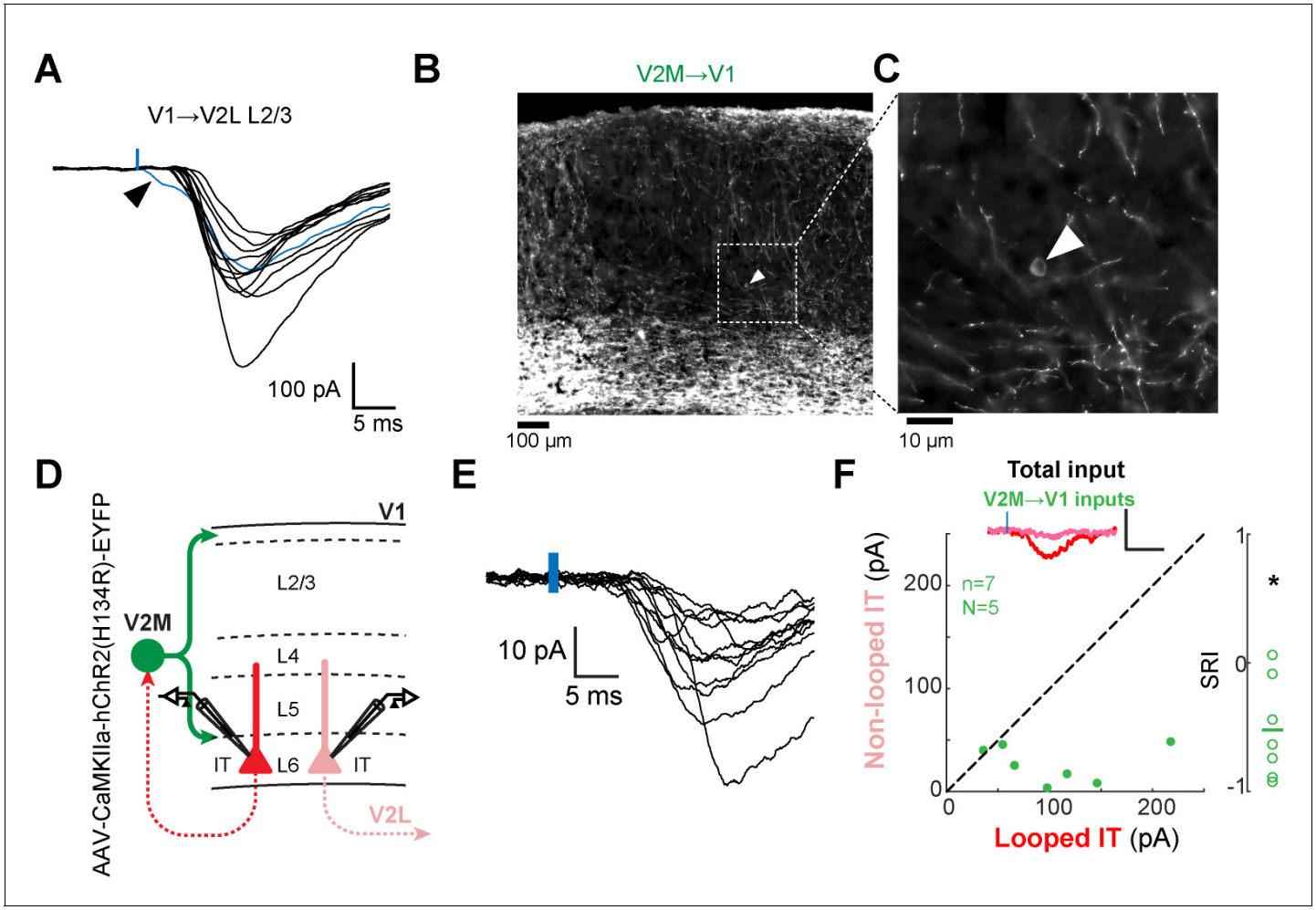

Figure 2—figure supplement 2. Analysis of the incidence of retrograde infection of projection neurons by adeno-associated viruses (AAVs). (**A**) Example of subcellular channelrhodopsin-2 (ChR2)-assisted circuit mapping (sCRACM) traces from individual neurons (data from L2/3 looped intratelencephalic [IT] neurons). Each trace corresponds to the average excitatory postsynaptic current (EPSC) in the location eliciting the largest amplitude. Blue tick, laser pulse. The arrowhead indicates a single neuron (trace in blue) in which the laser pulse evoked an early-onset EPSC, suggestive of a non-synaptic response. Ten neurons with early-onset EPSCs were detected in the entire dataset and removed from further analysis. (**B**) Anti-green fluorescent protein (GFP) immunostained section of primary visual cortex (V1) showing fluorescent medial visual area (V2M) axons in an animal injected with AAV2/1-CAG-ChR2-Venus. (**C**) Higher magnification image of a region in (**B**). The arrow indicates an example of a retrogradely infected neuron in V1. (**D**) Configuration of experiment comparing strength of V2M feedback (FB) input to pairs of L6 looped and non-looped IT neurons in V1 using AAV5-CaMKIIa-hChR2(H134R)-EYFP. (**E**) sCRACM traces from 11 looped IT neurons recorded in L6 from the experiment in (**D**). (**F**) Left, paired comparisons of total FB input to looped vs. non-looped IT neurons from the experiment in (**D**). Inset traces represent group averages for each projection class. Blue tick, light pulse. Right, sCRACM Response Index (SRI) of the same data. *, p=0.0116.

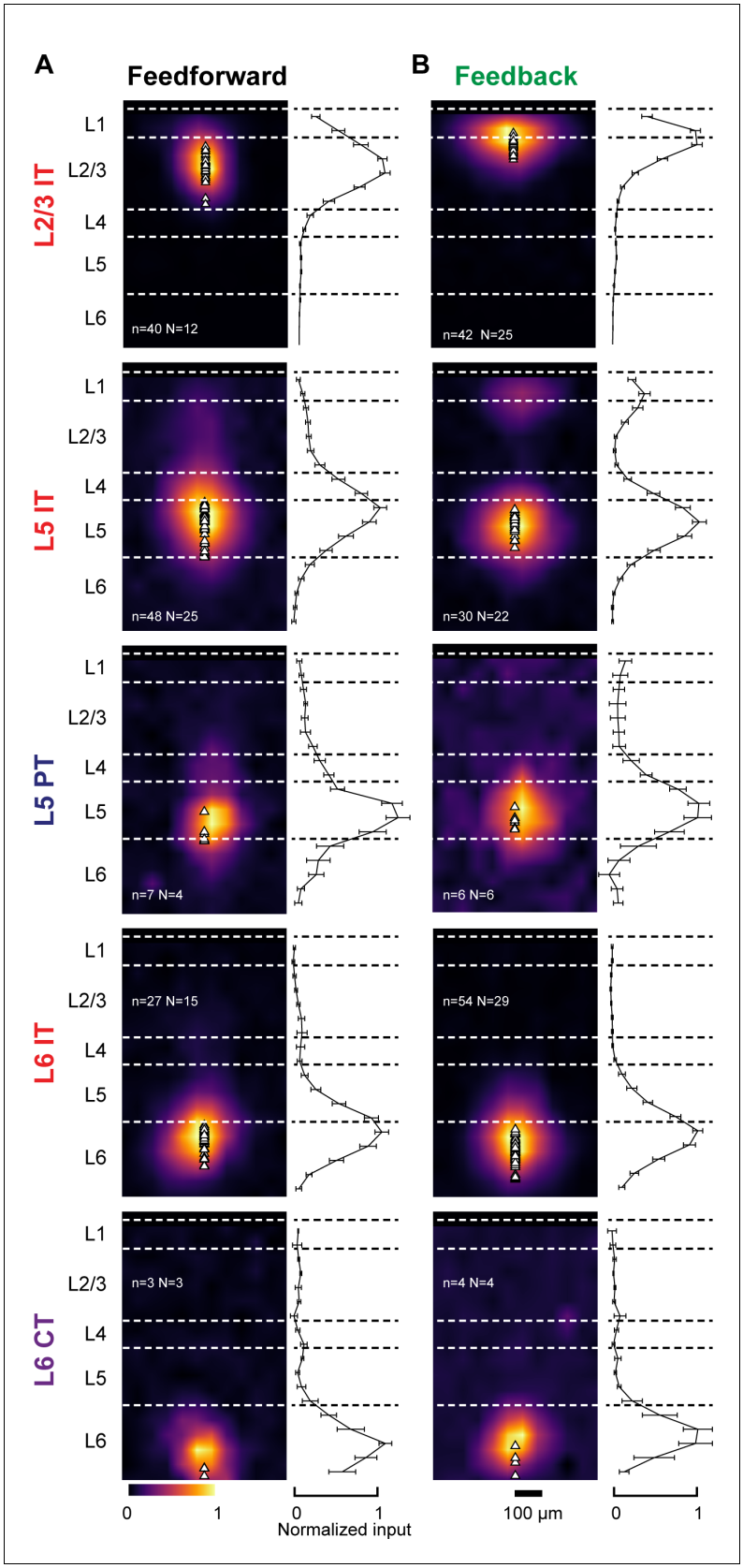

Figure 3. Dendritic distribution of feedforward (FF) and feedback (FB) inputs to different projection neuron classes. (**A**) Left, group averages of subcellular channelrhodopsin-2 (ChR2)-assisted circuit mapping (sCRACM)

Figure 3 continued on next page

Figure 3 continued

maps aligned by pia position showing primary visual cortex (V1) FF input to the different cell types (combining V1→V2L and V1→V2M inputs in the case of intratelencephalic [IT] neurons). Triangles, soma position. Right, vertical profiles of input strength. Error bars, s.e.m.; n, number of neurons; N, number of mice. (**B**) Group averages and vertical profiles of sCRACM maps showing FB input to the different cell types in V1 (combining V2L→V1 and V2M→V1 inputs in the case of IT neurons).

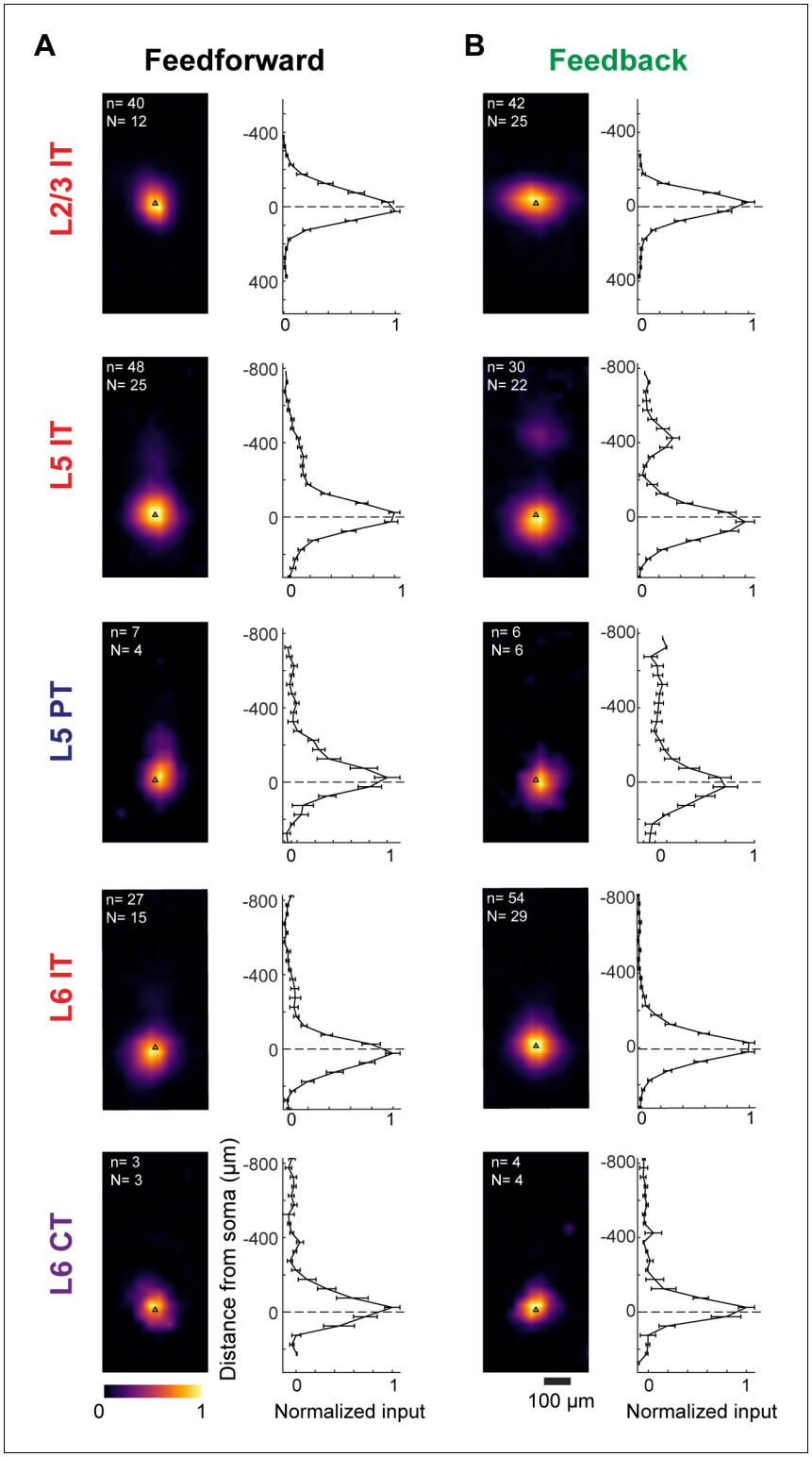

Figure 3—figure supplement 1. Soma-aligned dendritic distribution of feedforward (FF) and feedback (FB) inputs to different projection neuron classes. (**A**) Left, group averages of subcellular channelrhodopsin-2 (ChR2)-assisted circuit mapping (sCRACM) maps aligned by soma position showing primary visual cortex (V1) FF input to the different cell types (combining V1→V2L and V1→V2M inputs in the case of intratelencephalic [IT] neurons). Triangles, soma position. Right, vertical profiles of the mean distribution of inputs as a function of distance to soma. Error bars, s.e.m.; n, number of neurons; N, number of mice. (**B**) Group averages and vertical profiles of

Figure 3—figure supplement 1 continued on next page

Figure 3—figure supplement 1 continued

soma-aligned sCRACM maps showing FB input to the different cell types in V1 (combining V2L→V1 and V2M→V1 inputs in the case of IT neurons).

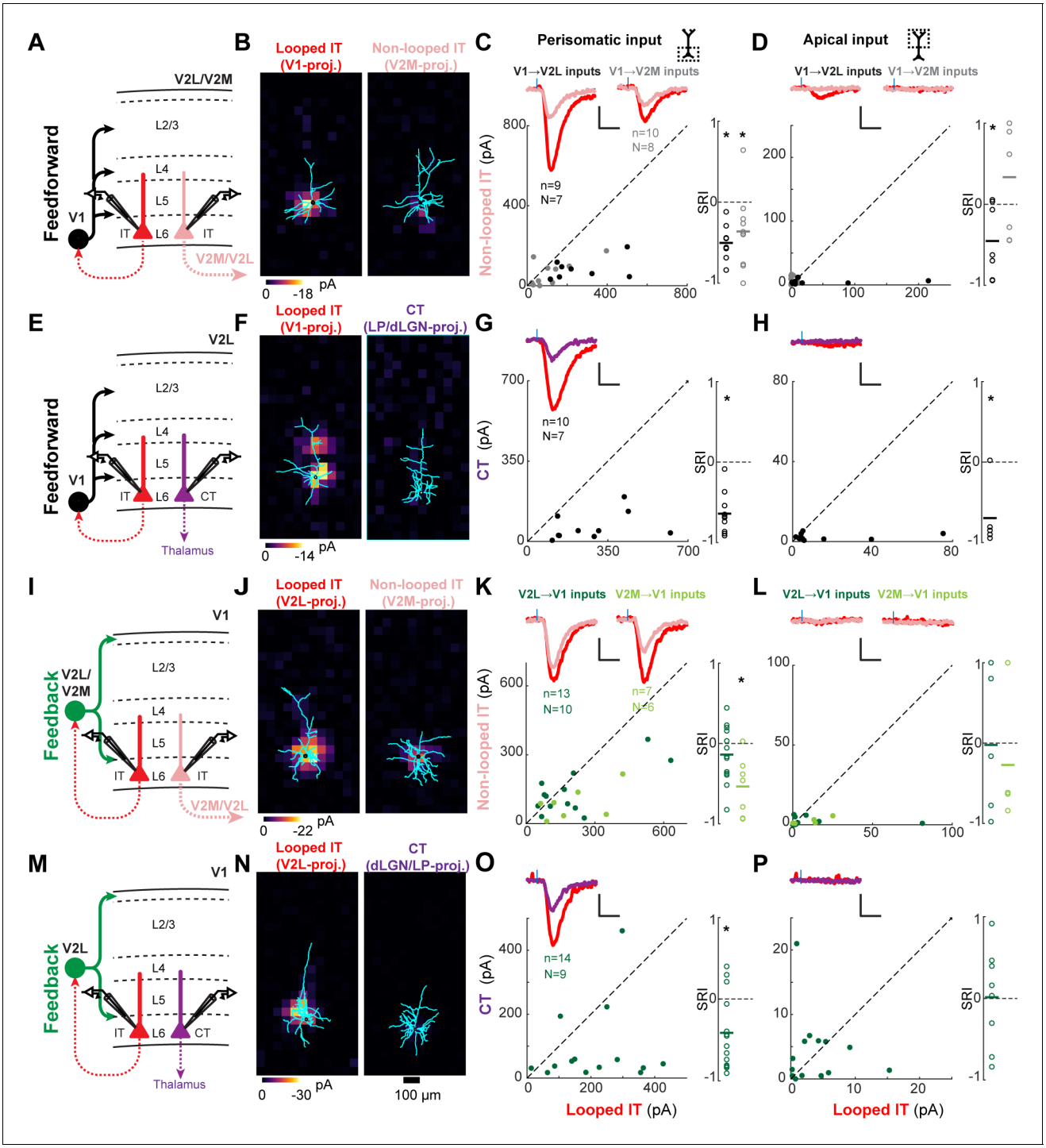

Figure 4. Most feedforward (FF) and feedback (FB) inputs are stronger in looped intratelencephalic (IT) neurons than in neighboring non-looped IT or corticothalamic (CT) neurons in L6. (**A**) Configuration of experiments comparing strength of primary visual cortex (V1) FF input to pairs of L6 looped and non-looped IT neurons in lateral visual area (V2L) or medial visual area (V2M). (**B**) Example pair of subcellular channelrhodopsin-2 (ChR2)-assisted circuit mapping (sCRACM) maps overlaid on reconstructed dendrites showing monosynaptic V1 FF inputs to a looped IT neuron (left) and an adjacent non-looped IT neuron (right) recorded in V2L. (**C**) Left, paired comparisons of perisomatic FF input to looped vs. non-looped IT neurons (n, number of cell pairs; N, number of mice); black dots, V1→V2L inputs; gray dots, V1→V2M inputs. Traces were generated by averaging the mean perisomatic excitatory postsynaptic current (EPSC) of each neuron across all neurons in the same projection class. Colors correspond to (**A**). Blue tick, laser pulse. Scale bars in all panels, 2 pA and 20 ms. Right, sCRACM Response Index (SRI) of the same data. Number of cell pairs and animals are the same as in the left plot unless otherwise specified. Horizontal line, mean. *, p<0.05, see text for exact value. (**D**) Same as C for apical inputs (SRI: V1→V2L, n = 7, N = 6;

Figure 4 continued on next page

Figure 4 continued

V1→V2M, n = 7, N = 6). (**E**) Configuration of experiment comparing strength of V1 FF input to pairs of L6 looped IT and CT neurons in V2L. (**F**) Example pair of sCRACM maps overlaid on reconstructed dendrites showing monosynaptic V1 FF inputs to a looped IT neuron (left) and an adjacent CT neuron (right) recorded in V2L. (**G**) Paired comparisons and SRI of perisomatic FF input to looped IT vs. CT neurons. (**H**) Paired comparisons and SRI (n = 5, N = 5) of apical FF input to looped IT vs. CT neurons. (**I**) Configuration of experiments comparing strength of V2L or V2M FB input to pairs of L6 looped and non-looped IT neurons in V1. (**J**) Example pair of sCRACM maps overlaid on reconstructed dendrites showing monosynaptic V2L FB inputs to a looped IT neuron (left) and an adjacent non-looped IT neuron (right) recorded in V1. (**K**) Paired comparisons and SRI of perisomatic FB input to looped vs. non-looped IT neurons. Dark green dots, V2L→V1 inputs; light green dots, V2M→V1 inputs. (**L**) Paired comparisons and SRI (V2L→V1, n = 5, N = 5; V2M→V1, n = 4, N = 4) of apical FB input to looped vs. non-looped IT neurons. (**M**) Configuration of experiment comparing strength of V2L FB input to pairs of L6 looped IT and CT neurons in V1. (**N**) Example pair of sCRACM maps overlaid on reconstructed dendrites showing monosynaptic V2L FB inputs to a looped IT neuron (left) and an adjacent CT neuron (right) recorded in V1. (**O**) Paired comparisons and SRI of perisomatic FB input to looped IT vs. CT neurons. (**P**) Paired comparisons and SRI (n = 8, N = 7) of apical FB input to looped IT vs. CT neurons.

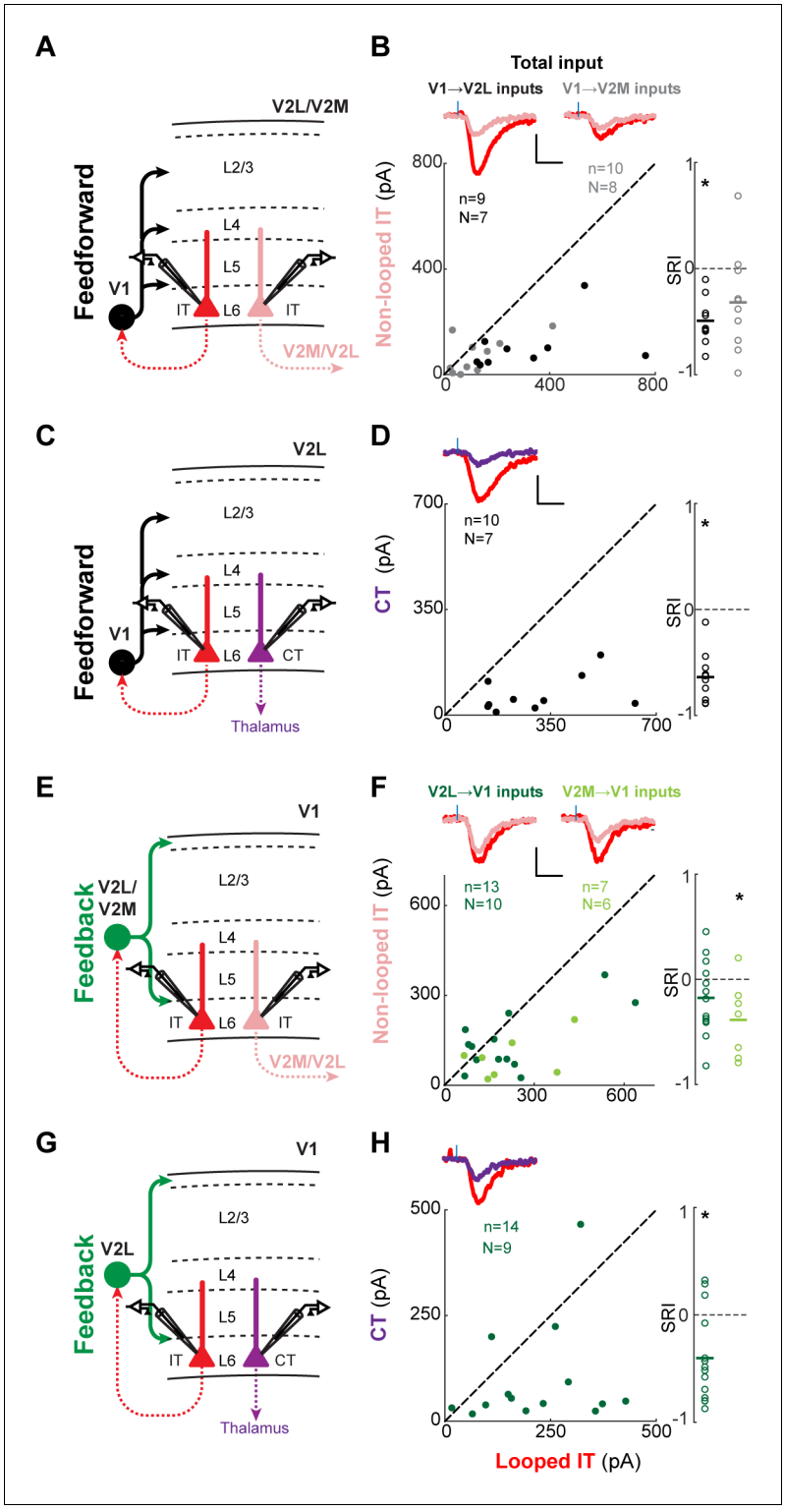

Figure 4—figure supplement 1. Total subcellular channelrhodopsin-2 (ChR2)-assisted circuit mapping (sCRACM) input to L6 neurons. (**A**) Configuration of experiments comparing strength of primary visual cortex (V1) feedforward (FF) input to pairs of L6 looped and non-looped intratelencephalic (IT) neurons in lateral visual areas (V2L) or medial visual areas (V2M). (**B**) Left, paired comparisons of total FF input to looped vs. non-looped IT neurons. Black dots, V1→V2L inputs; gray dots, V1→V2M inputs. Traces were generated by averaging the mean excitatory postsynaptic currents (EPSC) of each neuron across all neurons in the same projection class. Blue tick,

Figure 4—figure supplement 1 continued on next page

Figure 4—figure supplement 1 continued

laser pulse. Scale bars in all panels, 2 pA and 20 ms. Right, sCRACM Response Index (SRI) of the same data. Number of cell pairs and animals are the same as in the left plot. Horizontal line, mean. *, p=0.0002. (**C**) Configuration of experiment comparing strength of V1 FF input to pairs of L6 looped IT and corticothalamic (CT) neurons in V2L. (**D**) Paired comparisons and SRI of total FF input to looped IT vs. CT neurons. *, $p=1.2\times10^{-5}$. (**E**) Configuration of experiments comparing strength of V2L or V2M FB input to pairs of L6 looped and non-looped IT neurons in V1. (**F**) Paired comparisons and SRI of total FB input to looped vs. non-looped IT neurons. Dark green, V2L→V1 inputs; light green, V2M→V1 inputs. *, p=0.0311. (**G**) Configuration of experiment comparing strength of V2L FB input to pairs of L6 looped IT and CT neurons in V1. (**H**) Paired comparisons and SRI of total FB input to looped IT vs. CT neurons. * p=0.0032.

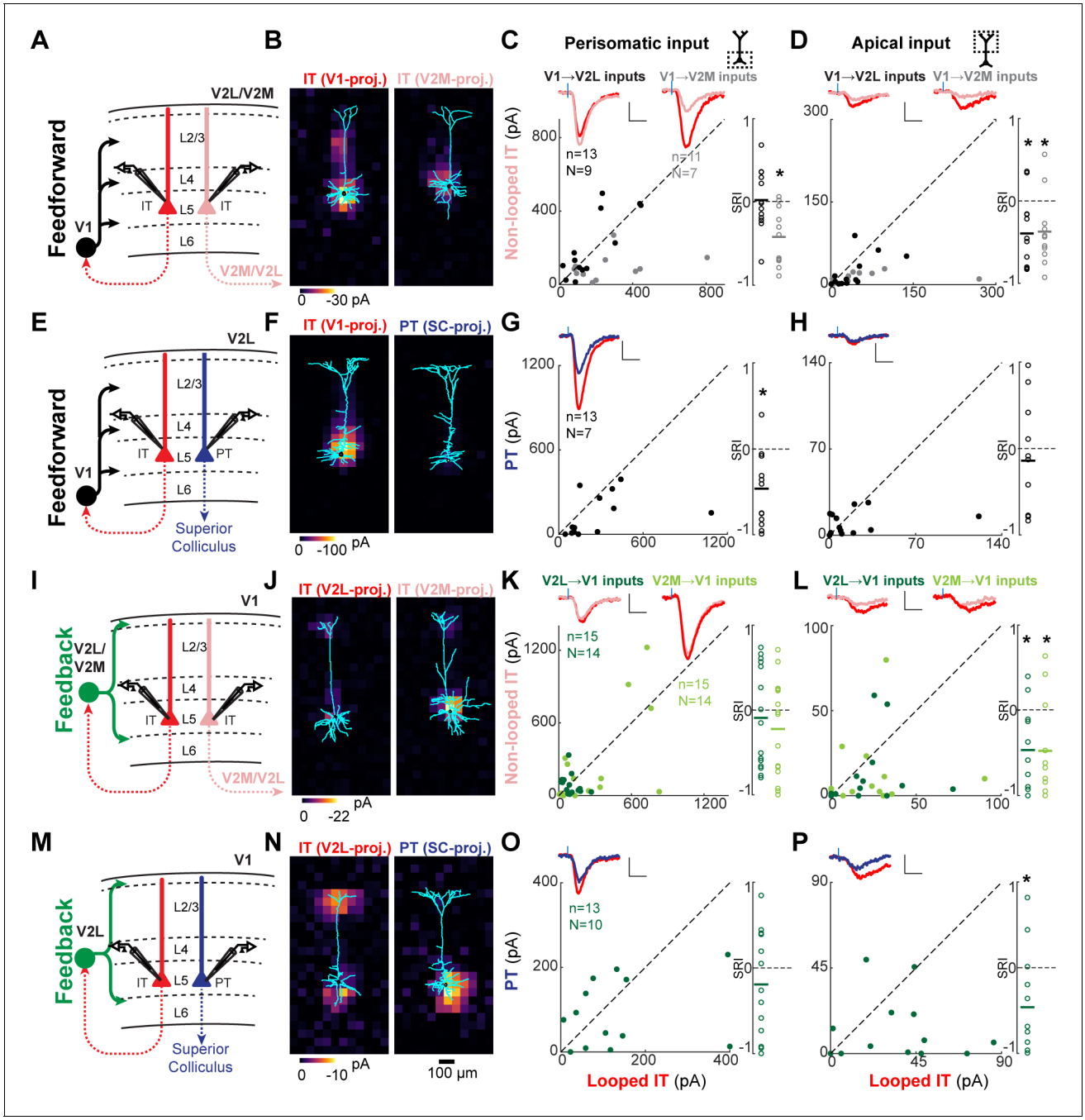

Figure 5. Feedforward (FF) and feedback (FB) inputs are stronger in looped intratelencephalic (IT) neurons than in neighboring non-looped IT or pyramidal tract (PT) neurons in L5. (**A**) Configuration of experiments comparing strength of primary visual cortex (V1) FF input to pairs of L5 looped and non-looped IT neurons in lateral visual (V2L) or medial visual (V2M) areas. (**B**) Example pair of subcellular channelrhodopsin-2 (ChR2)-assisted circuit mapping (sCRACM) maps overlaid on reconstructed dendrites showing monosynaptic V1 FF inputs to a looped IT neuron (left) and an adjacent non-looped IT neuron (right) recorded in V2L. (**C**) Left, paired comparisons of perisomatic FF input to looped vs. non-looped IT neurons; black dots, V1→V2L inputs; gray dots, V1→V2M inputs. Traces were generated by averaging the mean perisomatic excitatory postsynaptic current (EPSC) of each neuron across all neurons in the same projection class. Blue tick, laser pulse. Scale bars in all panels, 2 pA and 20 ms. Right, sCRACM Response Index (SRI) of the same data. Number of cell pairs and animals are the same as in the left plot unless otherwise specified. Horizontal line, mean. *, $p<0.05$, see text for exact value. (**D**) Same as C for apical inputs (SRI: V1→V2L, n = 12, N = 8; V1→V2M, n = 11, N = 7). (**E**) Configuration of experiment comparing strength of V1 FF input to pairs of L5 looped IT and PT neurons in V2L. (**F**) Example pair of sCRACM maps overlaid on reconstructed dendrites showing monosynaptic V1 FF inputs to a looped IT neuron (left) and an adjacent PT neuron (right) recorded in V2L. (**G**) Paired comparisons and SRI of perisomatic FF input to looped IT vs. PT neurons. (**H**) Paired comparisons and SRI (n = 11, N = 7) of apical FF input to looped IT vs. PT

Figure 5 continued on next page

Figure 5 continued

neurons. (**I**) Configuration of experiments comparing strength of V2L or V2M FB input to pairs of L5 looped and non-looped IT neurons in V1. (**J**) Example pair of sCRACM maps overlaid on reconstructed dendrites showing monosynaptic V2L FB inputs to a looped IT neuron (left) and an adjacent non-looped IT neuron (right) recorded in V1. (**K**) Paired comparisons and SRI of perisomatic FB input to looped vs. non-looped IT neurons. Dark green dots, V2L→V1 inputs; light green dots, V2M→V1 inputs. (**L**) Paired comparisons and SRI (V2L→V1, n = 11, N = 10; V2M→V1, n = 11, N = 10) of FB input in L1 to looped vs. non-looped IT neurons. (**M**) Configuration of experiment comparing strength of V2L FB input to pairs of L5 looped IT and PT neurons in V1. (**N**) Example pair of sCRACM maps overlaid on reconstructed dendrites showing monosynaptic V2L FB inputs to a looped IT neuron (left) and an adjacent PT neuron (right) recorded in V1. (**O**) Paired comparisons and SRI of perisomatic FB input to looped IT vs. PT neurons. (**P**) Paired comparisons and SRI (n = 12, N = 9) of FB input in L1 to looped IT vs. PT neurons.

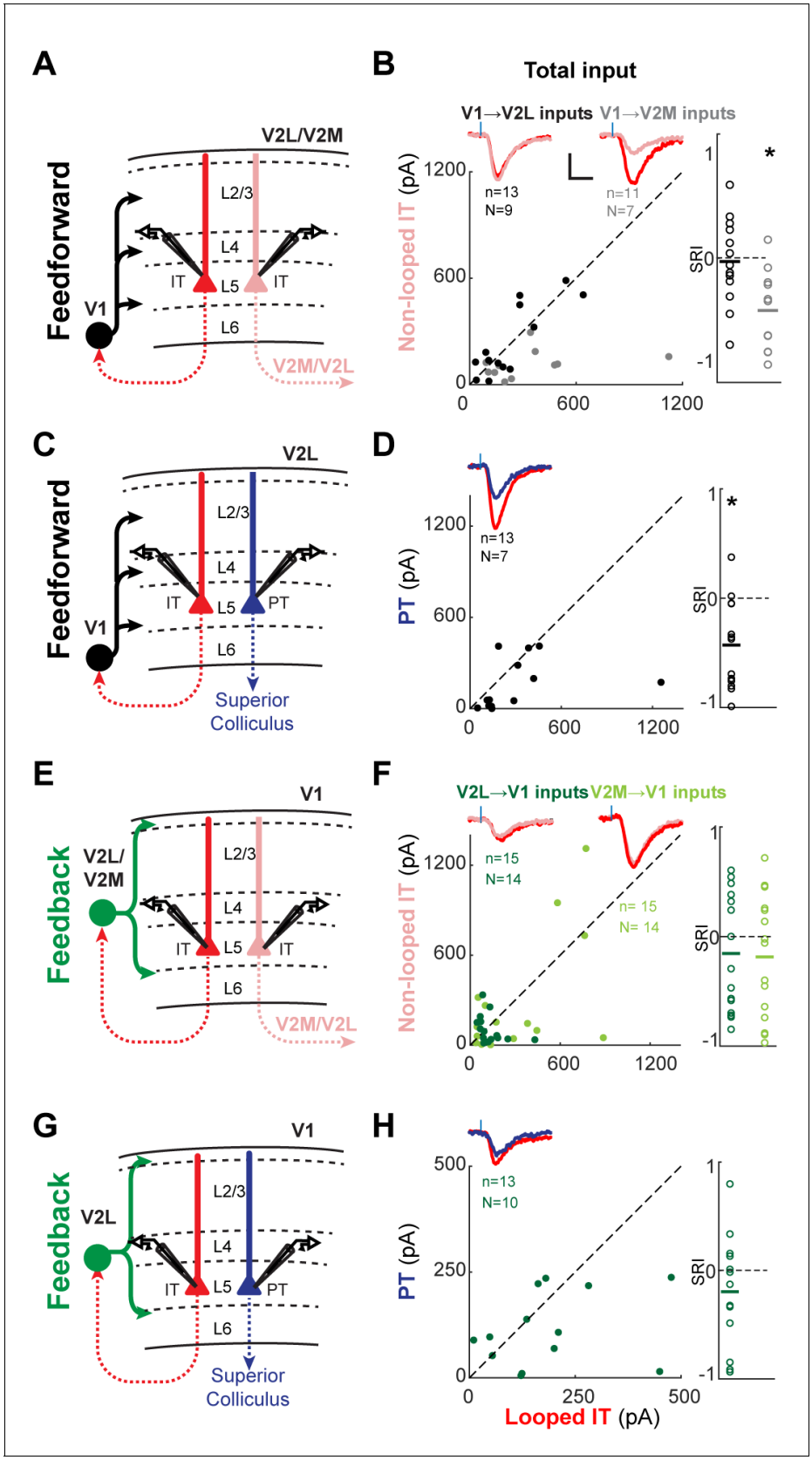

Figure 5—figure supplement 1. Total subcellular channelrhodopsin-2 (ChR2)-assisted circuit mapping (sCRACM) input to L5 neurons. (**A**) Configuration of experiments comparing strength of primary visual cortex (V1) feedforward (FF) input to pairs of L5 looped and non-looped

Figure 5—figure supplement 1 continued on next page

Figure 5—figure supplement 1 continued

intratelencephalic (IT) neurons in lateral visual areas (V2L) or medial visual areas (V2M). (**B**) Left, paired comparisons of total FF input to looped vs. non-looped IT neurons. Black dots, V1→V2L inputs; gray dots, V1→V2M inputs. Traces were generated by averaging the mean excitatory postsynaptic current (EPSC) of each neuron across all neurons in the same projection class. Blue tick, laser pulse. Scale bars in all panels, 2 pA and 20 ms. Right, sCRACM Response Index (SRI) of the same data. Number of cell pairs and animals are the same as in the left plot. Horizontal line, mean. *, p=0.0015. (**C**) Configuration of experiment comparing strength of V1 FF input to pairs of L5 looped IT and PT neurons in V2L. (**D**) Paired comparisons and SRI of total FF input to looped IT vs. PT neurons. *, p=0.0028. (**E**) Configuration of experiments comparing strength of V2L or V2M FB input to pairs of L5 looped and non-looped IT neurons in V1. (**F**) Paired comparisons and SRI of total FB input to looped vs. non-looped IT neurons. (**G**) Configuration of experiment comparing strength of V2L FB input to pairs of L5 looped IT and PT neurons in V1. (**H**) Paired comparisons and SRI of total FB input to looped IT vs. PT neurons.

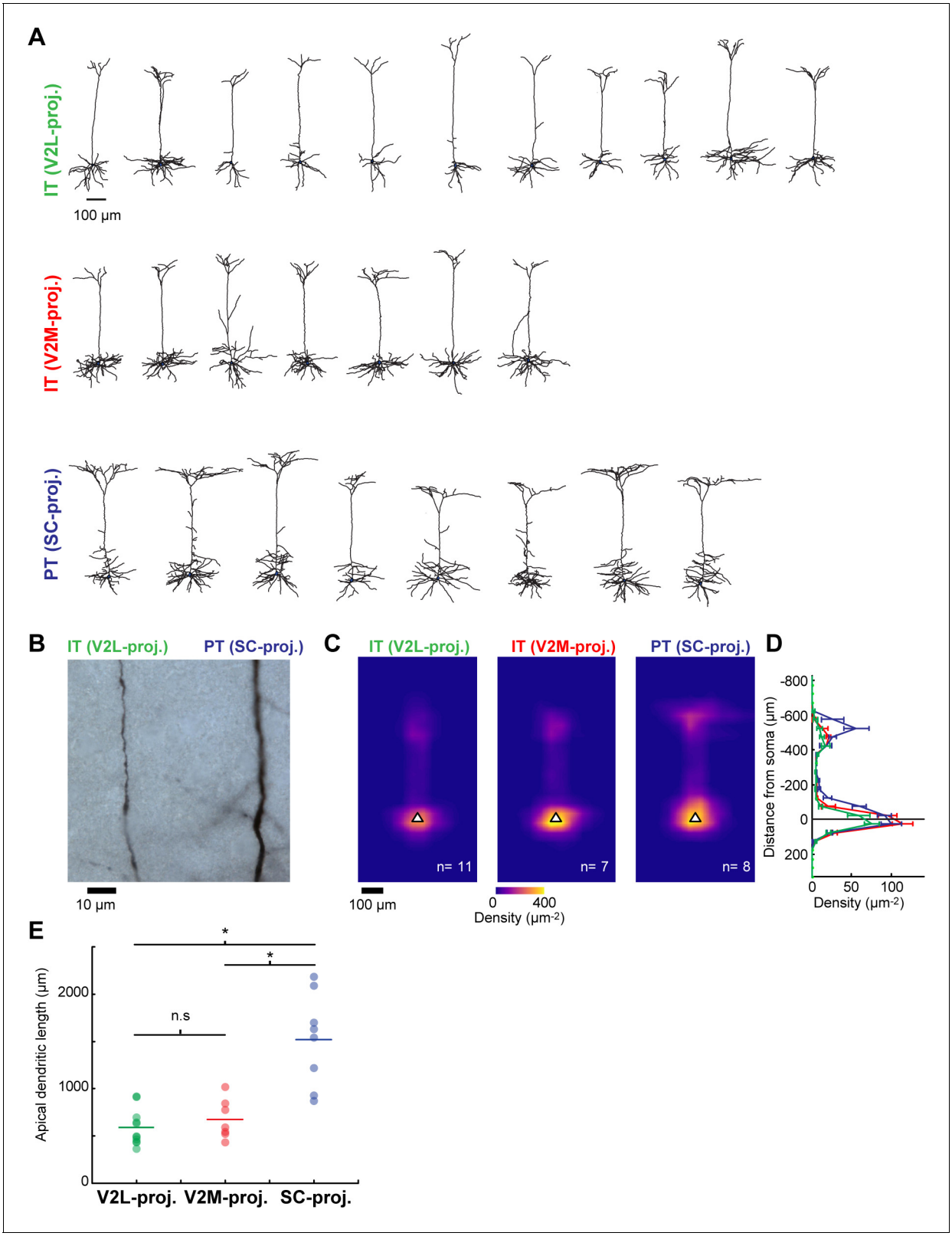

Figure 5—figure supplement 2. Dendritic morphology of the different L5 projection neuron types in primary visual cortex (V1). (**A**) Reconstructed dendritic morphologies of the three different L5 projection neurons recorded in V1. Top and middle, intratelencephalic (IT) neurons projecting to lateral visual (V2L) or medial visual (V2M) areas; bottom, pyramidal tract (PT) neurons projecting to superior colliculus (SC). (**B**) Brightfield image showing representative example of apical shaft segments from a pair of biocytin-stained IT and PT L5 neurons. The apical dendrites of SC-projecting PT neurons

Figure 5—figure supplement 2 continued on next page

Figure 5—figure supplement 2 continued

were of larger diameter than those of same-layer V2L- and V2M-projecting IT neurons. (**C**) Average normalized dendritic length density of the three cell types, aligned by soma position (white triangle). (**D**) Mean vertical profiles of dendritic length density (error bars, s.e.m). (**E**) Total apical tuft dendritic length for the three cell types. Apical tuft branches of SC-projecting PT neurons are more extensive than those of V2L- and V2M-projecting IT neurons (Kruskal-Wallis test followed by Tukey-Kramer honestly significant difference (HSD) post-hoc test, SC-projecting vs. V2L-projecting, p=0.0006; SC-projecting vs. V2M-projecting, p=0.0168; V2L-projecting vs. V2M-projecting, p=0.8044).

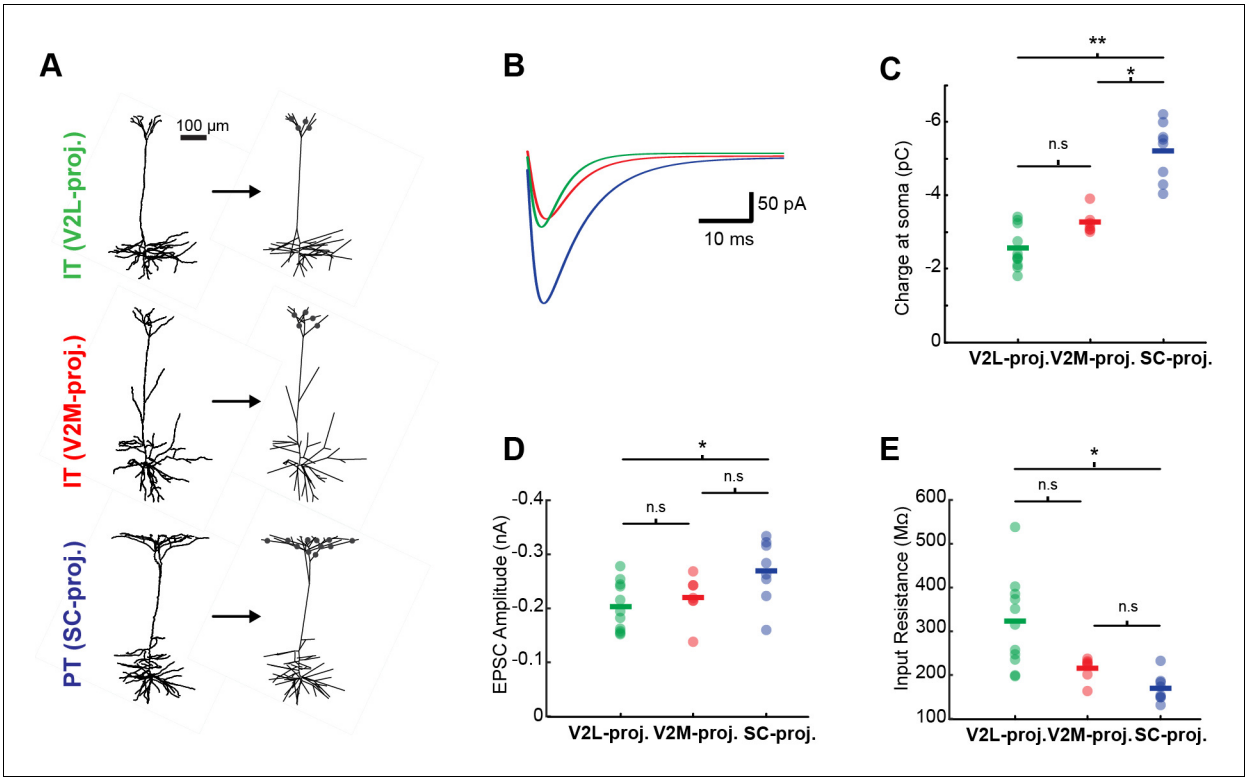

Figure 5—figure supplement 3. Simulations of the dendritic filtering of distal apical inputs. (**A**) Example simulations of L5 neurons. Reconstructed dendritic arbors were imported into the NEURON environment. Synapses were randomly placed with constant density along apical tuft dendritic segments. (**B**) Simulated excitatory postsynaptic current (EPSC) at the soma evoked by L1 input under voltage-clamp conditions for the three example neurons shown in A. (**C**) Mean somatic charge per cell (based on 100 simulations) resulting from apical tuft input across the three projection neuron populations. Apical inputs lacking cell-type selectivity and exhibiting equal synaptic density across the different cell types generate larger somatic currents in superior colliculus (SC)-projecting neurons vs. medial visual area (V2M)- or lateral visual area (V2L)-projecting neurons (Kruskal-Wallis test followed by Tukey-Kramer HSD post-hoc test, SC-projecting vs. V2L-projecting, p=0.0001; SC-projecting vs. V2M-projecting, p=0.0325; V2L-projecting vs. V2M-projecting, p=0.3626). (**D**) ESPC amplitude resulting from apical tuft input across the three projection neuron populations. EPSC amplitudes are larger in pyramidal tract (PT) neurons than in V2L-projecting neurons (Kruskal-Wallis test followed by Tukey-Kramer HSD post-hoc test, SC-projecting vs. V2L-projecting, p=0.0262; SC-projecting vs. V2M-projecting, p=0.1495; V2L-projecting vs. V2M-projecting, p=0.8753). (**E**) Input resistance measured from a voltage step during simulated somatic voltage-clamp in the model L5 cells. PT neurons have lower input resistance than V2L-projecting neurons (Kruskal-Wallis test followed by Tukey-Kramer HSD post-hoc test, SC-projecting vs. V2L-projecting, p=0.0003; SC-projecting vs. V2M-projecting, p=0.2082; V2L-projecting vs. V2M-projecting, p=0.1356).

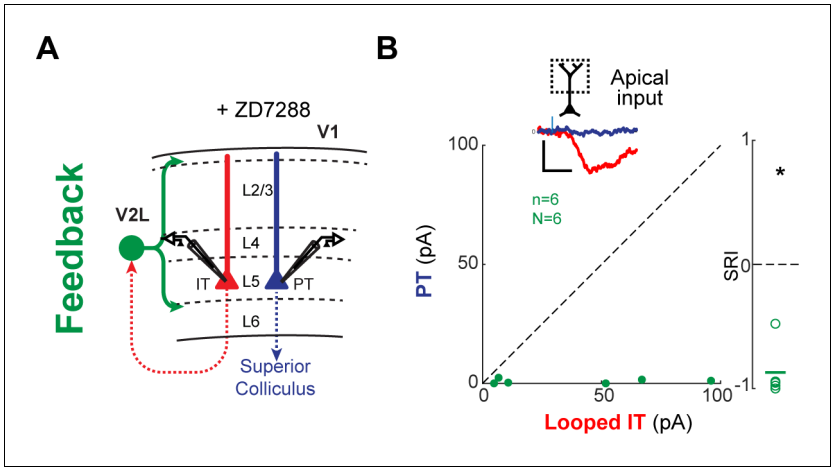

Figure 5—figure supplement 4. Feedforward (FB) input to looped L5 intratelencephalic (IT) neurons vs. pyramidal tract (PT) neurons in the presence of I_h blockers. (**A**) Configuration of experiment comparing strength of lateral visual area (V2L) feedback (FB) input to pairs of looped IT and PT neurons in primary visual cortex (V1) L5. ZD7288 was added to the bath solution to block I_h currents. (**B**) Left, paired comparisons of FB inputs to L1 apical dendrites of looped IT neurons vs. PT neurons in L5. Traces represent group-averaged excitatory postsynaptic currents (EPSCs) in L1. Right, sCRACM Response Index (SRI) of the same data (n = 5, N = 5). *, p=0.0009.

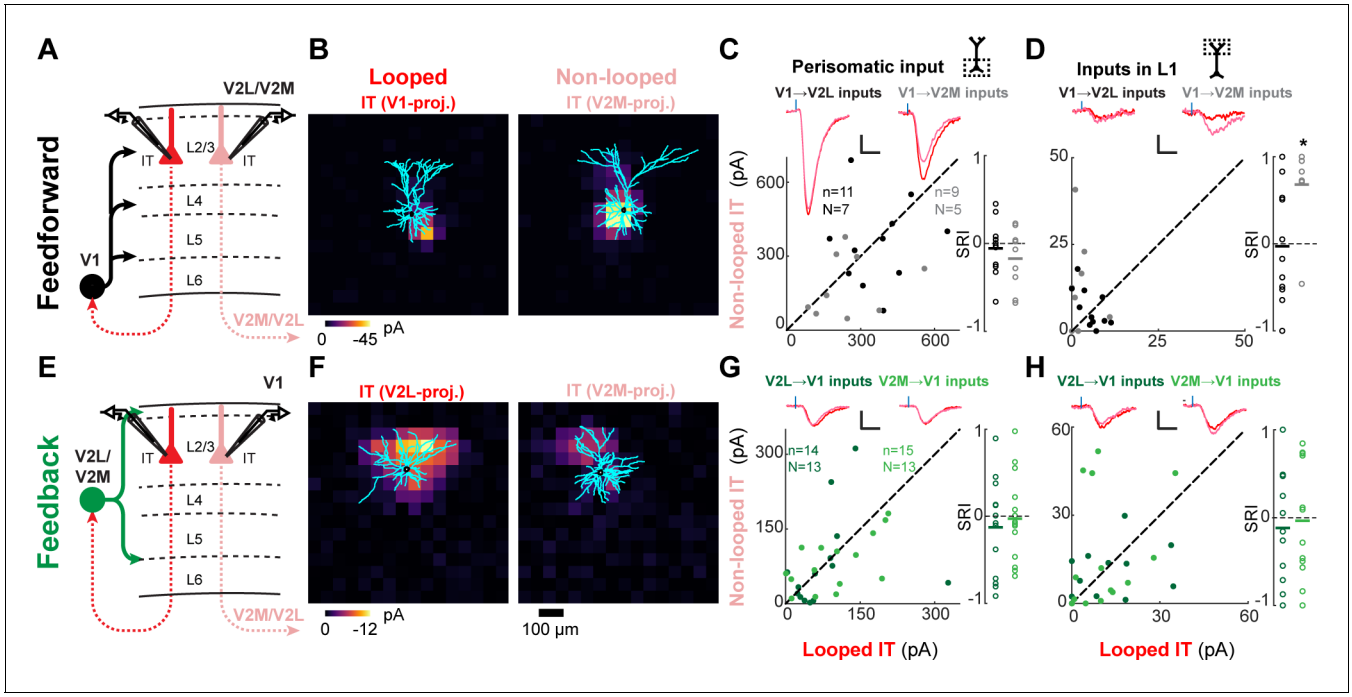

Figure 6. Feedforward (FF) and feedback (FB) connections are similar or weaker in looped L2/3 neurons. (**A**) Configuration of experiments comparing strength of primary visual cortex (V1) FF input to pairs of L2/3 looped and non-looped intratelencephalic (IT) neurons in lateral visual area (V2L) or medial visual area (V2M). (**B**) Example pair of subcellular channelrhodopsin-2 (ChR2)-assisted circuit mapping (sCRACM) maps overlaid on reconstructed dendrites showing monosynaptic V1 FF inputs to a looped IT neuron (left) and an adjacent non-looped IT neuron (right) recorded in V2L. (**C**) Left, paired comparisons of perisomatic FF input to looped vs. non-looped IT neurons; black dots, V1→V2L inputs; gray dots, V1→V2M inputs. Traces were generated by averaging the mean perisomatic excitatory postsynaptic current (EPSC) of each neuron across all neurons in the same projection class. Blue tick, laser pulse. Scale bars in all panels, 2 pA and 20 ms. Right, sCRACM Response Index (SRI) of the same data. Number of cell pairs and animals are the same as in the left plot unless otherwise specified. Horizontal line, mean. *, $p<0.05$, see text for exact value. (**D**) Same as C for inputs in L1 (SRI: V1→V2L, n = 11, N = 7; V1→V2M, n = 7, N = 5). (**E**) Configuration of experiments comparing strength of V2L or V2M FB input to pairs of L2/3 looped and non-looped IT neurons in V1. (**F**) Example pair of sCRACM maps overlaid on reconstructed dendrites showing monosynaptic V2L FB inputs to a looped IT neuron (left) and an adjacent non-looped IT neuron (right) recorded in V1. (**G**) Paired comparisons and SRI of perisomatic FB input to looped vs. non-looped IT neurons. Dark green dots, V2L→V1 inputs; light green dots, V2M→V1 inputs. (**H**) Same as G for inputs in L1 (SRI: V2L→V1, n = 11, N = 10; V2M→V1, n = 12, N = 11).

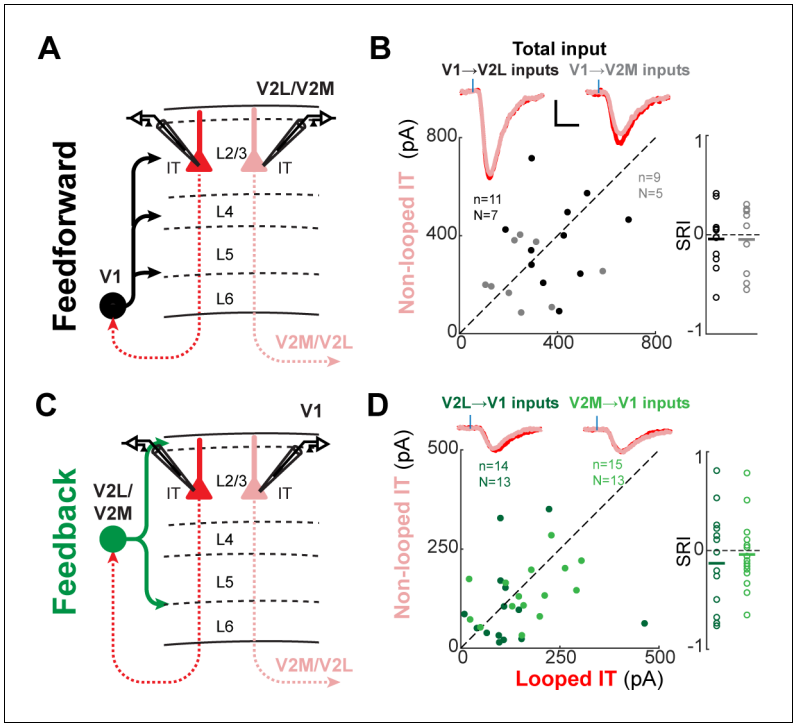

Figure 6—figure supplement 1. Total subcellular channelrhodopsin-2 (ChR2)-assisted circuit mapping (sCRACM) input to L2/3 neurons. (**A**) Configuration of experiments comparing strength of primary visual cortex (V1) feedforward (FF) input to pairs of L2/3 looped and non-looped intratelencephalic (IT) neurons in lateral visual area (V2L) or medial visual area (V2M). (**B**) Left, paired comparisons of total FF input to looped vs. non-looped IT neurons. Black dots, V1→V2L inputs; gray dots, V1→V2M inputs. Traces were generated by averaging the mean excitatory postsynaptic current (EPSC) of each neuron across all neurons in the same projection class. Blue tick, laser pulse. Scale bars in all panels, 2 pA and 20 ms. Right, sCRACM Response Index (SRI) of the same data. (**C**) Configuration of experiments comparing strength of V2L or V2M FB input to pairs of L2/3 looped and non-looped IT neurons in V1. (**D**) Paired comparisons and SRI of total FB input to looped vs. non-looped IT neurons. Dark green dots, V2L→V1 inputs; light green dots, V2M→V1 inputs.

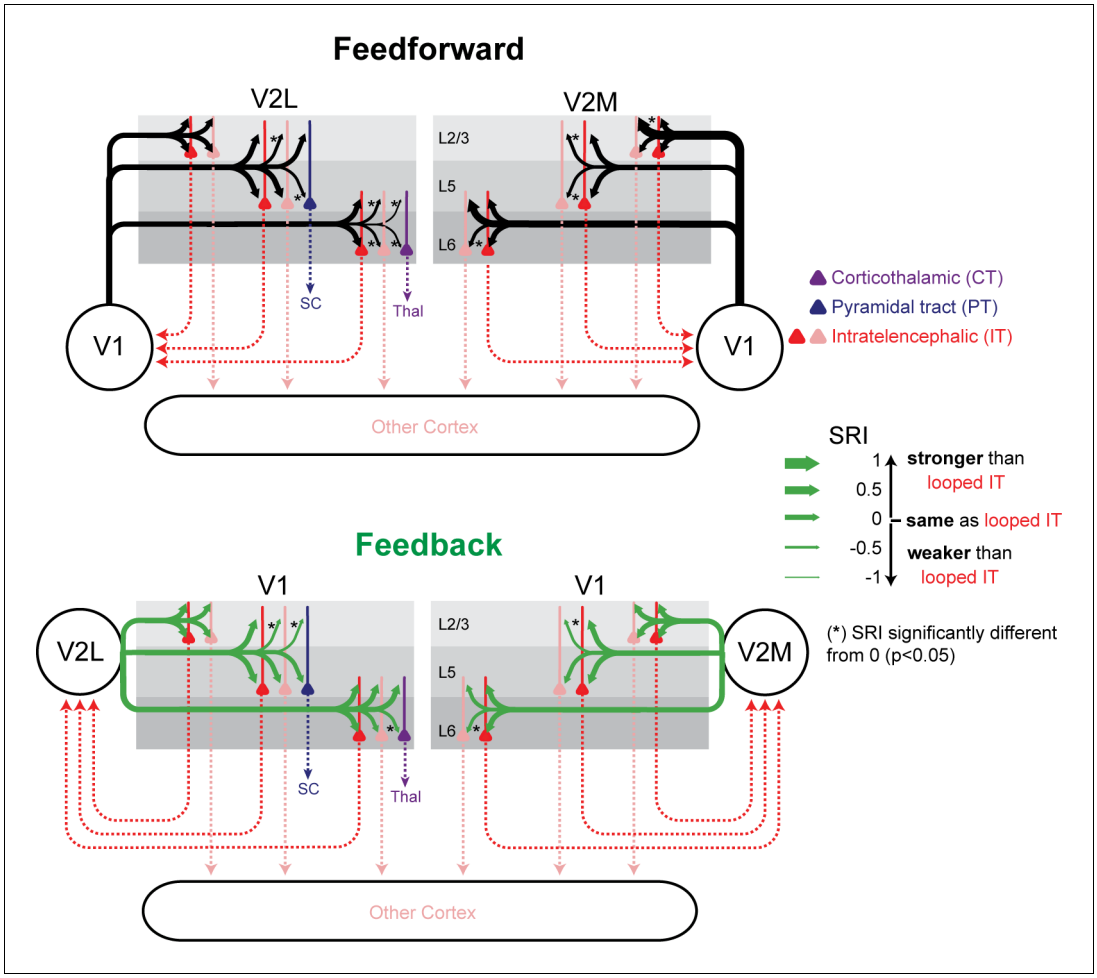

Figure 7. Summary of relative input strength across all experiments. The sCRACM Response Index (SRI) of feedforward (FF) and feedback (FB) inputs to the different cell types is represented by arrow thickness. The top and bottom arrows to L5 neurons indicate inputs to apical and perisomatic domains, respectively. Inputs to looped intratelencephalic (IT) cells in each cortical layer are assigned an SRI of 0 (medium arrow thickness). * signifies significant difference ($p<0.05$) from the looped IT population.

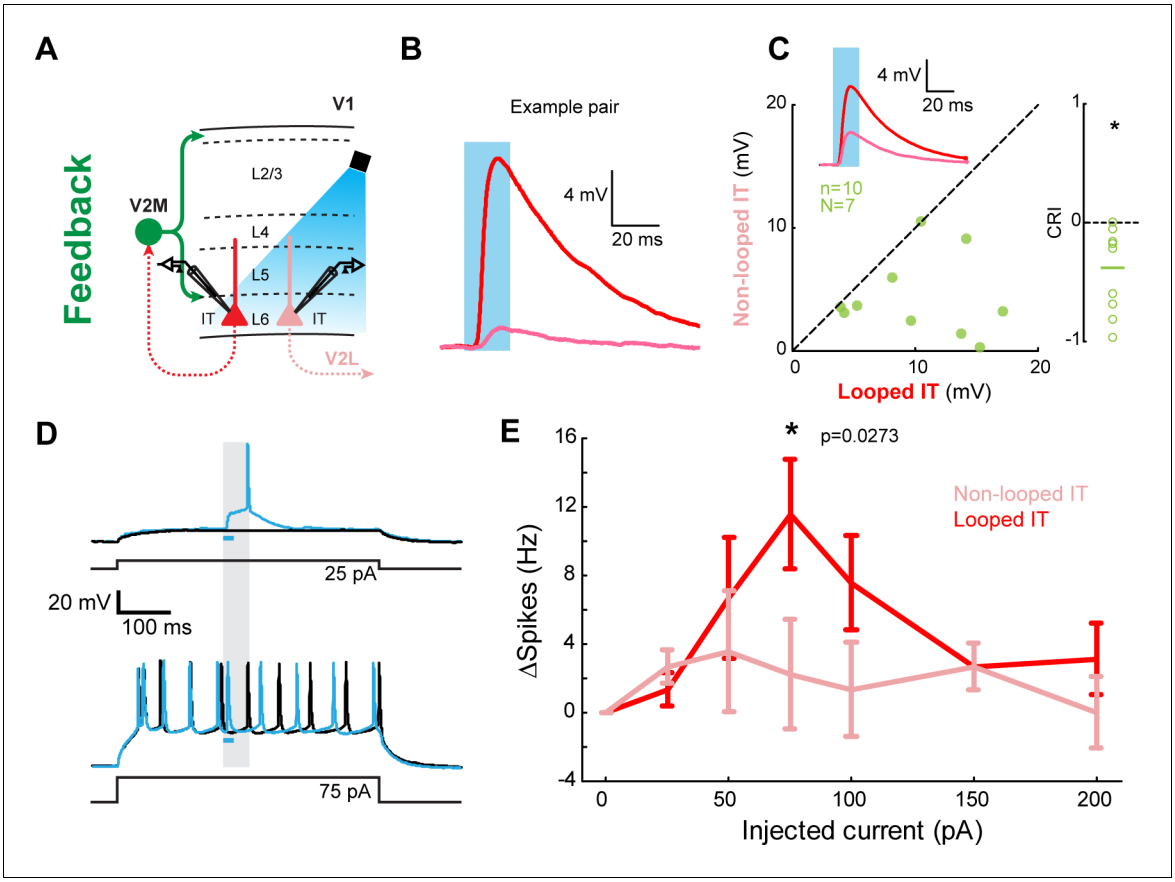

Figure 8. Feedback (FB) inputs in L6 can selectively modulate activity in looped intratelencephalic (IT) neurons. (**A**) Experiment configuration. In the absence of channel blockers, V2M→V1 FB axons were photostimulated using an LED during current-clamp recordings of looped and non-looped IT neurons in L6. (**B**) Example of excitatory postsynaptic potentials (EPSPs) from an example pair. Blue shade, light pulse. (**C**) Left, paired comparisons of EPSP amplitudes evoked in looped vs. non-looped IT neurons. Inset traces represent group averages for each projection class. Blue shade, light pulse. Right, CRACM Response Index (CRI) of the same data (n = 10, N = 7). (**D**) Example traces of FB modulation in a looped IT neuron. Cells were driven by a sustained positive current injection. Black traces, LED OFF trials; blue traces, LED ON trials. Blue bar, duration of the LED light pulse. Gray shading, time period used to analyze spiking activity in (**E**). (**E**) Spike rate difference between LED-ON and LED-OFF trials in looped and non-looped IT neurons as a function of the amount of current injected during the depolarization step. *, p=0.0273, paired t-test with Bonferroni correction for seven comparisons.

Chapter 3

"In case anyone thinks I'm at all complacent about area 17 being well in hand, let me reassure you; there are still problems enough even to keep all 5000 (or whatever the number is) area-17 physiologists busy. One has only to think of apical dendrites and that crowning mystery, layer 1. Or if that leaves you cold, there are those reciprocal connections – 18 to 17, 17 to the lateral geniculate – which, along with every other reciprocal connection in the nervous system...are utterly ununderstood."

Hubel (1982)

3

EXTENDED DISCUSSION

3.1 Summary

The purpose of this project was to establish whether or not feedforward (FF) and feedback (FB) cortico-cortical (CC) connections showed specificity with respect to their target neurons. To this end, we measured the connectivity strength of different FF and FB projections between higher order visual areas and primary visual cortex, and found that synaptic organization of these projections differs across superficial and deep layers. Specifically, we found that FF and FB projections generally form stronger connections onto projection neurons in layers 5/6 that loop back to the source of those projections when compared to other projection neurons that send axons to other cortical or subcortical targets. In contrast, we did not find such specificity for looped layer 2/3 neurons, which suggests distinct organizing principles for superficial and deep layers of the cortex. We shall now discuss how these results compare to rabies tracing studies, whether they accord with predictive coding and error-backpropagation models, possible alternative sources of input to CT and PT neurons, limitations of our method, and future avenues of research.

3.2 Rabies virus studies of looped connectivity

Of particular relevance to this project are two recent studies by Siu et al. (2020) and Kim et al. (2020) using monosynaptic rabies tracing in the primate and mouse, respectively, to examine FB loops in visual cortex. Rabies virus tracing is a technique that has been widely adopted in cortical connectivity studies to retrogradely and monosynaptically label presynaptic cells, though it is not yet understood how it spreads transynaptically and how successfully it infects all presynaptic cells (Beier, 2019; Luo, Callaway, & Svoboda, 2018).

The first study by Kim et al. (2020) found that L2/3 V1 cells projecting to either PM or AL received more of their higher visual area (HVA) inputs from the area that they projected to. While the HVAs in this study are not entirely the same as ours, the results nevertheless contrast with our findings in that we did not find evidence for preferential monosynaptic loops in L2/3. Using transgenic mouse lines expressing Cre in either L2/3 or L5, they retrogradely infected V1→PM or V1→AL cells by injecting AAVretro-FLEXloxp-Flp in PM or AL, respectively, and also injected AAV8-FLEXfrt-oG/TVAmCherry in V1. This resulted in V1→PM or V1→AL cells, in either L2/3 or L5, expressing the receptor TVA for the envelope protein EnvA and the rabies glycoprotein oG (TVA allows the rabies virus to enter and infect the cell, and oG allows the G-deleted rabies virus to spread transsynaptically). After enough time elapsed for expression of TVA and oG in these V1 projection neuron

populations, the EnvA pseudotyped, G-deleted rabies virus expressing eGFP (EnvA+RVdG-eGFP) was subsequently injected in V1 to fluorescently label direct monosynaptic inputs to V1→PM or V1→AL neurons in either L2/3 or L5.

The authors then counted the number of eGFP+ rabies-labeled FB neurons in each of the HVAs, and found that both V1→PM and V1→AL L2/3 neurons received a greater percentage of HVA inputs from the area they projected to when compared to other areas (41% for V1→PM, 51% for V1→AL). This bias for looped connectivity was also observed for V1→PM L5 neurons, which received 54% of their HVA inputs from PM. This last result shows similarity to our finding that V2M FB projections preferentially target looped L5 neurons in V1 (via their apical dendrites), since our V2M injections included PM. Additionally, the authors found that V1 L5 neurons projecting to AL, which we did not include in our study, instead received more HVA inputs from LM compared to AL (41% versus 28%). Thus, they find evidence for selective looped connectivity that is consistent across FB projections in L2/3, rather than in L5.

Such specificity of FB inputs may be layer-dependent. When the authors used AAVretro-Cre viruses rather than Cre transgenic mice and applied input tracing to V1 neurons across all cortical layers rather than from an individual layer, only V1→PM projection neurons received more inputs from the HVA they projected to, while V1→AL and V1→P/POR neurons received more inputs from area LM and areas LM, M and PM, respectively. It is interesting to note that

only FB projections from PM consistently displayed preferential looped connectivity across all their experiments, since we also found evidence that V2M selectively engages looped neurons in V1. It may be that FB projections from other HVAs not measured in our study exhibit different connectivity patterns with looped V1 neurons.

Nevertheless, given that V1→PM L2/3 neurons were found to receive FB selectively from the same area to which they project, how can we account for the differences between these results and ours? Firstly, it may be worth noting that monosynaptic rabies tracing measures the number of presynaptic neurons, rather than presynaptic strength. Recently, for example, a study using both sCRACM circuit mapping and rabies tracing reported large discrepancies between the two methods, with the proportion of rabies-labelled presynaptic neurons being a poor predictor of functional input strength (Galloni, Ye, & Rancz, 2021). Areas identified by rabies tracing as strong inputs were found to provide weaker-than-expected sCRACM input, and vice versa.

Secondly, as with other AAV vectors, AAV8 causes both retrograde and anterograde infection (Castle, Gershenson, Giles, Holzbaur, & Wolfe, 2014; Löw, Aebischer, & Schneider, 2013), as it can transduce axon terminals. This may have contributed to the presence of more GFP-positive cells in the target HVA of V1→PM and V1→AL L2/3 cells, since FB cells with axon terminals in V1 could have become infected with both the AAV8 virus and retrograde rabies virus and thus expressed TVA and GFP. Unfortunately, due to

the high sensitivity of the EnvA-TVA interaction, only a very small amount of TVA is necessary for successful rabies infection (Federspiel, Bates, Young, Varmus, & Hughes, 1994; Seidler et al., 2008), such that GFP-positive cells in HVAs could express GFP but not the mCherry fluorophore associated with the TVA, making it difficult to distinguish unintended starter cells that have been retrogradely labelled from genuine presynaptic GFP-positive cells that have been transynaptically labelled. While starter cells in HVAs would be unlikely to cause transsynaptic spread (since this would require high levels of the glycoprotein oG), they would nevertheless lead to artificially elevated levels of GFP-positive cells in the target HVA, particularly as the AAVretro-FLEXloxp-Flp used to target the specific V1 projection neuron population was not injected in any other HVA.

The authors control for this artefact by omitting injection of the glycoprotein oG, which enables transsynaptic spread. Unfortunately, it is not clear from their control experiments to what extent this potential confound did or did not apply to the GFP-positive cell count in HVAs. Given that we used AAV-mediated transfection of ChR2 in our own experiments, we also had to contend with retrograde infection (Chapter 2, Figure 2, figure supplement 2). Our electrophysiological recordings made it possible to detect early-onset (<2 ms) responses, suggestive of a retrogradely infected cell, and we removed these cells from the dataset. Using sections stained for the neural marker NeuN, we estimated that the number of such cells comprised 1 out of every ~1300 $NeuN^+$ V1 neurons, indicating

minimal retrograde infection. We also repeated recordings in animals injected with AAV5-ChR2, which is less prone to retrograde infection than AAV2/1-ChR2 (Kinnischtzke, Simons, & Fanselow, 2014), and obtained similar results. Together, these findings suggest that, at least in our own experiments, cells retrogradely infected with AAV2/1-ChR2 did not significantly contribute to our measurements, though it could potentially be an unaccounted factor that overestimates looped connectivity in rabies tracing experiments.

Finally, other factors associated with the monosynaptic tracing method, such as differential spread, may have contributed to the apparent differences between this study and ours. Since rabies tracing labels only a fraction of presynaptic inputs (Callaway & Luo, 2015), there may be biases in labelling such that certain presynaptic contacts are more likely to be labelled than others. For example, synaptic inputs to basal dendrites may be more likely to be transynaptically infected than inputs to apical dendrites, or vice versa. Indeed, the subcellular location of synaptic inputs has already been speculated to influence likelihood of labelling (Callaway & Luo, 2015). Given that preferential innervation of looped deep-layer neurons often involved specific dendritic compartments, and could not be detected when comparing total input (e.g. Chapter 2, Figure 5, figure supplement 1), the lower incidence of looped connectivity in L5 relative to L2/3 reported by Kim et al. (2020) may be a consequence of such biases in labelling. Indeed, because of these and other possible biases, Callaway & Luo (2015) recommend that rabies tracing be complemented by ChR2-assisted circuit mapping, to

identify and measure the connection strength of presynaptic contacts, respectively.

The second study by Siu et al. (2020) used rabies tracing in the macaque visual cortex to identify direct presynaptic inputs to V1→V2 projection neurons. They first injected AAV9-CAG-FLEXTVAmCherry and AAV9-CAG-FLEX-oG-WPRE in V1, followed by CAV2-CMV-Cre in V2, so that only V1→V2 projection neurons would express the Cre-dependent TVAmCherry and oG necessary for initial rabies infection. The EnvA-pseudotyped, G-deleted rabies virus carrying the eGFP gene (EnvA-RVdG-eGFP) was subsequently injected in V1, in order to label the starter cells and the cells that directly synapse onto them.

Similar to some of the projections in the previous study and our own, the researchers found that V1→V2 projection neurons receive more direct input from cells in the area they project to, V2, than from any other higher area. However, the specificity of this FF-FB interareal loop was far greater, with almost all presynaptic neurons being located in V2. Interestingly, they found that most of the V1 starter cells were located in L2/3, suggesting that superficial V1 cells receive more FB from the area they project to, in contrast to the findings reported here. Several observations support these results. First, unlike in the mouse, as much as 96–98% of V1→V2 projections arise from L2/3 (Federer et al., 2009; Sincich, Jocson, & Horton, 2010) which is consistent with the predominance of starter cells reported in L2/3, and second, the majority of V1 FF projection neurons in the macaque do not bifurcate their long-range axons and

only project to a single higher area (Bullier, Kennedy, & Salinger, 1984; Ferrer, Kato, & Price, 1992; Sincich & Horton, 2003), which suggests that FB axons in the macaque may also show a similar degree of specificity.

Indeed, perhaps surprisingly, in two of the three animals studied, presynaptic cells in HVAs other than V2 (including MT, V3, V4, and V6 which all send FB projections to V1) were completely absent, and in the third animal, just 0.6% of presynaptic cells were located in extrastriate cortical areas other than V2. This indicates that the specificity of FB axons is absolute rather preferential, and greater than that of FF axons, at least 5–10% of which bifurcate (Sincich & Horton, 2003).

Thus, while looped connectivity appears to be a prominent feature of cortico-cortical communication in both rodents and primates, there may well be important biological differences in how such loops are implemented. As with the previous rabies tracing study, it is possible that GFP-positive cells in V2 were retrogradely infected by both the TVAmCherry-encoding AAV and GFP-encoding rabies virus injected in V1. In fact, starter cells in V2 expressing both mCherry and GFP were found in two of the three macaques studied. While these double-labelled cells can be easily discarded from the GFP-positive cell count, given that only a minuscule amount of TVAmCherry is necessary for initial rabies infection, V2→V1 cells could potentially express low amounts of TVA without having visible mCherry fluorescence. As a result, some GFP-positive cells in V2 may

have arisen from retrograde infection rather than from transsynaptic spread. Repeating the experiment without injecting the rabies glycoprotein oG, which enables transsynaptic labelling, would help determine to what extent retrograde infection contributed to the GFP-positive cell count in V2.

3.3 CT cells, "mysterious creatures of the deep"

The relative paucity of CC inputs to CT neurons observed in this study contradicts the conventional wisdom that these cells are recipients of long-range cortical input, though our study is not the first to report weak CC input to CT cells relative to IT cells (Kinnischtzke, Fanselow, & Simons, 2016). Harris & Shepherd (2015) cite three studies as support for the view that CT neurons are innervated by higher-order cortical areas. However, it may be noted that 2 of these studies (Vélez-Fort et al., 2014; Zhang & Deschênes, 1998) do not attempt to distinguish between CT and IT neurons in L6. While the majority of cortico-thalamic projections emanate from L6 and this layer is often regarded as being cortico-thalamic, studies in the cat visual cortex (Gilbert & Kelly, 1975) and in the rat primary somatosensory cortex estimate that CT cells constitute just 50% of L6 neurons. As a result, the findings that L6 in the primary somatosensory area of the rat receives strong CC input from deep layers of the motor and secondary somatosensory cortices (Zhang & Deschênes, 1998), or that frontal brain regions such as secondary motor cortex and orbital cortex provide prominent CC input to pyramidal neurons in L6 of mouse motor cortex (Hooks et al., 2013),

does not mean that these CC projections make strong synapses with L6 CT cells. It is possible that such projections instead primarily target neighboring IT cells within the same layer.

The third study by Vélez-Fort et al. (2014) does distinguish between IT and CT neurons in L6, and reported that CT cells in mouse V1 receive more than 20% of their presynaptic inputs from areas V2L, V2M and retrosplenial cortex (RSC), in contrast to IT cells that receive less than 5% of their input from these same areas. In this study, the authors used modified rabies virus-based input tracing of individually recorded cells and genetically targeted populations to measure the presynaptic inputs to CT and IT neurons in L6 of V1. These results may nevertheless still be consistent with ours if a dissociation exists between the number of presynaptic neurons and connection strength, such that CC synapses in L6 of V1 are more numerous and/or stronger in IT neurons than in CT neurons, despite originating from relatively fewer neurons.

It has been noted that there appear to be two types of CT cells in L6, those in upper L6 that project to primary sensory thalamus and those in lower L6 that project to both primary sensory thalamic nuclei as well as to association thalamus and/or interlaminar nuclei (Thomson, 2010). Given that thalamocortical axons arborize mostly in L4 and upper L6, and that the lower L6 CT cells have apical dendrites terminating in L5 (in contrast to the upper L6 CT cells that have apical dendrites terminating in L4), it has been proposed that the principal synaptic drive for lower L6 CT cells is CC rather than

thalamo-cortical (Zhang & Deschênes, 1998). Thus, since our recordings of CT cells are distributed across both upper and lower L6 of V1 and V2L (Chapter 2, Figure 2, figure supplement 1), it is possible that our measurements underestimate CC input strength to CT cells. However, in the V2L dataset in which lower L6 CT cells outnumbered upper L6 CT cells, all CT cells still received weaker V1 FF input than their partner IT cells. Thus, it seems that we have yet to definitively establish the principal source(s) of inputs to CT neurons, and much remains unknown about this class of neurons, described as "mysterious creatures of the deep" by Harris & Shepherd (2015).

3.4 PT cells, "awareness neurons"?

Perhaps one of the more surprising results of this study is that the elaborate, dense apical tufts of PT cells receive relatively little FB from V2L. Given the energy costs associated with developing and maintaining these rich apical branches, they likely receive long-range inputs, albeit from other sources. This begs the question: what might these other sources be?

Using monosynaptic rabies tracing, Kim et al. (2015) reported that both IT and PT neurons in L5 of mouse V1 received more input from HVAs than from any other structure. Indeed, for both IT and PT neurons, the greatest proportion of presynaptic neurons was found in area V2L (40% and 25% of all presynaptic neurons, respectively). Thus, if these results and ours are to be believed, it appears that V2L

selectively avoids the apical dendrites of PT neurons in V1, despite being their greatest source of long-range input.

The authors also reported the RSC and V2M as being prominent sources of long-range input to PT neurons (23% and 11% of all presynaptic neurons, respectively), along with a small fraction of inputs (<2%) emanating from the basal forebrain. Thus, it is possible that the apical tufts of PT neurons receive stronger innervation from these areas. Moreover, if the principal role of PT neurons is to broadcast the final output of cortical computations, then the RSC and V2M may be more likely to innervate the apical dendrites of PT cells than area V2L, since they are both higher up the cortical hierarchy.

Interestingly, a recent sCRACM study revealed an unlikely candidate for long-range inputs to the apical dendrites of PT neurons located in V2M (Galloni et al., 2021). Axons from V1 were found to strongly innervate their apical tufts, more so, on average, than other dendritic regions, despite the fact that V1→V2M axonal projections were densest in L2/3 and L5 and sparse in L1. Other regions providing >50% of their input to the apical tufts of PT neurons included the anterior thalamic nuclei and lateral posterior nucleus of the thalamus, which is more consistent with their dense axonal projections to L1 of V2M. The authors also used rabies tracing to identify presynaptic inputs to PT neurons in V2M, and found that the RSC provided nearly 30% of all input, similar to the study by Kim et al. (2015), though unlike that study, V2L provided much weaker inputs (<5% of all input). In sCRACM recordings, RSC did indeed

innervate the apical dendrites of PT cells, but to a lesser degree than other input areas such as V1 and the secondary thalamic nuclei.

Since PT cells target predominantly subcortical areas rather than cortical ones, their apical dendrites may serve as antennae for non-looped cortical communication and enable them to more effectively broadcast the output of cortical computations to deep brain structures involved in movement and behavior. Indeed, our simulations showed that, all else being equal, inputs arriving on the more extensive apical dendrites of PT neurons (Chapter 2, Figure 5, figure supplement 2) generate a larger response at the soma compared to the thin-tufted IT cells (Chapter 2, Figure 5, figure supplement 3). Furthermore, their intrinsic bursting firing patterns and dense coding properties may make PT neurons ideally suited for relaying the results of these computations to subcortical areas related to action selection and motor control (Harris & Mrsic-Flogel, 2013; Harris & Shepherd, 2015). This is because a burst discharge may be more likely to initiate action potentials in the postsynaptic neuron through significant temporal summation and amplification of EPSPs (Williams & Stuart, 1999).

In this study, PT cells were defined by their projections to the superior colliculus, which has been implicated in the regulation of spatial attention (Krauzlis, Lovejoy, & Zénon, 2013). Interestingly, a recent study of PT neurons in mouse primary somatosensory cortex found that activation of PT apical dendrites, but not IT apical dendrites, is critical for tactile detection (Takahashi et al., 2020). The

authors reported that whisker-based perceptual detection was correlated with Ca2+ currents in the apical tufts of PT neurons, but only when the tactile stimulus carried behavioral relevance.

It has been proposed that the apical dendrites of cortical L5 pyramidal neurons and their Ca2+ currents may mediate not just tactile perception, but conscious perception more generally (Bachmann, 2015; K. Meyer, 2015; Suzuki & Larkum, 2020). Over a quarter-century ago, in their essay titled 'Some Further Ideas Regarding the Neuronal Basis of Awareness', Koch & Crick posited that PT neurons may play a pivotal role in conscious awareness (Koch & Davis, 1994). They wrote that "If at any given point in time only 1% of all the neurons in cortex fire significantly, about one billion cells in sensory, motor, and association cortices would be active and we would never be able to distinguish any particular event out of this vast sea of active nerve cells. We strongly expect that the majority of neurons will be involved in doing computations, while only a much smaller number will express the results of these computations. It is probably that we become aware of only the latter".

This accords with previous proposals that the content of consciousness is composed of the output of neural computations rather than the computations themselves (Johnson-Laird, 1988). Since PT neurons convey the results of cortical computations, Koch & Crick speculated that awareness may arise from these bursting cells: "Thus a very simplistic answer to the question 'Which neurons fire in

such a way that they correlate with awareness?' would be 'The large pyramidal cells in layer 5 that fire in bursts and project outside the cortical system!' It would be marvelous if this were true but the answer is unlikely to be as simple as that".

Intriguingly, this proposed property of PT cells formed part of Koch & Crick's "lower-layers hypothesis" in which neural correlates of visual awareness occur in the deep layers of the cortex, L5 and L6, while L2/3 and L4 are mainly associated with unconscious processing. This hypothesis stemmed from their observations that burst-generating cortical output neurons reside in L5 and that neurons in cat V1 that fire more strongly in the awake state compared to slow-wave sleep are predominantly found in L5 and L6 (Livingstone & Hubel, 1981).

Thus, we may speculate that there are two fundamentally different types of CC connections in lower layers of visual cortex. The apical dendrites of PT cells in V1, which received only weak inputs in our study, may instead receive CC inputs from frontal and associative areas (Kim et al., 2015) that mediate attention and awareness of sensory stimuli (Manita et al., 2015; Takahashi et al., 2020; Takahashi, Oertner, Hegemann, & Larkum, 2016; Zhang et al., 2014). Such CC connections would be non-looped since, by definition, PT cells project outside the cortex rather than within it. Meanwhile, other looped CC connections in the visual hierarchy, such as the ones we have identified, may be more used for making sense of the world

through feature extraction and object identification, as we shall explore further in the next section.

3.5 Implications for predictive coding frameworks

For much of the history of neuroscience, the representational framework has dominated our view of what the cortex does. This theory posits that sensory cortical areas, driven mainly by FF input, are tasked with extracting and identifying an object or feature from environmental stimuli. Thus, sensory neurons act as "feature detectors" that enable other neurons to act on the presence (or absence) of the detected feature (Marr, 1982). From simple cells in visual cortex (Hubel & Wiesel, 1959) to face cells in the temporal cortex (Perrett, Rolls, & Caan, 1982), this representational framework has been a cornerstone in how we think about neocortical function.

However, an alternative view has been gaining traction in the last few decades, which builds on ideas first put forward in the 1860s (Von Helmholtz, 1867), that the brain generates an internal model of the outside world, based on past experience, in order to make predictions about sensory inputs (Barlow, 1961; Bastos et al., 2012; Craik, 1952; Dayan, Hinton, Neal, & Zemel, 1995; Gregory, 1980; Keller & Mrsic-Flogel, 2018). In the predictive framework, the predicted and actual sensory inputs are compared, and any difference between the two, termed the "prediction error", updates the prediction or internal model.

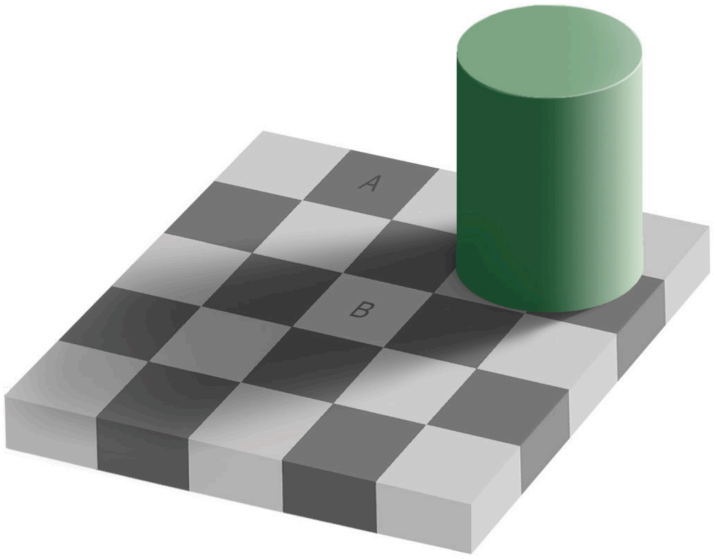

Figure 3.1 *Adelson's Checker-Shadow Illusion: squares marked A and B are, in fact, exactly the same shade of gray.*

Predictive coding theories help to explain optical illusions, such as when we see color where there is none because our prior experience tells us that objects seldom change color (Foster, 2011), or when we see two objects as being different colors when they are in fact the same (Adelson, 1995). For example, in Adelson's famous checkerboard shadow illusion (Figure 3.1), the color of square A looks very different to the color of square B, but the colors of these two squares are actually the same. Illusions like this one demonstrate that our visual perception of the world is not a faithful representation of reality. Rather, it is an interpretation. Our brain assumes that a shadow darkens the surface it is cast upon, so it compensates by making square B seem lighter than it really is, even though these two squares reflect exactly the same amount of light to

our eye. Thus, the brain is not a camera, and does not passively record the world. Instead, it actively constructs it based on prior expectations. For this reason, perception may be more accurately described as "controlled hallucination" (Clark, 2015). Presumably, predictive internal models carry evolutionary advantages, anticipating not just sensory inputs arising from our own actions, but also the actions of others. As Donald Hoffman puts it, "Perception is not about seeing truth. It's about having kids" (Hoffman, 2016). Moreover, internal models can be decoupled from their sensory inputs to simulate the sensory consequences of self-generated movements. As Keller and Mrsic-Flogel point out, these simulations "are likely what we refer to as thinking" (Keller & Mrsic-Flogel, 2018).

How do these predictive coding theories map onto the cortical circuit? L5 pyramidal cells in higher cortical areas are thought to send predictions of bottom-up input to lower cortical areas, while L2/3 pyramidal cells in lower cortical areas are thought to send prediction errors to higher cortical areas. Importantly, a predictive framework suggests specificity in both FF and FB connections: in order for an internal representation of the world to be updated by sensory input, higher areas would be expected to relay FB predictions to the same lower areas that they receive FF prediction errors from. In other words, predictive coding requires looped connectivity.

Given that prediction error signals in L2/3 neurons in mouse V1 occur in precise locations of the visual field (Zmarz & Keller, 2016), and that V1 arborizations in higher areas are retinotopically organized (Wang & Burkhalter, 2007), prediction errors may be relayed in a retinotopically specific manner to higher areas. Similarly, the receptive field properties of LM FB inputs in L1 of V1 were found to, on average, retinotopically match those of underlying L2/3 pyramidal cells in their vicinity (Marques, Nguyen, Fioreze, & Petreanu, 2018), consistent with predictive coding models in which prediction signals reciprocally target the same cells in lower areas that they receive information from (Sacramento, Bengio, Costa, & Senn, 2018).

However, although we measured robust FB inputs from V2L and V2M to looped L2/3 neurons in V1, which may be involved in predictive processing computations, we did not see a preference for looped connectivity in superficial layers, as neighboring non-looped L2/3 neurons received, on average, equal input. If prediction error responses are more prevalent in L2/3 than in L5, as has been reported (Hamm, Shymkiv, Han, Yang, & Yuste, 2021; Jordan & Keller, 2020; Saleem, Ayaz, Jeffery, Harris, & Carandini, 2013), we might expect a preference of FB inputs for looped neurons in supragranular layers rather than in infragranular ones.

Considering that FB predictions are supposed to suppress prediction errors, their overall effect on cells in lower areas may be inhibitory, rather than excitatory. This is consistent with studies

showing enhanced neural responses to unexpected stimuli, which presumably reflects a failure of FB predictions to predict bottom-up sensory input and to reduce prediction errors (Garrido, Kilner, Stephan, & Friston, 2009). Considering also that FB axons densely innervate L1, which lacks excitatory neurons and contains interneurons with powerful inhibitory influences on L2/3 pyramidal cells (Chu, Galarreta, & Hestrin, 2003; Wozny & Williams, 2011), FB predictions may instead suppress prediction errors in superficial cells via their axon terminals in L1. Thus, the monosynaptic excitatory FB connections we measured in L2/3 cells may mediate other, non-predictive, processes such as attentional modulation (Hopfinger, Buonocore, & Mangun, 2000).

Alternatively, if FB monosynaptic inputs in L2/3 V1 cells do indeed convey predictions, then the lack of a preference for looped connectivity in L2/3 may not be so surprising, if one is to believe proposed microcircuits for predictive processing (Figure 3.2) (Keller & Mrsic-Flogel, 2018). Prediction errors may take one of two forms: either the prediction error neuron responds less strongly than predicted (negative prediction error), such as when a stimulus unexpectedly disappears, or it responds more strongly than predicted (positive prediction error), such as when an unexpected stimulus suddenly appears. It has been suggested that negative and positive prediction errors are encoded by two separate populations of neurons (Keller & Mrsic-Flogel, 2018; Rao & Ballard, 1999).

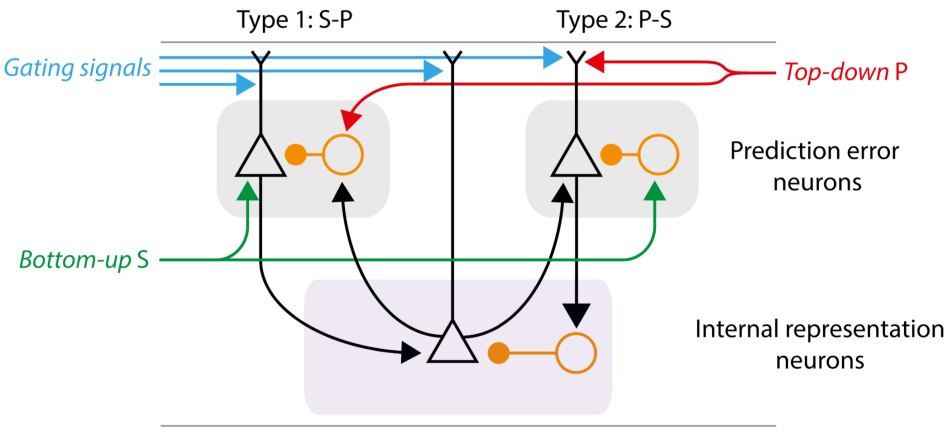

Figure 3.2 *Proposed microcircuit for predictive coding. Type 1 neurons (left) encode positive prediction errors, while Type 2 neurons (right) encode negative prediction errors. In Type 1 neurons, FB inputs are inhibitory and bottom-up inputs are excitatory, and in Type 2 neurons, FB inputs are excitatory and bottom-up inputs are inhibitory. Triangles, pyramidal cells; Circles, interneurons. Reproduced from (Keller & Mrsic-Flogel, 2018).*

Indeed, studies have uncovered evidence for each type of prediction error. For example, some L2/3 neurons in mouse V1 selectively respond to the absence of a predicted stimulus (Fiser et al., 2016), so-called negative prediction error neurons, while other neurons selectively respond to the presence of an unpredicted stimulus (T. Meyer & Olson, 2011), so-called positive prediction error neurons.

Since FB inputs are theorised to excite negative prediction error neurons and inhibit positive prediction error neurons (Figure 3.2), stronger FB excitation of looped negative prediction error

neurons in L2/3 of V1 may have been masked in our recordings by weaker FB excitation of looped positive prediction error neurons, assuming that these two populations of neurons are equally abundant and interspersed with one another. This might explain why we observed no predilection of FB inputs for looped neurons in L2/3. Of course, this still leaves the question of what function FB inputs to non-looped L2/3 neurons serve.

While the symmetry of negative and positive prediction-error circuits is appealing, it may also be inefficient and biologically implausible, since it necessitates two populations of prediction error neurons rather than one. Thus, like a gas-guzzling sports car, it might be aesthetically pleasing, but energetically rather expensive. In the dopaminergic system, for example, positive and negative prediction errors are encoded by the same neurons (Schultz, Dayan, & Montague, 1997). Indeed, it is not immediately obvious what the advantages are of having separate circuits for signalling the unexpected absence or presence of a stimulus. They may well be two sides of the same coin. After all, the absence of an expected stimulus is simply the presence of an unexpected stimulus in its place.

Thus, a neural response to the absence of a predicted sensory input ("negative prediction error") may instead reflect a response to the presence of an unpredicted sensory input. In other words, negative prediction error neurons may merely be positive prediction error neurons. If that is the case, excitatory FB inputs to L2/3 pyramidal cells might be more likely to mediate attentional

enhancement, as previously mentioned, increasing the gain of prediction error neurons, and overcoming FB suppression of responses to predictable stimuli. In this way, predictive (inhibitory) and attentional (excitatory) FB signals may work together synergistically in L2/3 to enhance the precision of perceptual inference, as demonstrated empirically (Kok, Rahnev, Jehee, Lau, & De Lange, 2012). Therefore, the excitatory FB inputs in L2/3 cells that we have measured in this study could be involved in top-down attentional modulation (which does not require looped connectivity), leading to equal inputs in looped and non-looped neurons, consistent with our results.

3.6 Learning and error backpropagation

Recently, models have theorized that FB inputs to apical dendrites of looped FF neurons act as a teaching signal to optimise the global output of neuronal circuits, akin to the way backpropagation-of-error algorithms train artificial neural networks (Guerguiev, Lillicrap, & Richards, 2017; Lillicrap, Cownden, Tweed, & Akerman, 2016; Richards & Lillicrap, 2019; Roelfsema & Holtmaat, 2018; Sacramento et al., 2018). Such theories posit that FB inputs send error signals that adjust the synaptic weights of bottom-up inputs to FF cells so as to facilitate learning and improve the functioning of the entire network. By targeting looped FF cells, FB cells may modulate the information they receive in order to obtain the desired outcome.

For decades, the idea that the brain implements "backprop" has been deemed biologically implausible (Crick, 1989; Grossberg, 1987). Such perceived implausibility stems in part from the requirement of the backprop learning algorithm that neurons must know the synaptic weights of many other neurons, and that FF and FB connections must exhibit precise symmetry. However, more recently, this idea has been revisited and such architectural constraints have been lifted. It has been argued that only a modest symmetry between FF and FB weights is required for rapid learning, and that even random FB weights are able to deliver useful teaching signals (Lillicrap et al., 2016).

Several attempts have been made to develop more biologically realistic models for how backprop could be implemented by neural circuits (Guerguiev et al., 2017; Sacramento et al., 2018). By segregating FF and FB inputs to distinct dendritic compartments – a basal compartment for bottom-up sensory information and an apical compartment for top-down feedback information – these models provide dendritic solutions to the "credit assignment problem" (Richards & Lillicrap, 2019). This problem refers to the difficulty in assigning credit or blame to neurons at lower hierarchical levels for errors that occur several synapses away at higher hierarchical levels. For example, if a neuron in sensory cortex contributes to errors in motor cortex, how can the brain correctly change the synaptic connections of this neuron if the behavioural effects of those changes also depend on intermediary synaptic connections downstream that link this sensory neuron with the final output?

The implications of these more biologically feasible models bear relevance to our own findings, since the distal apical dendrites of looped pyramidal neurons play a central role in their proposed solution to the credit assignment problem. Our results are consistent with these models in that we observe a preference for looped connectivity in CC projections, and these models predict alignment of FF and FB synaptic weights. In the presence of weight alignment, non-looped neurons, which by definition have zero synaptic weight with the source of CC input, would be expected to receive less CC input relative to looped neurons, which is what we find. Thus, the prefential innervation of looped neurons that we observe may provide a biological substrate for learning, and the apical dendrites of looped IT neurons may be specialised for this purpose.

However, while our results are consistent with a degree of weight alignment in cortical circuits, they do not prove the existence of symmetric FF and FB synaptic weights in bidirectionally connected pairs of neurons located at different hierarchical levels. This is because sCRACM measures the strength of inputs from a presynaptic population rather than from an individual presynaptic cell. Consequently, the monosynaptic connections that we measure are at the area-to-cell level, rather than at the cell-to-cell level. Moreover, we cannot know whether the looped cells labelled in this study contact the same cells that they receive monosynaptic inputs from.

3.7 Limitations of our study

It is worth mentioning several potential limitations of our approach. First, it is possible that the specificity of FF or FB connections varies across projections. Given that we recorded similar numbers of cells across different projections, nonsignificant results could therefore reflect underpowered data rather than lack of specificity. Such variations are conceivable given that the HVAs targeted, namely LM and AM, lie at opposite ends of the visual cortical hierarchy, with LM even receiving direct thalamocortical projections from dLGN (Antonini, Fagiolini, & Stryker, 1999; Oh et al., 2014). Thus, while V1→V2L L6 projection neurons, for example, did not receive stronger FB from V2L compared to non-looped neurons, this could be due to an insufficient number of cell pairs recorded.

Another potential drawback pertains to FF connections. Unlike FB axons, which are widely distributed across V1, FF projections tend to be restricted to a narrow column (~200/250 microns wide) of the HVA that they target. While we recorded pairs no more than 200 microns apart, it is possible that in some cases, cells may have received less input than their partner cell because of being located just outside of, or on the border of, this FF axonal column. In addition, given that the boundaries we used to define cortical layers are approximate, it may be that some cells with somas very closely positioned to estimated laminar borders were incorrectly assigned to layers.

We recorded from mice ~P40/P45, almost a month after eye opening, though it is not clear if full maturation of FF or FB axonal connectivity has occurred by this time point, and there is evidence to suggest that interareal CC connections continue to develop several months after eye opening (Dong, Wang, Valkova, Gonchar, & Burkhalter, 2004). Ideally, our recordings would have been carried out in older mice, though whole-cell patch clamp recordings become increasingly difficult to perform with age.

Given that our injections in V2L and V2M may have in some cases targeted more than one HVA, it is possible that this added noise to our FB datasets such that ChR2+ve FB inputs to a V1 neuron labelled as looped may have come from a different area to the one it projected to. This would be expected, however, to reduce specificity of FB connections rather than to increase it, and the likelihood of a mismatch between looped neurons and the source of FB was reduced by coinjecting the ChR2 and retrobeads in the same pipette.

Given that the sCRACM method has a spatial resolution of ~60 μm (Petreanu, Mao, Sternson, & Svoboda, 2009), specificity of FF and FB connections for looped neurons could arise from stronger synapses, more synapses, or a mixture of the two, and we cannot distinguish between these scenarios. Similarly, given that ChR2 was expressed in many cells across cortical layers, we cannot say whether cells presynaptic to looped and non-looped neurons differed in either quantity or identity.

3.8 Future directions

Aside from the potential future experiments already discussed, such as establishing whether or not deep-layer FF-FB loops involve cell-to-cell specificity rather than simply area-to-cell specificity, several other interesting lines of research remain to be investigated. For example, it remains to be determined whether or not FF-FB loops involve non-visual areas as well, and how prevalent they are across the cortex. As stated by Ungerleider and colleagues (1994), "…it may be that the rules that have been used for establishing hierarchical relationships within both the visual and somatosensory systems do not extend, in any simple way, to connections with frontal lobe areas". Given the lack of selectivity for looped neurons observed in various CC projections to the somatosensory and motor cortex (Mao et al., 2011; Suter & Shepherd, 2015; Yamawaki, Radulovic, & Shepherd, 2016), it appears unlikely that selective targeting of looped cells is a consistent property of CC connections (though it is possible that in these studies, separately analyzing apical and basal inputs would have revealed dendrite-specific preferences for looped connectivity in some cases). As of the time of writing, work in the lab suggests that L5 V1 neurons projecting to RSC, implicated in spatial and episodic memory and navigation, receive stronger FB inputs from RSC compared to adjacent V2L-projecting neurons (Figure 3.3).

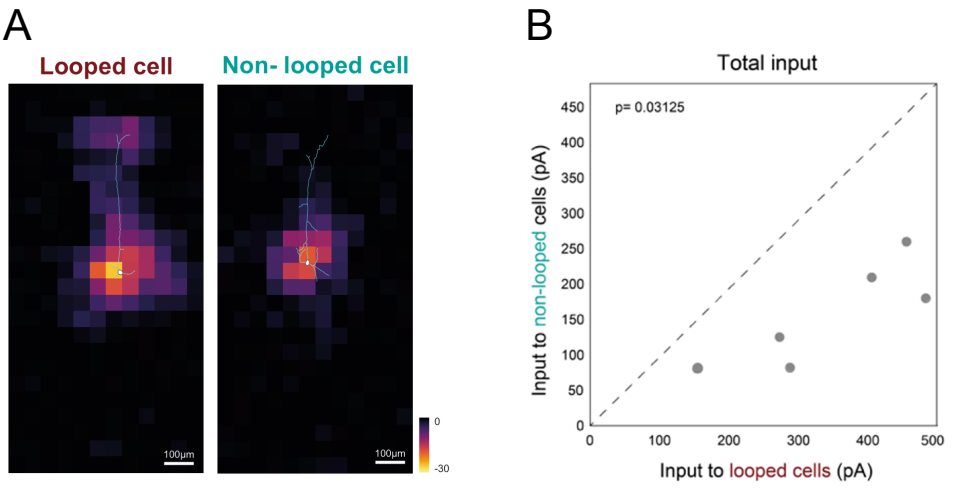

Figure 3.3 *A) sCRACM maps of an example pair of V1 L5 neurons overlaid on their reconstructed dendrites. Responsive locations are color-coded to represent mean amplitude. The looped cell projects to the retrosplenial cortex, the source of FB, while the non-looped cell projects to V2L B) Paired comparisons of total FB input to looped vs. non-looped neurons. Unpublished data collected by Beatriz Moura.*

It is likely that the selective modulation of looped neurons that we have identified in this study occur in other long-range projections arising from the cortex. For example, it has already been shown that both CT and PT cells in the primary somatosensory cortex of the mouse preferentially target looped over non-looped neurons in the thalamus (Guo, Yamawaki, Barrett, Tapies, & Shepherd, 2020). Indeed, cortico-thalamo-cortical loops may be critical for communication in hierarchical models of cortical organization (Shepherd & Yamawaki, 2021). Further cases may remain to be uncovered. For instance, corticoclaustral projection neurons have been identified in L6 and, rarely for L6 neurons, have apical

dendrites extending to L1 (Katz, 1987), while reciprocal claustrocortical projections strongly innervate L6 and L1 (LeVay, 1986).

FF and FB connections may also show specificity with respect to local inhibitory neurons, not just excitatory neurons. They may, for example, preferentially synapse onto inhibitory neurons connecting either to looped neurons or to other interneurons that connect to looped neurons. One such candidate recipient of specific CC connections are interneurons expressing the vasoactive intestinal polypeptide, which are known to receive considerable long-range and neuromodulatory inputs (Wickersham et al., 2007; S. Zhang et al., 2014), and to mainly suppress somatostatin-expressing interneurons, leading to the disinhibition of pyramidal cells (Kepecs & Fishell, 2014; Pfeffer, Xue, He, Huang, & Scanziani, 2013). Understanding the precise wiring of FB axons with regard to inhibitory neurons also promises to inform the predictive coding models that we discussed earlier, in which FB is posited to suppress prediction errors.

Another area that has been neglected is the role of FB connections targeting the basal dendrites of cells in lower areas. We observed that, in all layers including L5, FB axons strongly innervated the perisomatic region. Presumably, these inputs amplify local FF input and increase the likelihood of action potential initiation in the axon hillock and axon initial segment. Using full-field LED illumination to activate FB inputs (both perisomatic and apical),

we found that FB does indeed induce greater spiking activity in infragranular looped neurons with concomitant bottom-up input (Chapter 2, Figure 8). However, teasing apart the contributions of perisomatic and apical FB input to action potential generation might shed light on the different functions they likely play. Most models of cortical computation emphasize the part played by apical dendrites and L1 in FB processing, and overlook the fact that FB axons may make stronger connections to basal dendrites than to apical ones. Answering these questions could help to reveal the full complexity of long-range connectivity in the cortex, which will likely take scientists many decades, if not centuries, to unravel.

Adelson, E. H. (1995). Checkershadow illusion.

Antonini, A., Fagiolini, M., & Stryker, M. P. (1999). Anatomical correlates of functional plasticity in mouse visual cortex. *Journal of Neuroscience*, *19*(11), 4388–4406. https://doi.org/10.1523/jneurosci.19-11-04388.1999

Bachmann, T. (2015). How a (sub)cellular coincidence detection mechanism featuring layer-5 pyramidal cells may help produce various visual phenomena. *Frontiers in Psychology*, *6*(DEC), 1–9. https://doi.org/10.3389/fpsyg.2015.01947

Barlow, H. (1961). Possible Principles Underlying the Transformations of Sensory Messages. *Sensory Communication*, *1*. https://doi.org/10.7551/mitpress/9780262518420.003.0013

Bastos, A. M., Usrey, W. M., Adams, R. A., Mangun, G. R., Fries, P., & Friston, K. J. (2012). Canonical Microcircuits for Predictive Coding. *Neuron*, *76*(4), 695–711. https://doi.org/10.1016/j.neuron.2012.10.038

Beier, K. T. (2019). Hitchhiking on the neuronal highway: Mechanisms of transsynaptic specificity. *Journal of Chemical Neuroanatomy*, *99*(April), 9–17. https://doi.org/10.1016/j.jchemneu.2019.05.001

Bullier, J., Kennedy, H., & Salinger, W. (1984). Branching and laminar origin of projections between visual cortical areas in the cat. *Journal of Comparative Neurology*, *228*(3), 329–341. https://doi.org/10.1002/cne.902280304

Callaway, E. M., & Luo, L. (2015). Monosynaptic circuit tracing with

glycoprotein-deleted rabies viruses. *Journal of Neuroscience*, *35*(24), 8979–8985. https://doi.org/10.1523/JNEUROSCI.0409-15.2015

Castle, M. J., Gershenson, Z. T., Giles, A. R., Holzbaur, E. L. F., & Wolfe, J. H. (2014). Adeno-associated virus serotypes 1, 8, and 9 share conserved mechanisms for anterograde and retrograde axonal transport. *Human Gene Therapy*, *25*(8), 705–720. https://doi.org/10.1089/hum.2013.189

Chu, Z., Galarreta, M., & Hestrin, S. (2003). Synaptic interactions of late-spiking neocortical neurons in layer 1. *Journal of Neuroscience*, *23*(1), 96–102. https://doi.org/10.1523/jneurosci.23-01-00096.2003

Clark, A. (2015). *Surfing uncertainty: Prediction, action, and the embodied mind*. Oxford University Press.

Craik, K. J. W. (1952). *The nature of explanation* (Vol. 445). CUP Archive.

Crick, F. (1989). The recent excitement about neural networks. *Nature*. https://doi.org/10.1038/337129a0

Dayan, P., Hinton, G. E., Neal, R. M., & Zemel, R. S. (1995). The Helmholtz machine. *Neural Computation*, *7*(5), 889–904. https://doi.org/10.1162/neco.1995.7.5.889

Dong, H., Wang, Q., Valkova, K., Gonchar, Y., & Burkhalter, A. (2004). Experience-dependent development of feedforward and feedback circuits between lower and higher areas of mouse visual cortex. *Vision Research*, *44*(28 SPEC.ISS.), 3389–3400.

https://doi.org/10.1016/j.visres.2004.09.007

Federer, F., Ichida, J. M., Jeffs, J., Schiessl, I., McLoughlin, N., & Angelucci, A. (2009). Four projection streams from primate V1 to the cytochrome oxidase stripes of V2. *Journal of Neuroscience*, *29*(49), 15455–15471. https://doi.org/10.1523/JNEUROSCI.1648-09.2009

Federspiel, M. J., Bates, P., Young, J. A. T., Varmus, H. E., & Hughes, S. H. (1994). A system for tissue-specific gene targeting: Transgenic mice susceptible to subgroup A avian leukosis virus-based retroviral vectors. *Proceedings of the National Academy of Sciences of the United States of America*, *91*(23), 11241–11245. https://doi.org/10.1073/pnas.91.23.11241

Ferrer, J. M. R., Kato, N., & Price, D. J. (1992). Organization of association projections from area 17 to areas 18 and 19 and to suprasylvian areas in the cat's visual cortex. *Journal of Comparative Neurology*, *316*(3), 261–278. https://doi.org/10.1002/cne.903160302

Fiser, A., Mahringer, D., Oyibo, H. K., Petersen, A. V., Leinweber, M., & Keller, G. B. (2016). Experience-dependent spatial expectations in mouse visual cortex. *Nature Neuroscience*, *19*(12), 1658–1664. https://doi.org/10.1038/nn.4385

Foster, D. H. (2011). Color constancy. *Vision Research*, *51*(7), 674–700. https://doi.org/10.1016/j.visres.2010.09.006

Galloni, A. R., Ye, Z., & Rancz, E. (2021). Dendritic distribution of synaptic inputs to layer 5 pyramidal neurons Dendritic domain-

specific sampling of long-range axons shapes feedforward and feedback connectivity of L5 neurons. *BioRxiv*, 2021.01.31.429033. Retrieved from https://doi.org/10.1101/2021.01.31.429033

Garrido, M. I., Kilner, J. M., Stephan, K. E., & Friston, K. J. (2009). The mismatch negativity: A review of underlying mechanisms. *Clinical Neurophysiology*, *120*(3), 453–463. https://doi.org/10.1016/j.clinph.2008.11.029

Gilbert, C. D., & Kelly, J. P. (1975). The projections of cells in different layers of the cat's visual cortex. *Journal of Comparative Neurology*, *163*(1), 81–105. https://doi.org/10.1002/cne.901630106

Gregory, R. L. (1980). Perceptions as hypotheses. *Philosophical Transactions of the Royal Society of London. Series B, Biological Sciences*, *290*(1038), 181–197. https://doi.org/10.1098/rstb.1980.0090

Grossberg, S. (1987). Competitive learning: From interactive activation to adaptive resonance. *Cognitive Science*, *11*(1), 23–63. https://doi.org/10.1016/S0364-0213(87)80025-3

Guerguiev, J., Lillicrap, T. P., & Richards, B. A. (2017). Towards deep learning with segregated dendrites. *ELife*, *6*, 1–37. https://doi.org/10.7554/eLife.22901

Guo, K. H., Yamawaki, N., Barrett, J. M., Tapies, M., & Shepherd, G. M. G. (2020). Cortico-thalamo-cortical circuits of mouse forelimb S1 are organized primarily as recurrent loops. *Journal of Neuroscience*, *40*(14), 2849–2858. https://doi.org/10.1523/JNEUROSCI.2277-19.2020

Hamm, J. P., Shymkiv, Y., Han, S., Yang, W., & Yuste, R. (2021). Cortical ensembles selective for context. *Proceedings of the National Academy of Sciences of the United States of America*, *118*(14). https://doi.org/10.1073/pnas.2026179118

Harris, K. D., & Mrsic-Flogel, T. D. (2013). Cortical connectivity and sensory coding. *Nature*, *503*(7474), 51–58. https://doi.org/10.1038/nature12654

Harris, K. D., & Shepherd, G. M. G. (2015). The neocortical circuit: themes and variations. *Nature Neuroscience*, *18*(2), 170–181. https://doi.org/10.1038/nn.3917

Hoffman, D. D. (2016). The Interface Theory of Perception. *Current Directions in Psychological Science*, *25*(3), 157–161. https://doi.org/10.1177/0963721416639702

Hooks, B. M., Mao, T., Gutnisky, D. A., Yamawaki, N., Svoboda, K., & Shepherd, G. M. G. (2013). Organization of cortical and thalamic input to pyramidal neurons in mouse motor cortex. *Journal of Neuroscience*, *33*(2), 748–760. https://doi.org/10.1523/JNEUROSCI.4338-12.2013

Hopfinger, J. B., Buonocore, M. H., & Mangun, G. R. (2000). The neural mechanisms of top-down attentional control. *Nature Neuroscience*, *3*(3), 284–291. https://doi.org/10.1038/72999

Hubel, D. H. (1982). Cortical Neurobiology. *Annual Review of Neuroscience*, *5*, 363–370.

Hubel, D., & Wiesel, T. (1959). RECEPTIVE FIELDS OF SINGLE

NEURONES IN THE CAT ' S STRIATE CORTEX By D . H . HUBEL * AND T . N . WIESEL * From the Wilmer Institute , The Johns Hopkins Hospital and In the central nervous system the visual pathway from retina to striate cortex provides an. *The Journal of Physiology*, *148(3)*, *57*, 574–591.

Johnson-Laird, P. (1988). The Computer And The Mind.

Jordan, R., & Keller, G. B. (2020). Opposing Influence of Top-down and Bottom-up Input on Excitatory Layer 2/3 Neurons in Mouse Primary Visual Cortex. *Neuron*, *108*(6), 1194-1206.e5. https://doi.org/10.1016/j.neuron.2020.09.024

Katz, L. C. (1987). Local circuitry of identified projection neurons in cat visual cortex brain slices. *Journal of Neuroscience*, *7*(4), 1223–1249. https://doi.org/10.1523/jneurosci.07-04-01223.1987

Keller, G. B., & Mrsic-Flogel, T. D. (2018). Predictive Processing: A Canonical Cortical Computation. *Neuron*, *100*(2), 424–435. https://doi.org/10.1016/j.neuron.2018.10.003

Kepecs, A., & Fishell, G. (2014). Interneuron cell types are fit to function. *Nature*, *505*(7483), 318–326. https://doi.org/10.1038/nature12983

Kim, E. J., Juavinett, A. L., Kyubwa, E. M., Jacobs, M. W., & Callaway, E. M. (2015). Three Types of Cortical Layer 5 Neurons That Differ in Brain-wide Connectivity and Function. *Neuron*, *88*(6), 1253–1267. https://doi.org/10.1016/j.neuron.2015.11.002

Kinnischtzke, A. K., Fanselow, E. E., & Simons, D. J. (2016). Target-specific M1 inputs to infragranular S1 pyramidal neurons. *Journal of*

Neurophysiology, *116*(3), 1261–1274. https://doi.org/10.1152/jn.01032.2015

Kinnischtzke, A. K., Simons, D. J., & Fanselow, E. E. (2014). Motor cortex broadly engages excitatory and inhibitory neurons in somatosensory barrel cortex. *Cerebral Cortex*, *24*(8), 2237–2248. https://doi.org/10.1093/cercor/bht085

Koch, C., & Davis, J. (1994). Large-Scale Neuronal Theories of the Brain.

Kok, P., Rahnev, D., Jehee, J. F. M., Lau, H. C., & De Lange, F. P. (2012). Attention reverses the effect of prediction in silencing sensory signals. *Cerebral Cortex*, *22*(9), 2197–2206. https://doi.org/10.1093/cercor/bhr310

Krauzlis, R. J., Lovejoy, L. P., & Zénon, A. (2013). Superior colliculus and visual spatial attention. *Annual Review of Neuroscience*, *36*(May), 165–182. https://doi.org/10.1146/annurev-neuro-062012-170249

LeVay, S. (1986). Synaptic organization of claustral and geniculate afferents to the visual cortex of the cat. *Journal of Neuroscience*, *6*(12), 3564–3575. https://doi.org/10.1523/jneurosci.06-12-03564.1986

Lillicrap, T. P., Cownden, D., Tweed, D. B., & Akerman, C. J. (2016). Random synaptic feedback weights support error backpropagation for deep learning. *Nature Communications*, *7*, 1–10. https://doi.org/10.1038/ncomms13276

Livingstone, M. S., & Hubel, D. H. (1981). Effects of sleep and arousal on the processing of visual information in the cat. *Nature*, *291*(5816), 554–561. https://doi.org/10.1038/291554a0

Löw, K., Aebischer, P., & Schneider, B. L. (2013). Direct and retrograde transduction of nigral neurons with AAV6, 8, and 9 and intraneuronal persistence of viral particles. *Human Gene Therapy*, *24*(6), 613–629. https://doi.org/10.1089/hum.2012.174

Luo, L., Callaway, E. M., & Svoboda, K. (2018). Genetic Dissection of Neural Circuits: A Decade of Progress. *Neuron*, *98*(2), 256–281. https://doi.org/10.1016/j.neuron.2018.03.040

Manita, S., Suzuki, T., Homma, C., Matsumoto, T., Odagawa, M., Yamada, K., … Murayama, M. (2015). A Top-Down Cortical Circuit for Accurate Sensory Perception. *Neuron*, *86*(5), 1304–1316. https://doi.org/10.1016/j.neuron.2015.05.006

Mao, T., Kusefoglu, D., Hooks, B. M., Huber, D., Petreanu, L., & Svoboda, K. (2011). Long-Range Neuronal Circuits Underlying the Interaction between Sensory and Motor Cortex. *Neuron*, *72*(1), 111–123. https://doi.org/10.1016/j.neuron.2011.07.029

Marques, T., Nguyen, J., Fioreze, G., & Petreanu, L. (2018). The functional organization of cortical feedback inputs to primary visual cortex. *Nature Neuroscience*, *21*(5), 757–764. https://doi.org/10.1038/s41593-018-0135-z

Marr, D. (1982). Vision: A computational investigation into the human representation.

Meyer, K. (2015). The Role of Dendritic Signaling in the Anesthetic Suppression of Consciousness. *Anesthesiology*, *122*(6), 1415–1431. https://doi.org/10.1097/ALN.0000000000000673

Meyer, T., & Olson, C. R. (2011). Statistical learning of visual transitions in monkey inferotemporal cortex. *Proceedings of the National Academy of Sciences of the United States of America*, *108*(48), 19401–19406. https://doi.org/10.1073/pnas.1112895108

Oh, S. W., Harris, J. A., Ng, L., Winslow, B., Cain, N., Mihalas, S., … Zeng, H. (2014). A mesoscale connectome of the mouse brain. *Nature*, *508*(7495), 207–214. https://doi.org/10.1038/nature13186

Perrett, D. I., Rolls, E. T., & Caan, W. (1982). Visual neurones responsive to faces in the monkey temporal cortex. *Experimental Brain Research*, *47*(3), 329–342. https://doi.org/10.1007/BF00239352

Petreanu, L., Mao, T., Sternson, S. M., & Svoboda, K. (2009). The subcellular organization of neocortical excitatory connections. *Nature*, *457*(7233), 1142–1145. https://doi.org/10.1038/nature07709

Pfeffer, C. K., Xue, M., He, M., Huang, Z. J., & Scanziani, M. (2013). Inhibition of inhibition in visual cortex: The logic of connections between molecularly distinct interneurons. *Nature Neuroscience*, *16*(8), 1068–1076. https://doi.org/10.1038/nn.3446

Rao, R. P. N., & Ballard, D. H. (1999). Predictive coding in the visual cortex: A functional interpretation of some extra-classical receptive-field effects. *Nature Neuroscience*, *2*(1), 79–87. https://doi.org/10.1038/4580

Richards, B. A., & Lillicrap, T. P. (2019). Dendritic solutions to the credit assignment problem. *Current Opinion in Neurobiology*, *54*, 28–36. https://doi.org/10.1016/j.conb.2018.08.003

Roelfsema, P. R., & Holtmaat, A. (2018). Control of synaptic plasticity in deep cortical networks. *Nature Reviews Neuroscience*, *19*(3), 166–180. https://doi.org/10.1038/nrn.2018.6

Sacramento, J., Bengio, Y., Costa, R. P., & Senn, W. (2018). Dendritic cortical microcircuits approximate the backpropagation algorithm. *ArXiv*, (NeurIPS).

Saleem, A. B., Ayaz, A. I., Jeffery, K. J., Harris, K. D., & Carandini, M. (2013). Integration of visual motion and locomotion in mouse visual cortex. *Nature Neuroscience*, *16*(12), 1864–1869. https://doi.org/10.1038/nn.3567

Schultz, W., Dayan, P., & Montague, P. R. (1997). A neural substrate of prediction and reward. *Science*, *275*(5306), 1593–1599. https://doi.org/10.1126/science.275.5306.1593

Seidler, B., Schmidt, A., Mayr, U., Nakhai, H., Schmid, R. M., Schneider, G., & Saur, D. (2008). A Cre-loxP-based mouse model for conditional somatic gene expression and knockdown in vivo by using avian retroviral vectors. *Proceedings of the National Academy of Sciences of the United States of America*, *105*(29), 10137–10142. https://doi.org/10.1073/pnas.0800487105

Shepherd, G. M. G., & Yamawaki, N. (2021). Untangling the cortico-thalamo-cortical loop: cellular pieces of a knotty circuit puzzle. *Nature Reviews Neuroscience*, *0123456789*.

https://doi.org/10.1038/s41583-021-00459-3

Sincich, L. C., & Horton, J. C. (2003). Independent projection streams from macaque striate cortex to the second visual area and middle temporal area. *Journal of Neuroscience*, *23*(13), 5684–5692. https://doi.org/10.1523/jneurosci.23-13-05684.2003

Sincich, L. C., Jocson, C. M., & Horton, J. C. (2010). V1 interpatch projections to V2 thick stripes and pale stripes. *Journal of Neuroscience*, *30*(20), 6963–6974. https://doi.org/10.1523/JNEUROSCI.5506-09.2010

Suter, B. A., & Shepherd, G. M. G. (2015). Reciprocal interareal connections to corticospinal neurons in mouse MI and S2. *Journal of Neuroscience*, *35*(7), 2959–2974. https://doi.org/10.1523/JNEUROSCI.4287-14.2015

Suzuki, M., & Larkum, M. E. (2020). General Anesthesia Decouples Cortical Pyramidal Neurons. *Cell*, *180*(4), 666-676.e13. https://doi.org/10.1016/j.cell.2020.01.024

Takahashi, N., Ebner, C., Sigl-Glöckner, J., Moberg, S., Nierwetberg, S., & Larkum, M. E. (2020). Active dendritic currents gate descending cortical outputs in perception. *Nature Neuroscience*, *23*(10), 1277–1285. https://doi.org/10.1038/s41593-020-0677-8

Takahashi, N., Oertner, T. G., Hegemann, P., & Larkum, M. E. (2016). Active cortical dendrites modulate perception. *Science (New York, N.Y.)*, *354*(6319), 1587–1590. https://doi.org/10.1126/science.aah6066

Thomson, A. M. (2010). Neocortical layer 6, a review. *Frontiers in Neuroanatomy*, *4*(MARCH), 1–14. https://doi.org/10.3389/fnana.2010.00013

Vélez-Fort, M., Rousseau, C. V., Niedworok, C. J., Wickersham, I. R., Rancz, E. A., Brown, A. P. Y., … Margrie, T. W. (2014). The stimulus selectivity and connectivity of layer six principal cells reveals cortical microcircuits underlying visual processing. *Neuron*, *83*(6), 1431–1443. https://doi.org/10.1016/j.neuron.2014.08.001

Von Helmholtz, H. (1867). *Handbuch der physiologischen Optik: mit 213 in den Text eingedruckten Holzschnitten und 11 Tafeln* (Vol. 9). Voss.

Wang, Q., & Burkhalter, A. (2007). Area map of mouse visual cortex. *Journal of Comparative Neurology*, *502*.

Webster, M. J., Bachevalier, J., & Ungerleider, L. G. (1994). Connections of inferior temporal areas TEO and TE with parietal and frontal cortex in macaque monkeys. *Cerebral Cortex (New York, N.Y. : 1991)*, *4*(5), 470–483. https://doi.org/10.1093/cercor/4.5.470

Wickersham, I. R., Lyon, D. C., Barnard, R. J. O., Mori, T., Finke, S., Conzelmann, K. K., … Callaway, E. M. (2007). Monosynaptic Restriction of Transsynaptic Tracing from Single, Genetically Targeted Neurons. *Neuron*, *53*(5), 639–647. https://doi.org/10.1016/j.neuron.2007.01.033

Williams, S. R., & Stuart, G. J. (1999). Mechanisms and consequences of action potential burst firing in rat neocortical pyramidal neurons. *Journal of Physiology*, *521*(2), 467–482.

https://doi.org/10.1111/j.1469-7793.1999.00467.x

Wozny, C., & Williams, S. R. (2011). Specificity of synaptic connectivity between layer 1 inhibitory interneurons and layer 2/3 pyramidal neurons in the rat neocortex. *Cerebral Cortex*, *21*(8), 1818–1826. https://doi.org/10.1093/cercor/bhq257

Yamawaki, N., Radulovic, J., & Shepherd, G. M. G. (2016). A corticocortical circuit directly links retrosplenial cortex to M2 in the mouse. *Journal of Neuroscience*, *36*(36), 9365–9374. https://doi.org/10.1523/JNEUROSCI.1099-16.2016

Zhang, S., Xu, M., Kamigaki, T., Do, J. P. H., Chang, W. C., Jenvay, S., … Dan, Y. (2014). Long-range and local circuits for top-down modulation of visual cortex processing. *Science*, *345*(6197), 660–665. https://doi.org/10.1126/science.1254126

Zhang, Z. W., & Deschênes, M. (1998). Projections to layer VI of the posteromedial barrel field in the rat: A reappraisal of the role of corticothalamic pathways. *Cerebral Cortex*, *8*(5), 428–436. https://doi.org/10.1093/cercor/8.5.428

Zmarz, P., & Keller, G. B. (2016). Mismatch Receptive Fields in Mouse Visual Cortex. *Neuron*, *92*(4), 766–772. https://doi.org/10.1016/j.neuron.2016.09.057

Financial Support

Hedi Young was supported by fellowships from Fundação para a Ciência e a Tecnologia (SFRH/BD/52221/2013 & Congento LISBOA-01-0145-FEDER-022170) and the Champalimaud Foundation.

ITQB-UNL | Av. da República, 2780-157 Oeiras, Portugal
Tel (+351) 214 469 100 | Fax (+351) 214 411 277

www.itqb.unl.pt